GEOLOGY AND GEOCHEMISTRY OF THE JONES CAMP MAGNETITE DEPOSITS, SOCORRO COUNTY, NEW MEXICO

by

John E. Jenkins

Submitted in Partial Fullfillment
of the Requirements for the Degree of
Master of Science in Geology

New Mexico Institute of Mining and Technology

Socorro, New Mexico

1985

Abstract of Thesis

The Jones Camp magnetite deposits occur near the southern edge of the Chupadera Mesa in eastern Socorro County, New Mexico. The deposits are interpreted as hydrothermal replacement type. The ore occurs as conformable pods of variable strike length, thickness, and grade adjacent to the Jones Camp dike and associated dikes and sills of probable Oligocene age. The ore replaces limestone, gypsum, and sandstone of the Permian Yeso, Glorieta, and San Andres Formations. Relatively minor ore bodies occur as replacements of intensely altered Jones Camp dike.

The Jones Camp ore consists of magnetite, secondary martite and maghemite; some pyrite is associated with gypsum hosted ore. No base or precious metal mineralization is present. Approximately 100,000 tons of Jones Camp ore has been mined in the 60's and 70's. There is renewed interest in the deposits as an ore source for a mini-steel mill.

Forceful emplacement of the Jones Camp dike and associated dikes and sills created favorable structures for the localization of ore. Shattering along the contacts developed secondary permeability and created the principal channelways for the ascending hydrothermal solutions. The intrusive rocks provided the thermal energy necessary for a convective hydrothermal system which leached, transported, and deposited the iron. Circulating groundwaters are believed to be the principal source of the fluids.

The mafic margins of the Jones Camp dike have been extensively altered by ascending hydrothermal solutions. Chemical analysis of intensely altered samples show a depletion in iron of approximately 3-4% which is believed to be the principal source of iron in the deposits.

Eleven samples collected from two locations in the district contained fluid inclusions hosted by calcite cogenetic with magnetite mineralization. Heating and freezing data suggest the system was non-boiling and under a hydrostatic pressure of 154 bars. A mean temperature of trapping of 169 degrees centigrade was determined. The salinity in terms of NaCl equivalents was not measured but the fluids are believed to be saline or hyper-saline.

Significant complexing of iron with chlorine in the acid-saline solutions must have occurred. The solutions apparently reached saturation around a calculated solubility minimum for the system which is approximately coincident with the temperatures obtained from fluid inclusion analysis. A reciprocal reaction between the dissolution of the host rocks by hydrolysis (hydrogen ion consuming reactions) and the precipitation of magnetite (which liberates hydrogen ions) may be envisioned resulting in the gradual replacement of the various host rocks.

Table of Contents

List of Figures:

List of Tables:

List of Appendices:

List of Plates (in pocket):

ACKNOWLEDGMENTS

I wish to aknowledge my advisor, Dr. Clay T. Smith, for continued support, enthusiasm, and critical reviews of the manuscript; and to my committee members, Dr. Andrew Campbell and Dr. Jaimie Robertson, for their critical reviews of the text and helpful suggestions. I'd also like to thank my Jones Camp comrade, Ted Jochems, for assistance in the field and provactive disscusions of the geology of the district. Finally I'd like to thank Ed Bottinelli, President Zia Steel Inc., for generous financial support during the course of this study.

INTRODUCTION

Purpose and Scope

This investigation of the geology and geochemistry of the Jones Camp iron deposits was undertaken in order to describe the physical and chemical controls for the occurrence and origin of the hydrothermal-replacement magnetite ore bodies, currently of renewed interest for their iron content. The magnetite ore which occurs as discontinuous pods of variable thickness, strike length and grade may be genetically related to Jones Camp dike and later dikes and sills. Data was obtained by the following methods: a) field observations and geologic mapping on a scale of 1:12000; b) petrographic examination of 46 thin sections of altered sedimentary and igneous rocks and 16 polished ore samples; c) fluid inclusion microthermometry and geobarometry from calcite cogenetic with magnetite mineralization; d) major and trace element data from Xray Fluorescence (XRF) analysis of unaltered Jones Camp syenodiorite and the later pyroxene syenodiorite dikes and sills.

Location and Accessibility

The iron deposits occur adjacent to the Jones Camp syenodiorite dike, a prominent east-west trending geologic feature which cuts Chupadera Mesa in eastern Socorro county

of south-central New Mexico. The deposits are easily accessible via the old Socorro-Carrizozo highway which parallels the Jones Camp dike on the north side. The old highway is about one mile north of Bingham, New Mexico located on U.S. highway 380, 36 miles east of San Antonio (Figure 1). Further access to the major ore outcroppings and old mine workings is possible via less well maintained ranch roads connected to the old highway or branching north from highway 380 approximately 5 miles east of Bingham.

History of Ownership and Mine Production

The discovery of the Jones Camp magnetite deposits is credited to local prospector P.G. Bell in 1902. He named the district in honor of Fayette A. Jones, then president of the New Mexico School of Mines. Mining records show the first claims to have been established on the Jones Camp property in 1927.

Rights to several lode and placer claims were obtained in 1964-65 by Carl Dotson of the International Mineral Company, Socorro, who was the first to begin mining operations on the deposits since their discovery. Between 1964 and 1969 approximately 100,000 tons of ore was removed by surface mining at several locations in sections 14 and 13 (township 5 south, range 7 east). The bulk of the ore mined was used by a local cement manufacturer in the production of high density cement with lesser tonnages sold to be used as

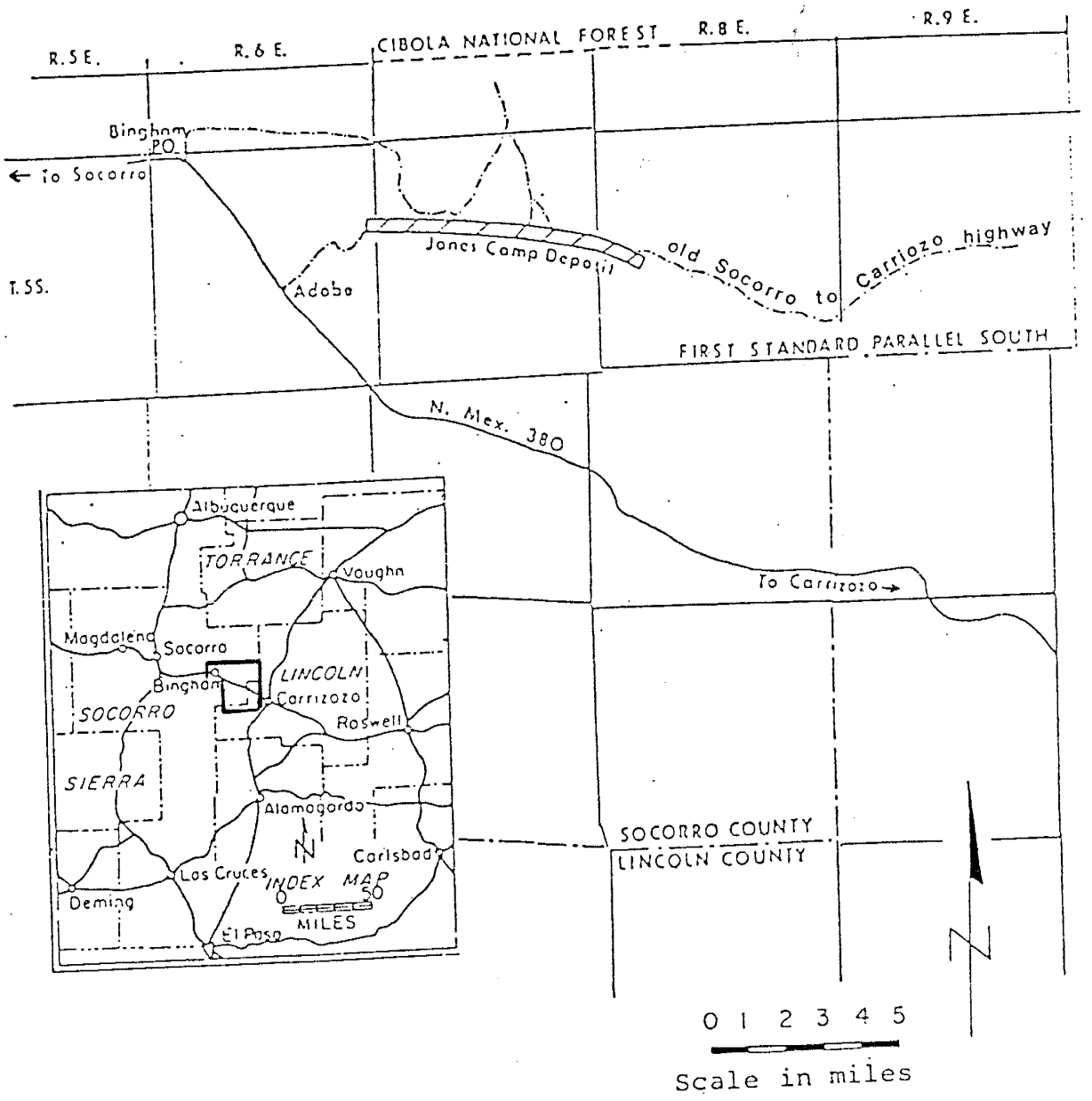

FIGURE 1: Location map of Jones Camp District in Socorro Co., New Mexico. The district is coincident with the Jones Camp dike. Note the area of detail is outlined in the larger scale map inset.

a water purifying agent.

In 1977 the claims were sublet by Dotson to Aweco International Ltd. which was interested in mining the ore to be processed in a 500 ton/day billet mill. Current ownership of the claims is by Zia Steel Inc., Edward Bottinelli, president. Developmental work and plans for a mini-steel mill operation are in progress.

Previous Work

Early accounts of the geology and nature of mineralization in the Jones Camp district include: Keyes (1904); Jones (1904); Emmons (1906); Schrader (1910); Lindgren, Graton and Gordon (1910); and Lasky (1932). During the Second World War the Jones Camp district was included as part of an extensive exploratory program carried out by the U.S. Bureau of Mines aimed at extending domestic iron ore reserves. This work, done in 1942, included extensive trenching, sampling and chemical analyses of ore and was published as Report of Investigation 1070 (Grantham and Soule, 1947). An account of the geology, a detailed geologic map, and estimates of the reserves, and grade of ore are included in V.C. Kelley's publication on the iron deposits of New Mexico (Kelley, 1949).

More recent investigations of the deposits were completed by Noguiera (1971), Bickford (1980), and Gibbons (1981). These papers provide additional geological, geophysical, and geochemical data pertaining to the Jones Camp deposits.

STRATIGRAPHY

The Jones Camp syenodiorite dike and associated pyroxene syenodiorite dikes and sills intrude sediments of Pennsylvanian and Permian age. Upper Permian strata are exposed in the study area and include (in ascending order) rocks of the Yeso Formation, the Glorieta Formation, and the San Andres Formation. Figure two is a stratigraphic column of the Permian and Pennsylvanian rocks of eastern Socorro county. The thicknesses of the units exposed in the study area are after Bickford (1980).

Yeso Formation

The Yeso Formation was first named and described by Lee (1909) for a section exposed on Mesa del Yeso northeast of Socorro, New Mexico. It has been subsequently redescribed and subdivided by Needham and Bates (1943) into four members: (in ascending order) the Meseta Blanca member, the Torres member, the Canas member, and the Joyita member. Only the upper three members are exposed in the study area.

Torres Member

The Torres member is comprised of a succession of interbedded limestone, gypsum, siltstone and silty sandstone layers. A maximum of 200 feet (61 m) measured by Bickford (1980, plate two) is present at the western end of the study

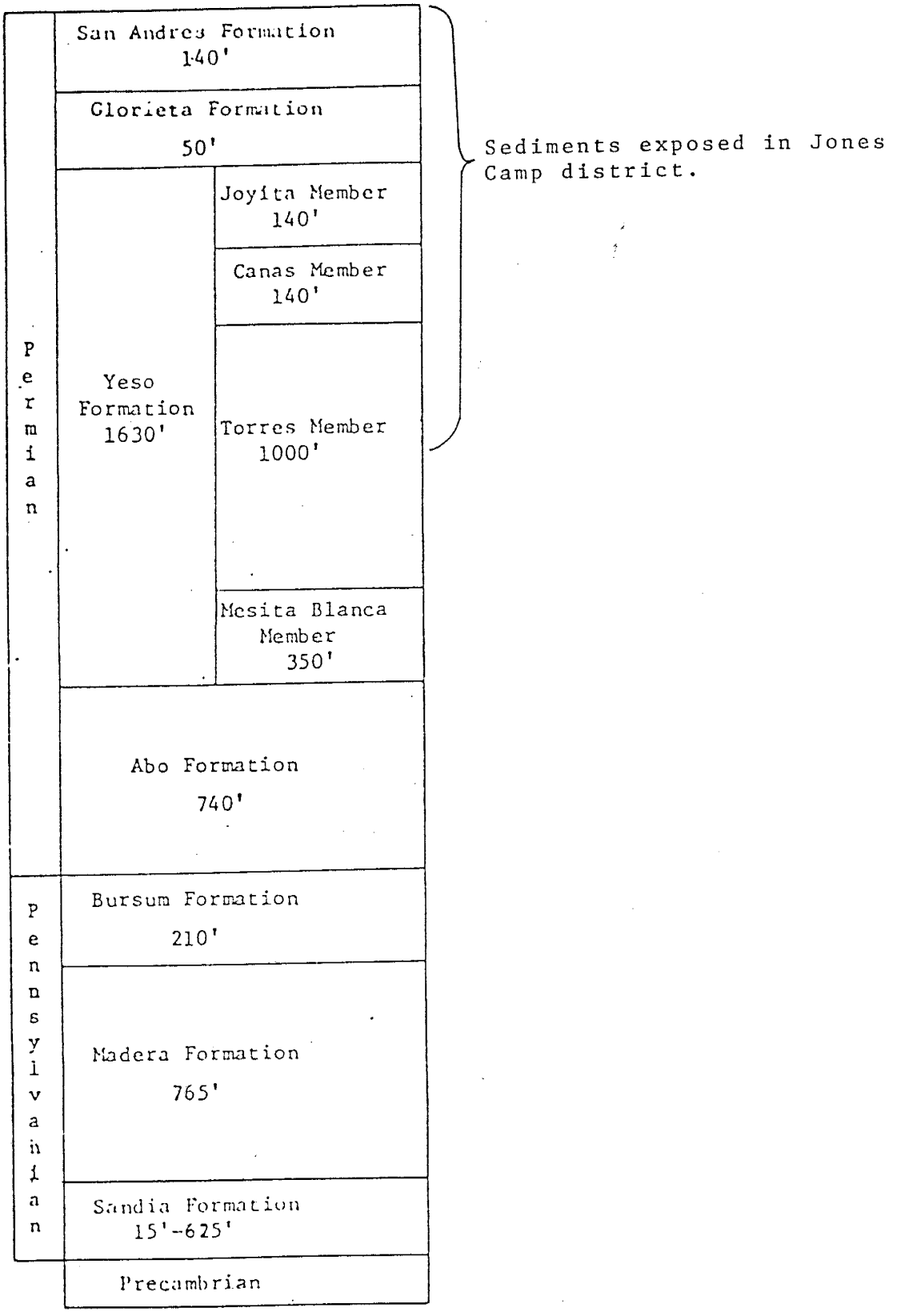

Figure 2: Stratigraphic section of Pennsylvanian and Permian rocks intruded by the Jones Camp dike. Thickness of units exposed in Jones Camp district after Bickford (1980).

area where the deepest level of erosion occurs. The stratigraphic section is recognized as being rhythmic, each cycle being marked by a thickly-bedded limestone. Physiographically these limestones form ridges or cap small cuestas and are useful markers which are easily mapped (see plate 1- geologic map). Each cycle begins with the thickly-bedded limestone which grades into finely-laminated limestone interbedded with thickly-laminated gypsum. The gypsum is interbedded with several thin-to thickly-bedded siltstones and sandstones. Discontinuous sandstones are typically found at the top of each cycle which grade laterally into gypsum and are in sharp contact with an overlying limestone. The upper Torres limestone is the thickest (up to 30 feet). It is dolomitic, and the top marks the contact with the overlying Canas. The majority of the ore bodies in the Jones Camp district are hosted by Torres member limestones, gypsum and sandstones.

Canas Member

The Canas member is distinguished from the Torres member by a predominance of bedded gypsum over interbedded limestones, sandstones, and siltstones. Both nodular and laminated gypsum are present in subequal amounts. Several distinct grey, gypsiferous limestone layers two to four feet (0.6-1.2 m) thick occur interbedded with the gypsum as do thin, one to two foot (0.3-0.6 m) thick, discontinuous siltstones or fine-grained sandstones. Bickford (1980)

measured 100 to 140 feet (31-43 m) of Canas member. The contact between the Canas member and the overlying Joyita member is sharp and conformable but is generally poorly exposed; the contact may be readily inferred by a difference in soil color and/or a change in slope due to a difference in susceptibility to erosion.

Joyita Member

The Joyita member is recognized by a distinctive reddish coloration. It consists predominantly of a red, fine-grained, massive to thinly-bedded sandstone. Two gypsum units occur interbedded with the sandstone: the lower thickly-laminated or nodular gypsum bed is six to eight feet (1.8-2.4 m) thick and is located 8 to 20 feet (2-6 m) above the base; the upper thickly-laminated gypsum bed is also 6 to 8 feet thick and marks the contact with the overlying (conformable) Glorieta Formation. The thickness of the Joyita member varies from approximately 106 feet (32 m) to 140 feet (43 m) (Bickford, 1980 plate 2).

Glorieta Formation

The Glorieta Formation was named and described by Keyes (1915) for Glorieta Mesa near Santa Fe, New Mexico. The Glorieta has commonly been included as a basal member of the conformable San Andres Formation (Read and Andrews, 1944) but is regarded in this study as deserving formational

status in agreement with Bickford (1980) and Gibbons (1981).

The Glorieta Formation consists of yellow-buff, fine-grained, thinly-bedded sandstone. It generally does not outcrop well but may be well-exposed in drainages or on steep slopes. The average thickness of the Glorieta is 53 feet (16 m). The contact with the overlying San Andres Formation is sharp and conformable.

San Andres Formation

The San Andres Formation was originally described by Lee (1909) from its type locality in the San Andres Mountains of south-central New Mexico. In the Jones Camp district it consists of grey, thickly-bedded limestone which may be fossiliferous or show horizons of bedded ferruginous chert nodules. In the Jones Camp district it is largely dolomitized. A ten to twenty foot (3-6 m) sandstone, lithologically similar to the Glorieta sandstone, occurs approximately 18 feet (6 m) above the base. This sandstone thins eastward and pinches out in section 29 T5S, R8E (Bickford, 1980). Erosion has truncated the San Andres and it shows a maximum exposed thickness of 140 feet (42 m) (Bickford, 1980 plate 2). The San Andres Formation covers most of Chupadera Mesa and forms the prominent cliffs which define the cuestas to either side of the Jones Camp dike.

STRUCTURE

Regional Structure

The prominent west-westnorthwest trending Jones Camp syenodiorite dike nearly crosses the southern half of Chupadera Mesa a broad north-northeast trending homocline which dips gently (1-2 degrees) to the east. Chupadera Mesa extends from an arbitrary northwesterly trending boundary with the Oscura uplift (near the Yeso-San Andres contact) to the southwestern corner of the Estancia Valley. The mesa is approximately 45 miles (72 km) long and 10 to 15 miles (16-24 km) wide. The southeast edge is bounded by the north-northeast trending Carrizozo anticline. The Jornada del Muerto anticline on the eastern side of the Jornada del Muerto Basin defines the western edge of the mesa. Chupadera Mesa is bounded on the east by the Chupadera fault which marks the boundary with the Claunch Sag. The otherwise nearly flat surface of Chupadera Mesa is modified by an anticlinal arch over the Jones Camp syenodiorite dike and similar structures created by other smaller, similarily trending intrusives to the south (the Iron Horse dike -Kelley, 1949) and two unnamed intrusives to the north.

The Jones Camp dike crops out for approximately 11 miles and is part of an east-west alignment of igneous features which has been referred to as the Capitan Lineament (Kelley and Thompson, 1964; Chapin, et al., 1978). The

geologic features which define the lineament from west to east are: the Jones Camp syenodiorite dike; the vents for the Quaternary Broken Back and Carrizozo basalt flows; the Capitan Stock; the dikes near Roswell, New Mexico; and the Matador Arch in west Texas. The Capitan Lineament is extended west of the Jones Camp into Arizona (near Springerville) where it terminates at the intersection with the Jemez lineament (Chapin, et al., 1978, figure 1). The western extension of the lineament is based on gravity and aeromagnetic data but is recognized as problematic (C.E. Chapin, personal communication, 1984). The clearly defined Capitan lineament strongly suggests that a prominent basement structure, probably of Precambrian age, has exerted control on the location and ascent of these igneous masses. The lineament is notable because it is roughly normal to the post-Precambrian tectonic fabric developed in the region.

The Jones Camp syenodiorite and other igneous rocks have been dated by the K-Ar method in eastern Socorro Co. and northern Lincoln Co. All yield mid-Tertiary Oligocene ages. The age on the Jones Camp syenodiorite was recently recalculated using the new K-Ar decay constants as 27.9 ±1.1 m.y. (C.E. Chapin personal communication, 1984). This is the same age as that recently determined for the Railroad dike near Roswell, New Mexico. Other relevant dates include a dike dated as 30.2 ±2.0 m.y., located west of Chupadera Mesa and approximately 26 miles (42 km) N-NW of Jones Camp (C.E. Chapin personal communication, 1984). Two intrusions

in the Sierra Blanca volcanic field to the southeast have dates of 31.8 ±2.0 m.y. and 34.4 ±1.2 m.y. (Weber, 1971 -not recalculated dates).

Isotopic dates on the Lincoln County porphyry belt are not available but based on composition and geologic information the porphyries are believed to be Oligocene or possibly Eocene in age (Kelley and Thompson, 1964). The trend on these intrusives and the other principal pre-Oligocene post-Precambrian structures in the region show a north or northeast trend essentially normal to the Jones Camp dike. This lends support to the hypothesis that the basement structure controlling the location of the Jones Camp dike is Precambrian in age and was not formed as a result of the stress regimes active in forming the later structures in the area.

Local Structure

The Jones Camp dike forms a resistant ridge with as much as 225 feet (69 m) of local relief above the soft strata of the Yeso Formation (plate 1). The strike of the dike is approximately N75W and is believed to dip steeply to the south (Nogueira, 1971; Bickford, 1980). At its eastern-most exposure the Jones Camp dike plunges beneath the Joyita member of the Yeso Formation. Strata of the overlying Glorieta and San Andres Formations are anticlinally arched and may be traced along strike of the

dike for an additional 1.2 miles (1.9 km) (Bickford, 1980). Successively older beds contact the dike westward. The dike extends for about three miles beyond the western escarpment of Chupadera Mesa where it is eventually covered by alluvium at the stratigraphic level of the Torres or Mesita Blanca members of the Yeso Formation. Total outcrop length of the Jones Camp dike is approximately 11 (18 km) miles and varies from approximately 250-825 feet (76-251 m) in width. Numerous roof pendants of mainly sandstone in the upper Torres or Joyita members of the Yeso Formation are present along the dike and are common in sections 15, 16 and 17 on the western half of the dike and in section 29 at the eastern end. This indicates that the present erosional surface is at, or near the top of, the Jones Camp dike.

As noted above, intrusion of the Jones Camp dike has resulted in a broad anticlinal arching of the overlying sediments which extends for up to 2000 feet (610 m) beyond either side of the central dike. Based on regional structural patterns and the lack of field evidence in the study area, there is little evidence that the Jones Camp dike was emplaced along a prexsisting fault or anticline in the Paleozoic strata but rather that the principal structural control was imposed by the extended basement structure described above.

A zone of greater structural complexity exists within about 200 feet (62 m) of the dike contact where expansion of the dike during emplacement has resulted in sharp upturning or pervasive folding and faulting of the sediments. Pervasive small scale asymmetrical anticlines and lesser synclines parallel the contact within this zone. These structures are well defined in places by outcrops of the upper Torres member limestone. Steeply dipping faults paralleling the axis of the folds are demonstratable in places (see Figure 8). Normal faults are perpendicular to the Jones Camp dike at points where it widens or where it is intruded by later dikes and sills.

At least two pulses of intrusion of later dikes and sills are recognized in the field based on crosscutting relationships and well developed chilled contacts. They intrude the margins of the Jones Camp dike and adjacent sediments. This intrusion has resulted in further upturning or shouldering of the sediments and engulfing of large blocks of sediments as inclusions. The sills are up to 75 feet (23 m) thick and may extend into the sediments for at least a half mile beyond the central Jones Camp dike. The gypsum layers in the Canas, Torres, and Joyita members of the Yeso Formation are favored stratigraphic horizons for intrusion of the sills. Sills are also emplaced along the Glorieta-San Andres contact and in the lower San Andres. Assimilation and/or plastic flow of the gypsum during emplacement of the igneous rocks may also explain changes in

thicknesses and/or complete displacement of the gypsum layers in the Canas, Torres, and Joyita members of the Yeso Formation.

IGNEOUS ROCKS

Introduction

The Jones Camp dike and the later, less voluminous dikes and sills represent two distinct intrusive events in the Jones Camp district. The genetic relationship between these two intrusions is interesting with regard to understanding the origin of the Jones Camp magnetite deposits. Modal analysis and textural descriptions, combined with chemical data, are required for a model of their origin. Detailed petrographic and geochemical data was obtained for the Jones Camp dike by Gibbons (1981) who presented a model for its origin. Major and trace element data were obtained in this study, of unaltered Jones Camp dike and the later pyroxene syenodiorite dikes and sills. These data aided the understanding of the origin of the igneous rocks. Prior to this study only a single chemical analysis of the pyroxene syenodiorite is known to the author and is included in Appendix I (Nogueira 1971). The trace elements Ba, Rb, Sr, Zr, Nb, Y, V, and Pb were analyzed in eleven samples of these rocks. The petrographic and chemical data of Gibbons (1981), Bickford (1980) and Noguiera (1971) are included in the author's analysis and are essential for the current model.

Field Characteristics

Jones Camp syenodiorite

The Jones Camp syenodiorite dike is resistant to erosion forming prominent outcrops which display well developed cooling joints in favorable locations. A greater textural and mineralogical variability exists in the Jones Camp syenodiorite than the later pyroxene syenodiorite dikes and sills. These differences are due to greater chemical variability as a result of differentiation in-situ and extensive hydrothermal alteration of the Jones Camp syenodiorite dike margins. The main dike consists of a fine to medium-grained, holocrystalline, hypidiomorphic granular pyroxene-hornblende diorite or monzodiorite. Lesser biotite, magnetite, zircon and occasional quartz are also observed in outcrop. There is a trend in the more leucocratic zones to a porphyritic texture containing phenocrysts of alkali feldspar. Variable sized miarolitic cavities containing coarser grained crystals of feldspar, hornblende and pyroxene with euhedral terminations are common.

The margins of the Jones Camp syenodiorite dike have been extensively altered by ascending hydrothermal solutions. The margins are very fine grained to aphanitic, green colored and show pronounced banding or layering. The layering structure is parallel to the strike of the dike and

may be related to cooling joints measured in section 17. The intensity of alteration (based on a overall decrease in grain size and development of mottled texture) is greatest at the dike contacts and decreases inwards. The effects of this hydrothermal alteration are recognized throughout the length of the dike but the overall intensity is variable.

Pyroxene syenodiorite

The later dikes and sills have been referred to in the literature as diabase after Kelley (1949). This is a misnomer as these intrusives are neither chemically nor texturally compatible with this classification. This discrepancy was noted by Bickford (1980) who referred to them as pyroxene syenodiorites. This latter classification is supported by the chemical data of this study and will be adopted as such.

The pyroxene syenodiorite dikes and sills lack the textural and mineralogical variability of the Jones Camp syenodiorite and lack extensive recrystallization due to hydrothermal activity. They are recognized as a dark green to greenish gray, fine-grained, porphyritic, intergranular pyroxene syenodiorite. They typically show 3-7% fine to medium-grained phenocrysts of feldspar (chiefly plagioclase) set in a matrix of fine to very fine-grained plagioclase and interstitial clinopyroxene, biotite, and magnetite. Deviations from this homogenous character are limited to

some of the thick sills which may be fine to medium-grained and non-porphyritic. No well-developed cooling joints are apparent.

Extensive alteration of the pyroxene syenodiorite is limited to no more than a few feet from the contact with ore. Altered rock does not sharply contrast with unaltered rock except that it tends to be more deeply weathered and may show extensive fractures and veins of secondary calcite which typically host grains of magnetite. Specular hematite, not associated with calcite, is also seen on fracture surfaces.

The pyroxene syenodiorite was emplaced in at least two pulses which are recognized by well developed chilled margins at the contacts between pulses. The fine-grained chilled texture is also typically developed at contacts with the Jones Camp syenodiorite dike or sediments where exposed.

Petrography

Jones Camp syenodiorite

Based on modal mineralogy the Jones Camp syenodiorite is classified as a diorite to monzodiorite following Streckeisen (1976). The texture is variable: fine to medium-grained, hypidiomorphic granular, inequigranular-hiatal to equigranular. It may be porphyritic. The primary mineralogy and texture of the margins of the Jones Camp dike

are often obscured by the extensive hydrothermal alteration.

The Jones Camp syenodiorite shows variable concentrations of the essential and varietal minerals; these include plagioclase, alkali feldspar, hornblende, clinopyroxene, orthopyroxene, magnetite, biotite, and quartz. Total ferromagnesian minerals plus magnetite range from approximately 35% in the margins of the dike to 5-10% in the central core. Plagioclase occurs as subhedral to euhedral laths which are often normally zoned and show variably developed sericite and/or saussurite alteration. Composition has been determined using the Michel-Levy method based on extinction angles. It ranges from about An 49 (andesine) to An 30 (oligoclase).

Alkali feldspar is euhedral to anhedral and predominantly fine-grained. Microperthitic texture is common. Nogueira (1971) recognized sutured phenocrysts of orthoclase in the core facies. Often anhedral alkali feldspar occurs rimming plagioclase laths in the more felsic zones. Late stage feldspar of uncertain composition also occurs as fine-grained anhedral or subhedral masses typically showing variably developed radial or spherulitic texture. This may be an intergrowth of alkali and plagioclase feldspar and might include some quartz. This texture is not restricted to any zone.

Hornblende is generally euhedral and fine to medium-grained; however, needles observed in the field are up to 12 mm in length. The pyroxenes are fine-grained, euhedral or subhedral and include augite, aegirine-augite and sporadic hypersthene. Magnetite is largely subhedral and is finer grained than the above minerals. It is recognized as an early crystallizing phase and may occur as inclusions in hornblende. Interstitial biotite is finer grained and common in some thin sections. Primary zircon and apatite are present as accessory minerals in almost all of the thin sections. Sporadic quartz and sphene are also present. Quartz constitutes 8.5% of the rock in the central quartz diorite subfacies of Nogueira (1971).

Pyroxene syenodiorite

The pyroxene syenodiorite dikes and most of the sills are fine to very fine-grained, porphyritic and show a well developed intergranular texture. Phenocrysts are plagioclase and occasional orthoclase. Groundmass feldspar is predominantly plagioclase of andesine composition and is commonly sericitized or saussuritized. Subhedral clinopyroxene, magnetite and biotite are interstitial to the plagioclase laths. These minerals typically constitute 30-35% of the rock in the following proportions: magnetite averages 3-5%; biotite 2-3%; and clinopyroxene makes up the remaining 25-27%. In a few locations primary hornblende in addition to clinopyroxene is present and may be the

predominant ferromagnesian mineral. Plagioclase is oligoclase in composition and a decrease in the ratio of plagioclase to alkali feldspar is noted. In some of the thin sections collected from these locations by Bickford (1980), an increase in grain size and a non-porphyritic, equigranular texture similar to the Jones Camp syenodiorite is present.

Geochemistry of the Igneous Rocks

A total of eleven samples of Jones Camp syenodiorite and pyroxene syenodiorite were collected for major and trace element analysis. XRF analyses were completed using a Rigakau DMAX spectrometer. The results of these analyses are contained in Tables 1A and 1B. An effort was made to collect samples as free as possible from secondary alteration. Hand specimen descriptions of these rocks are included in Appendix II. The locations of these samples is outlined in figure 3.

A silica variation diagram for the major element data for these samples is plotted in Figure 4. The pyroxene syenodiorite compositions are plotted as an average excluding 84-11 which was enriched in K_2O above the average of 1.10 wt.% by a factor of three. Figure 4 also includes the chemical data of Gibbons (1981) for two suites of Jones Camp syenodiorite dike samples collected normal to the

TABLE 1A: Major and trace element analysis. Major element concentrations are weight percent; trace element concentrations are parts per million.

Pyroxene syenodiorite:	84-5A	84-5B	84-15A	84-15B	84-15C	84-11
SiO_2	52.30	51.69	52.21	52.11	51.37	51.98
TiO_2	1.54	1.49	1.51	1.52	1.52	1.45
Al_2O_3	16.10	15.86	15.84	16.08	15.95	15.72
*Fe_2O_3	10.28	10.14	10.04	10.26	10.08	10.01
MgO	4.46	4.69	4.65	4.55	4.56	4.51
CaO	6.30	6.94	6.22	6.27	6.08	5.01
Na_2O	5.16	4.07	4.41	4.98	4.65	4.58
K_2O	0.72	1.05	1.43	1.26	1.03	3.27
MnO	0.10	0.10	0.12	0.12	0.11	0.12
P_2O_5	0.61	0.61	0.57	0.59	0.59	0.59
LOI	1.20	2.26	1.58	1.61	2.29	2.63
H_2O-	0.81	0.62	0.58	0.50	0.92	0.35
TOTAL	100.39	100.14	99.74	100.45	100.07	100.55
Y	35	34	36	36	34	44
Sr	686	678	714	678	636	567
Nb	16	15	16	17	16	17
Zr	217	223	224	221	224	264
Rb	6	17	33	23	20	72
Pb	3	2	8	3	5	8
V	171	156	211	181	180	176
Ba	646	773	983	779	659	1067

Jones Camp dike:	84-33	84-34	84-35	84-36	84-37
SiO_2	59.89	59.13	60.18	60.76	56.16
TiO_2	1.19	1.33	1.26	1.25	1.40
Al_2O_3	16.94	17.16	17.17	16.23	16.94
*Fe_2O_3	5.94	5.81	5.89	5.72	6.35
MgO	2.08	2.22	2.03	2.03	2.34
CaO	3.73	3.87	3.14	3.42	4.67
Na_2O	5.99	6.83	8.32	4.69	6.99
K_2O	2.51	1.81	1.04	4.27	1.78
MnO	0.09	0.07	0.07	0.08	0.08
P_2O_5	0.45	0.54	0.50	0.45	0.56
LOI	0.85	1.04	0.77	0.85	1.78
H_2O-	0.30	0.54	0.23	0.48	0.40
TOTAL	99.96	100.35	100.60	100.23	99.45
Y	47	49	44	50	49
Sr	1058	1023	751	796	899
Nb	18	18	19	21	18
Zr	262	293	314	342	276
Rb	37	36	15	56	31
Pb	-	-	2	1	3
V	83	83	91	67	89
Ba	933	754	498	1088	673

*Fe_2O_3 as total iron.

TABLE 1B: Normative concentrations.

Pyroxene syenodiorite:

	84-5A	84-5B	84-15A	84-15B	84-15C	84-11
Q	--	1.42	--	--	--	--
Or	4.40	6.48	8.79	7.68	6.40	20.03
Ab	45.13	35.94	38.79	43.48	41.36	38.89
An	19.30	22.86	19.96	18.37	20.61	13.14
Ne	--	--	--	--	--	0.70
Di	7.35	7.33	6.77	8.03	5.79	7.06
Hy	12.27	18.53	17.99	7.63	16.55	--
Ol	4.11	--	0.34	7.43	1.76	12.17
Mt	3.00	3.03	3.02	2.99	3.05	3.76
Tl	3.02	2.95	2.98	2.98	3.04	2.86
Ap	1.46	1.46	1.37	1.41	1.44	1.42

Jones Camp dike:

	84-33	84-34	84-35	84-36	84-37
Q	5.66	2.88	0.01	8.30	--
Or	15.06	10.87	6.19	25.60	10.86
Ab	51.48	58.71	70.93	40.26	59.03
An	12.11	10.99	6.48	10.78	9.90
Ne	--	--	--	--	1.09
Di	2.97	4.19	4.74	2.76	8.33
Hy	5.69	5.12	4.43	5.17	--
Ol	--	--	--	--	4.07
Mt	3.69	3.68	3.65	3.68	3.74
Il	2.30	2.57	2.41	2.41	2.74
Ap	1.06	1.27	1.17	1.06	1.34

Explanation: Q=quartz; Or=orthoclase; Ab=albite; An=anorthite; Ne=nepheline; Di=diopside; Hy=hypersthene; Ol=olivine; Mt=magnetite; Il=ilmenite; Ap=apatite.

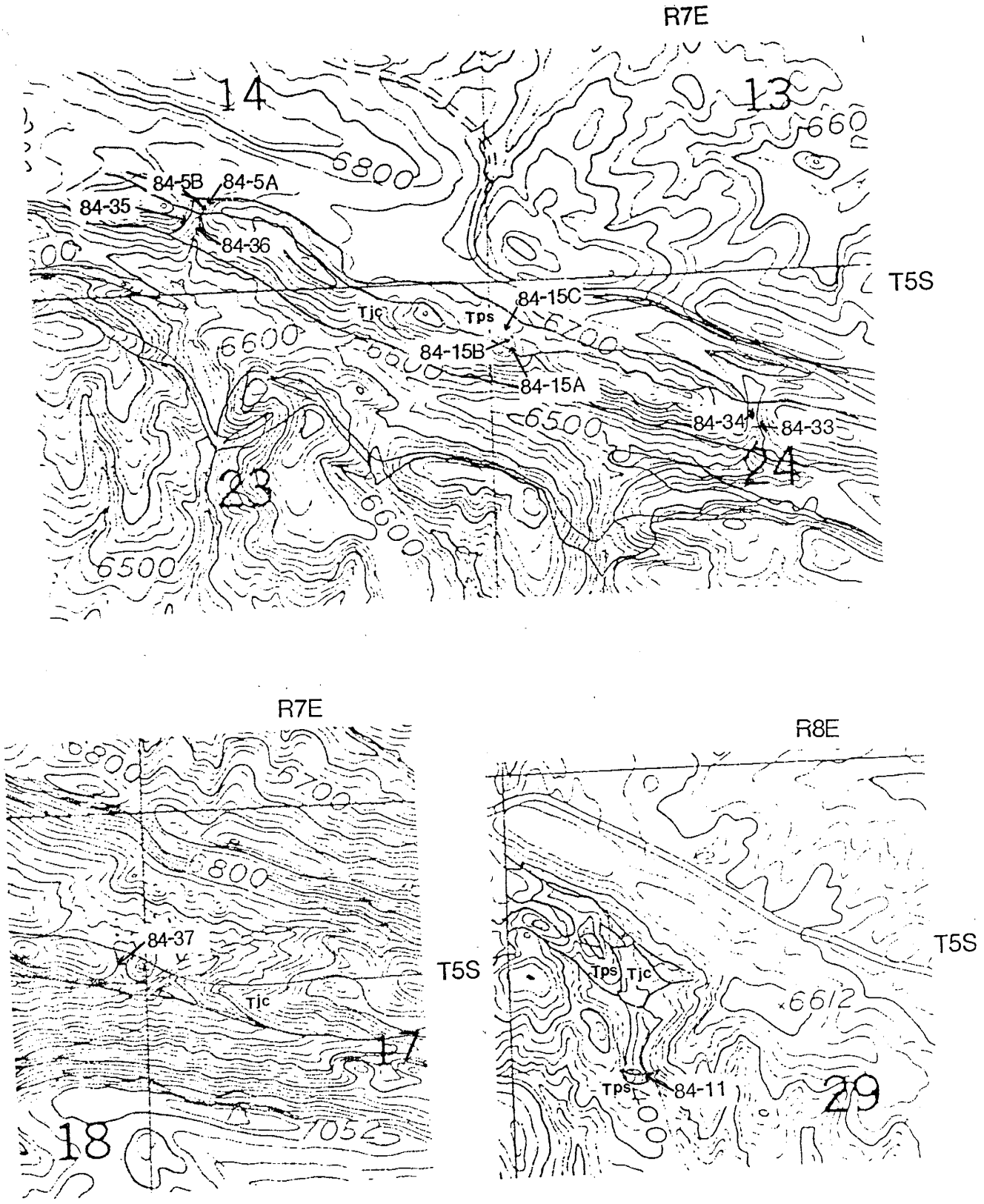

FIGURE 3: Location maps for chemical samples. See plate 2 for details of the geology.

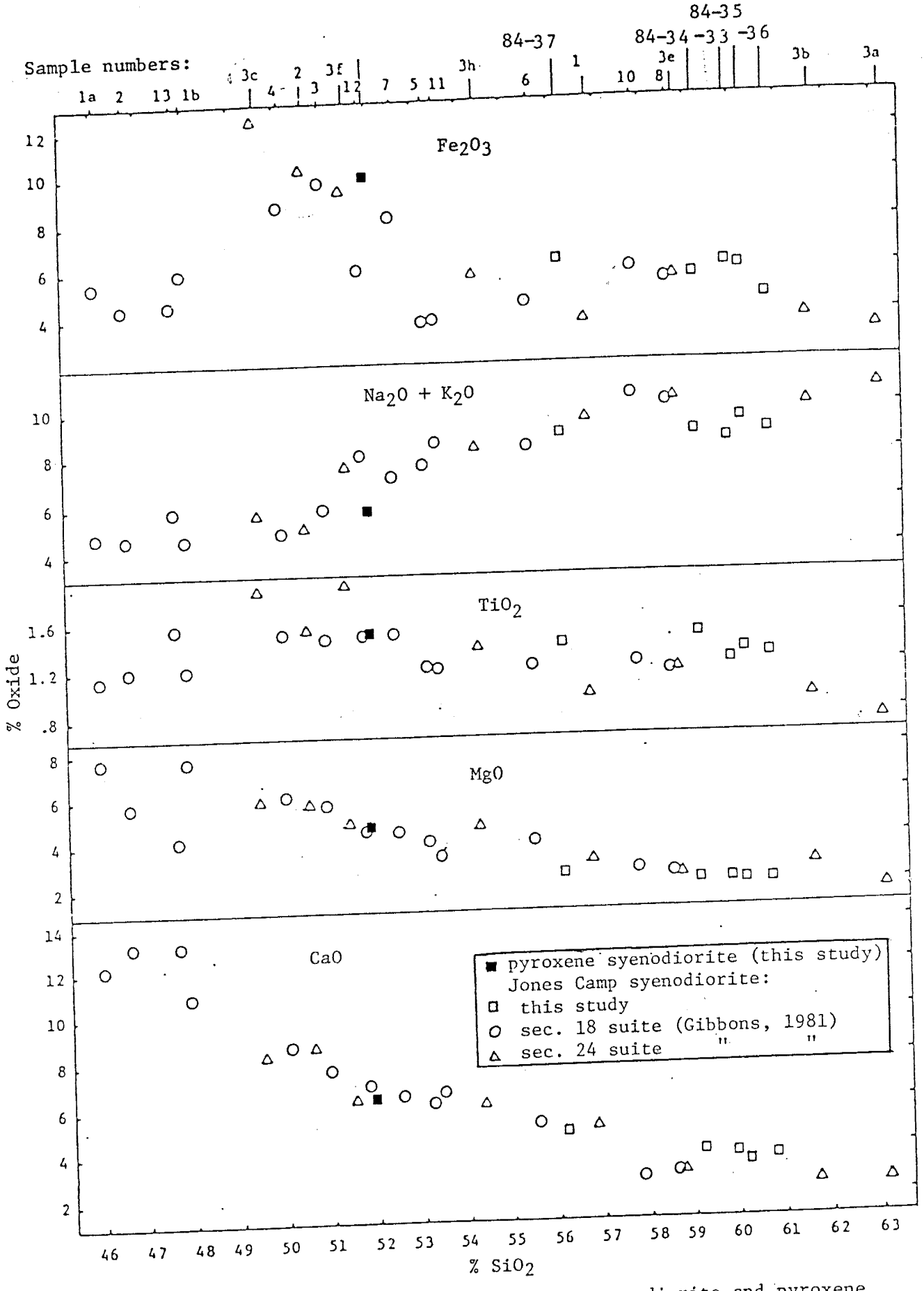

FIGURE 4: Silica variation diagram for Jones Camp syenodiorite and pyroxene syenodiorite. The latter is plotted as an average of five analyses.

strike of the dike in sections 18 and 24 (R7E, T5E). The chemical data for these rocks is contained in appendix III. Some of the samples of Gibbons included in figure 4 represent completely recrystallized marginal dike samples. Note that these samples are the lowest in SiO_2 and are enriched in CaO. The major and trace element concentrations for the pyroxene syenodiorite are remarkably similar, the greatest variations being in the concentrations of the alkalis and the large ion lithophile (LIL) elements Rb and Ba. The silica variation diagram of the trace elements for all eleven samples is plotted in Figure 5.

The rocks are classified as alkalic-calcic with a calcium-alkali-lime index of 52 after Peacock (1931). The rocks are also somewhat enriched in Na_2O relative to the diorite of LeMaitre (1976) and the average diorite of Nockolds (1954) hence may be classified as syenodiorites.

Geochemical Models

The chemical variations for the Jones Camp syenodiorite are compatible with a process of crystal fractionation. Major and trace element variations can be correlated to observed modal trends. These variations are controlled by fractionation of feldspars, hornblende, clinopyroxene, magnetite and biotite. Major element variations plotted against distance across the dike from the section 18 suite of (Gibbons, 1981, Figures 9a, 9b) show a symmetrically zoned body in which more mafic margins grade into a

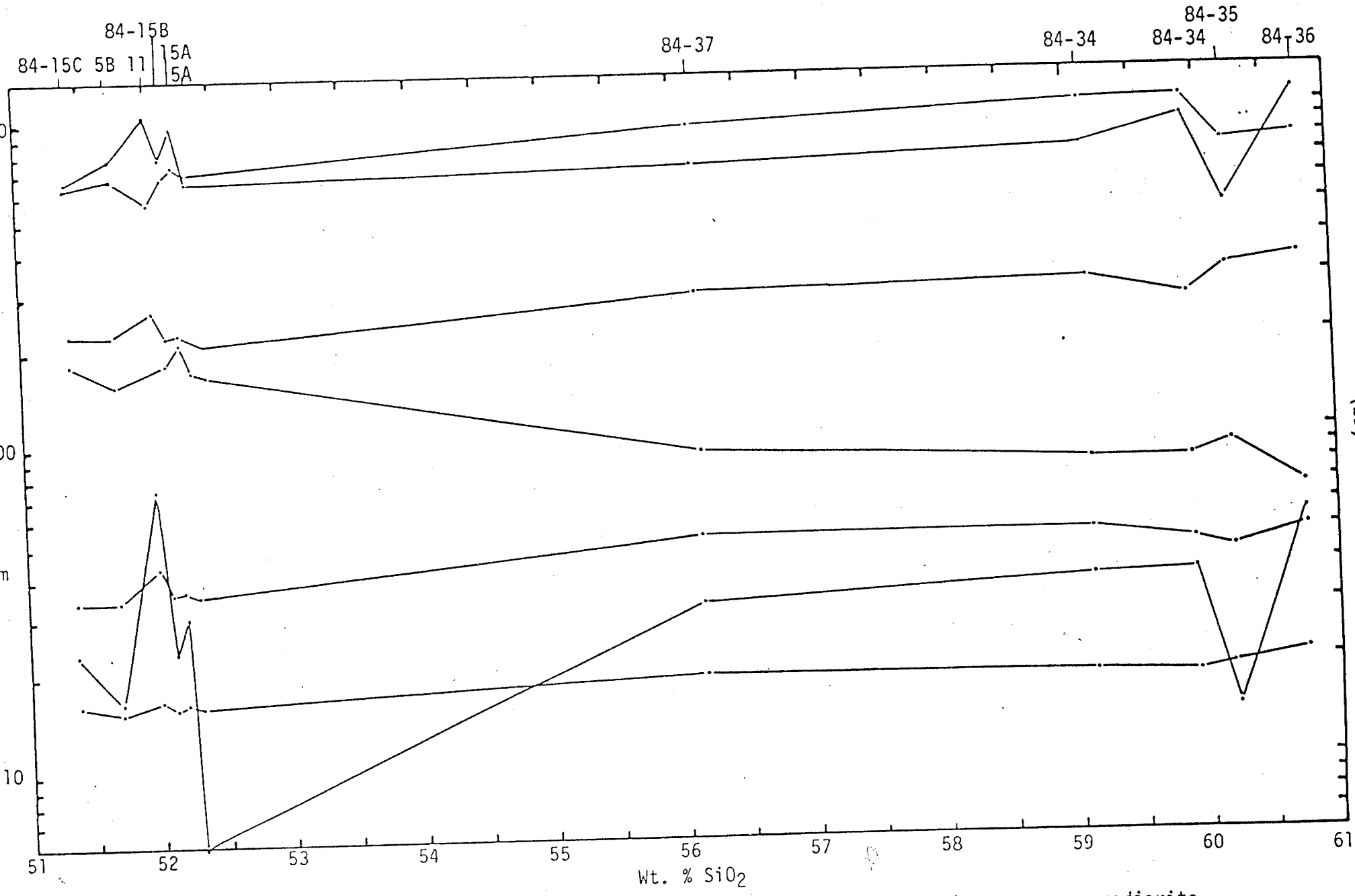

FIGURE 5: Trace element silica variation diagram for the Jones Camp syenodiorite and pyroxene syenodiorite.

relatively felsic core. A similar plot from the section 24 suite (figures 8a, 8b) shows several perturbations from the smooth trends seen in the section 18 suite. A model for the Jones Camp syenodiorite as a composite intrusive related to a single fractionating source was suggested. In this model, successive intrusions from a fractionating source, would be emplaced before the core of the previous intrusion had cooled (Gibbons, 1981). This model was called upon to explain the chemical variability of the Jones Camp syenodiorite and offers an explanation for perturbations in major oxide content across the dike. Possible field evidence found for this interpretation is indicated by distinct mineral zonations observed in places characterized by rapid changes in grain size and concentrations of ferromagnesian minerals (but no chilled contacts) in contrast to the gradational changes typically observed. There is also evidence for multiple intrusions into completely cooled dike as demonstrated by occasional outcrops showing xenoliths of earlier Jones Camp dike in a subsequent pulse (figure 6).

Although there is evidence that the Jones Camp syenodiorite dike was emplaced in more than one pulse, the chemical variability in the dike is probably the result of differentiation in-situ. This was first suggested by Nogueira (1971) based on chemical, petrographic and field data obtained for the Jones Camp dike in sections 13, 14, and 24. Differences in volatile content in the rocks during

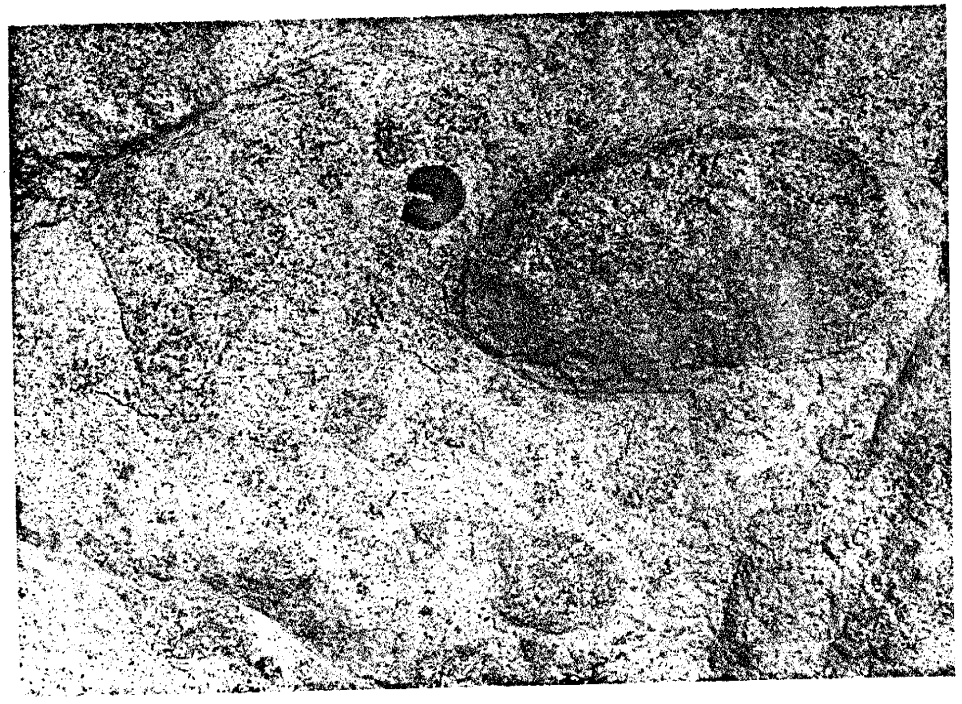

FIGURE 6: Outcrop of unaltered Jones Camp dike showing variably sized xenoliths of earlier Jones Camp dike indicating multiple intrusions. Magnet is 1" in length.

fractional crystallization may account for local deviations in grain size, percentage of ferromagnesian minerals and miarolitic cavities seen in the field. These zones were interpreted by Nogueira as "segregation pockets" enriched in volatiles during normal differentiation which would lower the freezing temperature and result in slower cooling, a coarser texture and a somewhat more felsic composition. This process may be more common at locations near the top of the dike which would be expected to be more enriched in volatile constituents during cooling. This process offers a possible explanation for the differences in major element chemistry between the section 18 and 24 suites of Gibbons. In both locations the top of the dike may be inferred from nearby roof pendants. The section 18 suite represents a deeper cross section (at least 300' below the top) whereas the section 24 suite is approximately 100' below the inferred top.

The major element compositions determined for the pyroxene syenodiorite are very close to the composition of the unaltered mafic end-members of Jones Camp syenodiorite dike (e.g. samples 3c, 3, 7, Gibbons, 1981). The modal mineralogy and approximate percentages of these rocks are also the same i.e. plagioclase, minor alkali feldspar, clinopyroxene, magnetite, and biotite. The lack of textural and chemical variation in the late intrusion indicates that these rocks cooled at a faster rate than the Jones Camp dike and no significant differentiation in-situ occurred. The

coarser grained, non-porphyritic pyroxene syenodiorite sills observed in thin sections of Bickford (1980) are an exception to this generalization. These rocks contain a lower plagioclase to alkali feldspar ratio and hornblende becomes the dominant ferromagnesian mineral. The differences in modal mineralogy suggest that these rocks have differentiated to some extent from the average pyroxene syenodiorite, as these differences are analogous to trends observed in the Jones Camp syenodiorite. No chemical analysis of this type of pyroxene syenodiorite has been obtained.

The samples collected for major and trace element analysis of the Jones Camp syenodiorite dike are from the more differentiated core zone. Despite the compositional gap not represented in these samples the major and trace element concentrations and variations suggest that the intrusive rocks are comagmatic. In this view the pyroxene syenodiorite represents an approximation to the undifferentiated Jones Camp syenodiorite and the chemistry of these rocks could probably be related by fractional crystallization. Quantitative testing of this conjecture, based on partial melting and fractional crystallization models described in the literature, is beyond the scope of this thesis. However, a consideration of the trace element data in view of the chemical and physical controls for the distribution of trace elements during fractional crystallization lends support to this hypothesis.

During fractional crystallization the concentration of a trace element in a melt relative to its concentration in the parent melt (C_l/C_o) is a function of the amount of fractional crystallization (commonly represented as the parameter F equal to the weight fraction of melt remaining) and the bulk distribution coefficient (D) for the crystals settling out. The bulk distribution coefficient for a given trace element is equal to the sum of the individual K_D values (mineral/melt distribution coefficient) times the weight fraction of the minerals (Hanson, 1978).

In a model based on the Rayleigh fractionation law, the concentration of trace elements with D values of 0.75 to 0 (i.e. incompatible to very incompatible) increases gradually in the fractionated melt with decreasing F up to F values of approximately 0.2 where a rapid increase occurs. The converse is essentially true for trace elements having a bulk distribution coefficient greater than one which would deplete the fractionated melt at a rate dependent on the size of the D value. For example, if D = 10, only 7.5% fractional crystallization reduces that elements concentration in the melt by a factor of 2 (Hanson, 1978).

Sympathetic variations in the concentrations of Rb, K, and Ba are probably related to the processes of secondary alteration and the mutual compatibility of these elements with respect to biotite (Rb, K, Ba) and alkali feldspar (K, Ba). The overall increase in concentrations of K, Rb, and

Sr in the Jones Camp syenodiorite samples (relative to the pyroxene syenodiorite) is typical for LIL elements during fractional crystallization and suggests that the bulk distribution coefficients were below unity. Late stage fluids or a volatile enriched phase may affect some trace element compositions by removing or mobilizing the elements. These fluids may be enriched in K, Rb, Ba (Hanson, 1978). This effect probably accounts for the sharp variations in these elements (and perhaps some variation in Sr which is also a mobile element) and is supported by petrographic observations of pervasive early hydrothermal alteration which is probably deuteric. This is particularly evident in samples 84-5A; 84-11; and 84-33.

Nb, Zr, and Y should behave as elements with small bulk distribution coefficients during fractionation of plagioclase, pyroxenes, hornblende, and Fe-Ti oxides, therefore the concentration of these elements should increase with increased fractionation. This trend is seen in Figure 5. Nb and Y show closely similar compatibilities for these minerals and thus the ratio should not vary significantly during a process of fractional crystallization which is also demonstrated by the data.

V is depleted by a factor of more than two in the Jones Camp dike samples. This is probably due to the high distribution coefficient of V for magnetite which is relatively abundant in the pyroxene syenodiorite and is

recognized as an early crystallizing phase in the Jones Camp syenodiorite thin sections (and is more concentrated in the more mafic samples). Therefore, early crystallization of magnetite would deplete the melt in V. This is also the probable explanation for the decrease in Ti which also has a high K_D for magnetite.

An understanding of the relationship between the Jones Camp syenodiorite and later pyroxene syenodiorite is significant with respect to a model for the ore deposits specifically with respect to the timing and duration of the hydrothermal system responsible for the deposition of the magnetite ore. Field evidence indicates that the ore is post-emplacement of the intrusive rocks and that the main stage of mineralization occurred at the lower temperature end of the hydrothermal system. The geochemical and petrographic data support geologic reasoning that the two intrusions are comagmatic. It is therefore likely that the hydrothermal system responsible for the mineralization was an effect of the emplacement and cooling of the intrusive rocks seen in the district. The life of the system may have been extended by the cooling of a larger pluton at depth which served as the source of the intrusive rocks.

MAGNETITE ORE

Field Occurrence

In the Jones Camp district high grade magnetite ore bodies are hosted by all of the various lithologies exposed in the Permian section. The ore bodies occur in sedimentary beds adjacent to the intrusive rocks; in the crests and limbs of anticlinal structures parallelling the Jones Camp dike; and as replacements of sedimentary inclusions in the pyroxene syenodiorite dikes emplaced along the Jones Camp syenodiorite dike. Lesser amounts are recognized replacing intensely altered (actinolitized) Jones Camp syenodiorite dike and occurring as replacements along fractures and intrusive contacts between pulses in the pyroxene syenodiorite. The bulk of the ore replaces the limestone, gypsum, and sandstone beds of the Torres member of the Yeso Formation and the gypsum and thin interbedded limestones and silty sandstones of the Canas member. The greatest concentration of exposed ore in the district is found in the central part of the study area in sections 13, 14, 19, 24 adjacent to the Jones Camp dike and pyroxene syenodiorite dikes and nearby sills (Plate 1). Ore occurrences found adjacent to the pyroxene syenodiorite sills that intrude higher in the section (i.e. the Joyita member of the Yeso and the Glorieta and San Andres Fms.) are thin and discontinuous. Because of the small size and relatively

difficult access, these occurrences are considered to be of low economic value.

In general the ore bodies are conformable to bedding in the sediments and are lenticular (or pod-like) in form. They are variable in thickness, length along strike, and grade. The largest exposed ore bodies in the upper Torres limestone and Canas gypsum show a maximum thickness of about 25 feet (8 m) and strike lengths of up to 1500 feet (457 m). The change from high grade ore to unmineralized host rock is rapid, on the order of 1-2 feet or less, and may be razor sharp as exemplified by some limestone hosted ore. The contact of ore and altered igneous rock is also very sharp.

The gypsum hosted ore presents some exceptions to the above generalizations. Magnetite is commonly widely disseminated. In these areas there seems to be less structural control imposed by bedding and the contacts between high grade ore (occurring as randomly oriented blocks or lenses) and unmineralized rock are often gradational. However, the prominent ore bodies hosted by Canas or Torres gypsum are more continuous and parallel the strike of the dike. These bodies may follow the interbedded limestones and/or sandstones.

The proximity of the magnetite ore to the igneous rocks is linked to the requirement of high porosity and permeability for leaching and transport of iron and other ions in solution. Extensive secondary permeability that

existed at the contacts of the intrusive rocks with the sediments provided the principal avenue for the ascending solutions with respect to the development and localization of ore. This accounts for the propensity of ore to occur at the contacts with the intrusive rocks. Figure 7 is an example of a ore body in the San Andres dolomite at the contact with a pyroxene syenodiorite sill.

A secondary porosity attained by dehydration and decarbonation reactions during contact metamorphism also may have facilitated the flow of hydrothermal solutions and is considered particularly important in the genesis of some of the gypsum hosted ore. The temperature of the Jones Camp syenodiorite magma was determined to be between 800 and 900 degrees centigrade based on the chemical composition (diorite) and estimate of the water pressure (Nogueira, 1971). The temperature obtained by the country rock is a function of the depth of burial, temperature of the dike, the thickness of the dike, and the distance from the contact with the dike (figure 10, Nogueira, 1971; after Winkler, 1967). Taking an average thickness of the dike of 600 feet (183 m) temperatures expected range from approximately 630 degrees centigrade at the contact to 375 degrees centrigrade at a distance of 300 feet (91 m). This distance includes all of the major ore bodies in the district. The dehydration of gypsum to anhydrite occurs at the relatively low temperature of 57-70 degrees centigrade, depending on the pressure (Holland and Malinin, 1979) thus it may

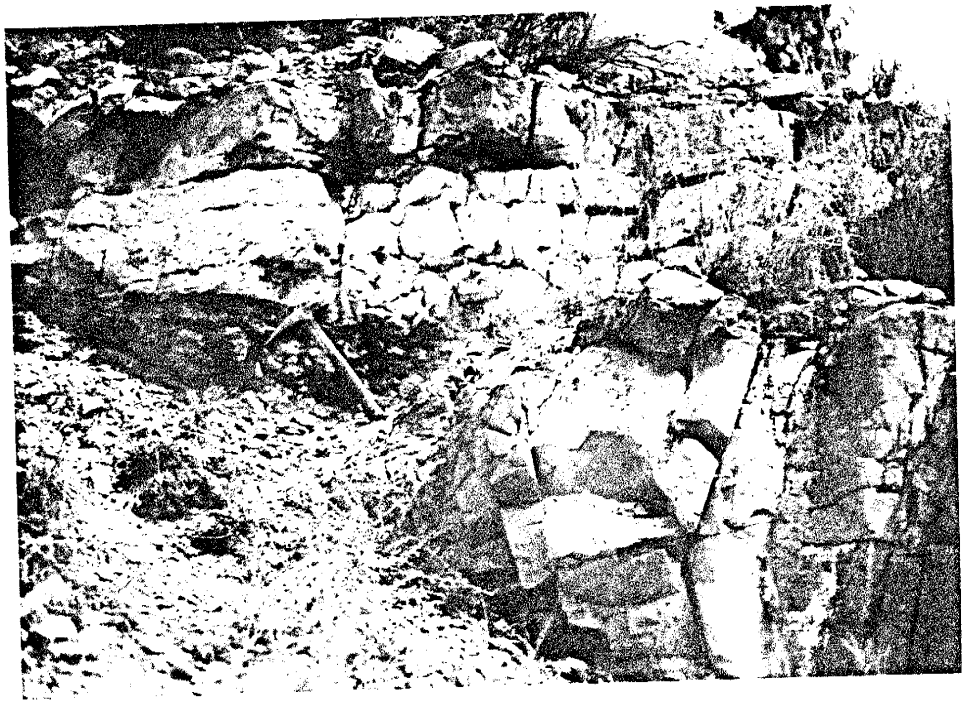

FIGURE 7: Outcrop of thin magnetite ore developed at contact of a pyroxene syenodiorite sill (bottom) intruding the San Andres dolomite. Hammer head is on contact of sill and the ore. Hammer is 13" in length. Note white marble in the dolomite and the unaltered character of the igneous rock.

be assumed that any gypsum present was dehydrated. This results in an increase in porosity of 38% (Schnake, 1977). The increase in porosity improved the permeability of these rocks to the mineralizing solutions.

Prexisting primary permeability in the sediments and at the contacts between units of differing lithology also played an important role in the localization of magnetite ore. This is exemplified by the high favorability of ore located in the crests and limbs of the anticlinal structures paralleling the Jones Camp dike. A well exposed cross section of the crest of a mineralized anticline is exposed in the section 24 pit (figure 8). This is also demonstrated by the common occurrence of ore bodies at steeply dipping sandstone-limestone and limestone-gypsum contacts.

At several different locations, outcrops of limestone hosted ore are found as inclusions in the pyroxene syenodiorite dikes. Only one such inclusion of ore (incompletely replaced sandstone) was found in the intensely altered margins of the Jones Camp dike. Most of the ore inclusions in the pyroxene syenodiorite, where exposed, have been excavated to some extent. In these exposures the igneous rock in contact with the ore is altered, which suggests that the inclusions were replaced in-situ. It is likely that significant amounts of unexposed ore inclusions exist in those areas where relatively wide pyroxene syenodiorite dikes intrude the margins of the Jones Camp

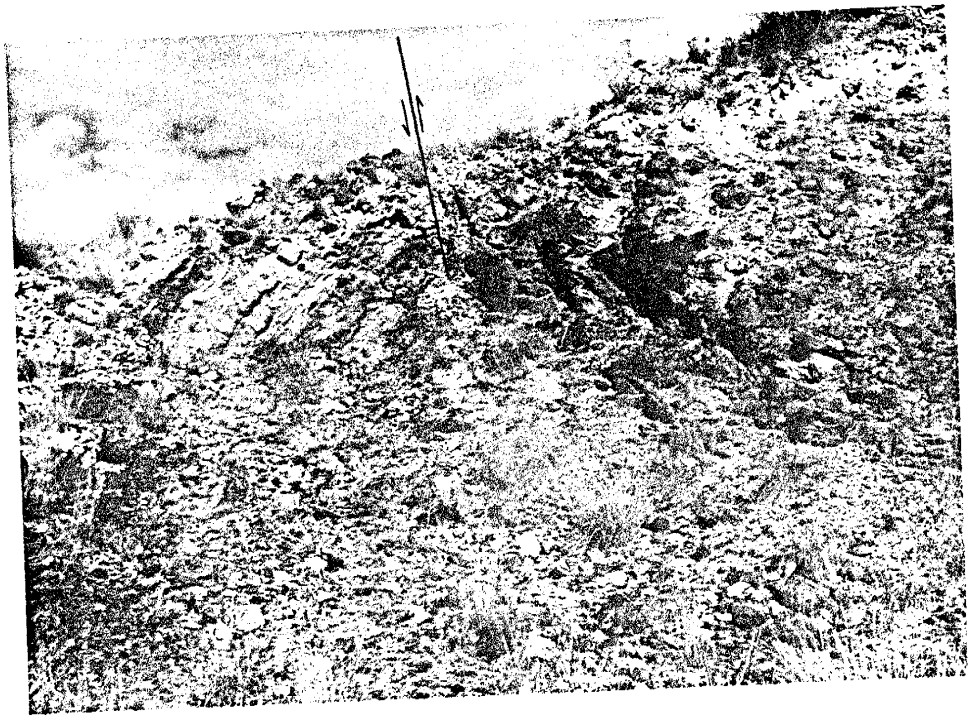

FIGURE 8: Outcrop of mineralized anticline exposed in the section 24 pit. Rock hammer is at the fold axis; Jones Camp dike is to the right. Note that axis of fold is faulted.

syenodiorite dike.

The subsurface extent of mineralization is not well known at this time. Favorable drilling locations have been identified by extensive magnetometer surveys of Bickford (1980), Jochems (masters thesis in progress), and work by the author. Two locations drilled in section 17 in 1979 did not intersect ore at a depth greater than 50 feet (15 m). No other drill hole data is available and the plans to begin a current drilling program are pending.

Despite the lack of drill hole data it is believed that significant tonnages of ore exist in the relatively shallow subsurface. Bickford (1980) estimated 1,117,940 tons of probable reserves and 1,575,630 tons of possible reserves based on an average ore horizon thickness of 6 feet (1.83 m) and a 75 foot (22.80 m) down-dip extent.

Ore Petrography

A petrographic anaylsis of 16 polished sections of ore from seven locations was made to determine the mineralogy and paragenesis of the ore and to see if any differences with respect to field occurrence or host rock existed. Descriptions of the individual samples, including textures and alteration, are found in appendix IV. These samples were collected at the same locations as samples collected for petrographic analysis of alteration mineralogy and

paragenesis. A description of the sample locations and aspects of the local geology is included at the end of appendix IV. Ore types examined included silicated and unsilicated gypsum and carbonate hosts, sandstone hosted ore and completely recrystallized-actinolitized Jones Camp dike rock.

Magnetite was found to be the only primary ore mineral present except for 0-15% pyrite associated with gypsum hosted ore. Minor copper sulfides and secondary copper carbonates were observed coating fractures in carbonate hosted ore in the West Pit and gypsum ore in the East Pit. Magnetite shows slightly different colored tints notably with respect to different stages in the paragenesis (e.g. magnetite phenocrysts vs. groundmass magnetite). This has been shown to reflect slightly different compositions, particularly with respect to high concentrations of unexsolved titanium which shows a light pink tint. However, in general this is not an unequivocal relationship and may not reflect any compositional differences (Ramdohr, 1980). Some zoning in some larger magnetite grains was observed. No twinning or exsolution textures were noted.

Maghemite is common in all the ore types examined petrographically. Maghemite is the metastable form of hematite with the structure of magnetite. As far as it is known, it only forms immediately adjacent to the surface of the earth (Ramdohr, 1980) and may occur in all intermediate

stages of oxidation of magnetite (Uyhenbogaardt, 1971). In the polished sections it is distinctly identifiable from magnetite in color and bireflectance. This is nicely displayed in some magnetite phenocrysts which are concentrically zoned with alternating zones of magnetite and maghemite (figure 9). The usual appearance of maghemite is as a patchy, incomplete replacement of magnetite with no preferred orientation. This is typical of maghemitization (Ramdohr, 1980).

The preferred alteration of magnetite to maghemite in certain zones in zoned crystals and in some magnetite which shows different colored tints, grain size or form may be due to different compositions. Maghemite appears to be more stable in magnetites high in unexsolved Ti and V and therefore may show preferential replacement of zones relatively enriched in these elements (Ramdohr, 1980).

Secondary hematite after magnetite (known as martite) was not found to be an abundant alteration product of magnetite. It typically occurs as a minor alteration of magnetite around grain edges or replacement controlled by crystallographic planes; however, it also occurs as psuedomorphs of magnetite phenocrysts in high grade ore (figure 10). Martite psuedomorphs of magnetite phenocrysts are relatively abundant at the Birthday Site and were confirmed by x-ray diffraction. Gibbons (1981) identified a greater abundance of martite in his samples and noted

FIGURE 9: Photomicrograph of limestone ore showing concentrically zoned magnetite phenocryst. Bluish grey zones are maghemite. Anhedral groundmass magnetite has slightly different tint. Section WP8A.

FIGURE 10: Photomicrograph of martite psuedomorphs of euhedral magnetite in limestone ore. Crystallographic control of alteration displayed in magnetite crystal in lower right corner. Section WPS-1 (Gibbons, 1981).

martite psuedomorphic after pyrite.

Pyrite is often associated with gypsum ore where it may be up to 15% of the rock (sample EP). It is euhedral or anhedral and occurs disseminated in a matrix of gypsum or anhydrite. Magnetite in gypsum ore is euhedral-subhedral and disseminated in a matrix of anhydrite or gypsum (figure 11). Gypsum ore that has been silicated then mineralized contains gangue of clinopyroxene and apatite. Clinopyroxene and gypsum or anhydrite may occur as inclusions in magnetite. In EP1, WP23, and WP26 pyrite may be seen partly replaced by magnetite particularly in zones where magnetite contacts pyrite when replacement has advanced to form a massive texture. Pyrite has also been observed to replace magnetite in some samples of Gibbons (1981).

Gangue in the limestone hosted ore includes primary or secondary carbonate and clinopyroxene or tremolite-actinolite in ore that has been subject to extensive metasomatism prior to mineralization. Clinopyroxene occurs as inclusions in magnetite in these samples. Gangue of earlier, higher temperature garnet, cordierite, and idocrase observed in thin sections of some altered carbonate was not recognized in polished section.

A layered texture of magnetite replacement is typical of the limestone hosted ore and is well displayed in less mineralized samples WP14A and WP14B and some thin sections. A bimodal grain size distribution of fine to medium-grained

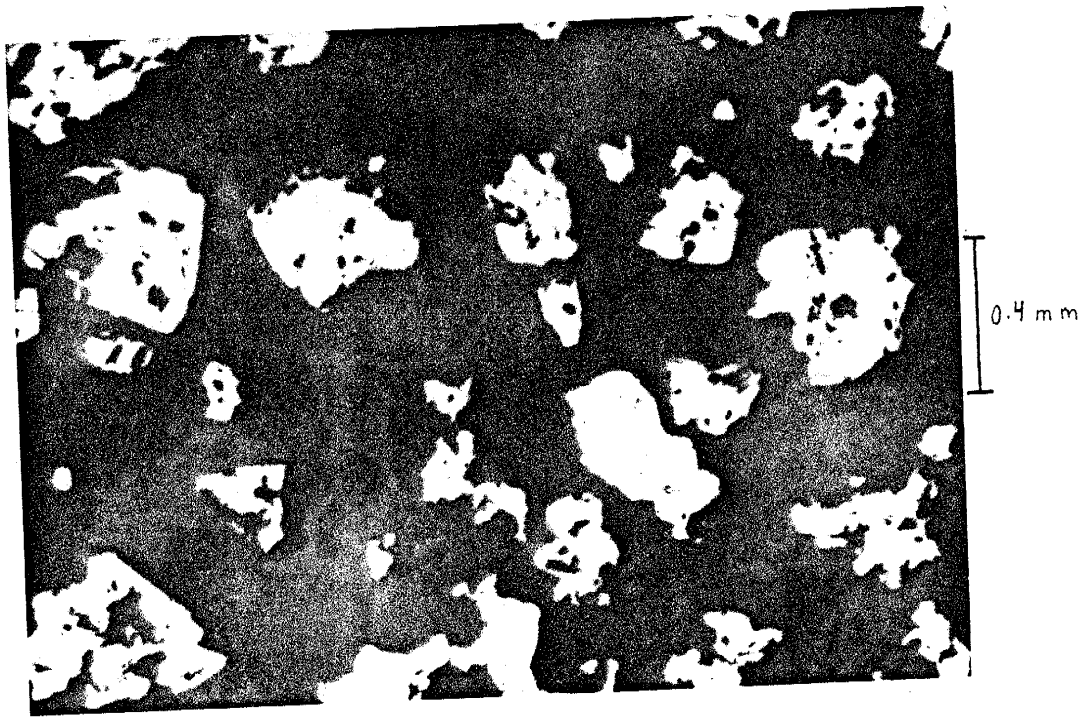

FIGURE 11: Photomicrograph of disseminated magnetite and pyrite (yellow tint) in gypsum ore. Gangue is clinopyroxene and gypsum. Section JCS 5 (Gibbons, 1981).

euhedral phenocrysts in a matrix of fine-grained (typically <0.5 mm diameter) groundmass magnetite is common. In high grade ore magnetite grain boundaries are typically indistinct describing a massive texture.

Gangue in sandstone ore includes detrital quartz and feldspar, carbonate, tremolite-actinolite, epidote, and clinopyroxene. Magnetite is anhedral or euhedral. It occurs as a replacement of detrital grains or of secondary carbonate and silicates.

Chemical Analysis of Ore

Extensive chemical analyses of Jones Camp ore were done by the U.S. Bureau of Mines (Grantham and Soule, 1947). This data is summarized by Kelly (1949, table 8). An average of these analysis yields the following percentages in weight percent: Fe 57.2, P 0.115, SiO_2 4.64, MnO 0.09, TiO_2 0.17, Al_2O_3 0.81, CaO 4.73, S 0.41 (Kelly, 1949, table 2). Trace element data for the Jones Camp ore was obtained by Gibbons (1981, table 4). Precious metals were not found in concentrations above the analytical uncertainty.

The wide range in the grade of ore is a function of the amount of gangue. Sulfur is the most deleterious element present and is highest in gypsum hosted ore where sulfur is present in pyrite, gypsum and anhydrite. Jones Camp ore does not contain excessive phosphorous or titanium.

Phosphorous is erratic in distribution (Kelley, 1949). Titanium is also erratic in distibution but an increase in titanium near igneous contacts and actinolite rock is noted (Kelly, 1949). A relationship between the highest titanium and vanadium concentrations was found by Gibbons (1981).

ALTERATION-MINERALIZATION OF SEDIMENTARY AND INTRUSIVE ROCKS

A determination of the alteration-mineralization paragenesis and textures of the various sedimentary and intrusive rocks in the Jones Camp district was accomplished by petrographic examination of 46 thin sections. Sample locations coincided with the areas in which ore was collected for polished sections and one of the two locations in which suitable samples were found for fluid inclusion analysis. These areas include the West Pit, East Pit, Roof site, Shaft site, "J" location, "B" location, and location B16. Petrographic descriptions of each thin section including textures and alteration paragenesis are contained in Appendix V. Descriptions of the sample locations and details of the local geology of these areas are found at the end of Appendix IV.

Jones Camp syenodiorite dike

The paragenesis of alteration of the Jones Camp dike was well demonstrated by a suite of ten thin sections from "J" location collected for this purpose. Complete exposure across the dike at this location allowed careful selection of samples to be as representative of the alteration as possible. The sequence of alteration is outlined in Figure 12. The paragenesis of secondary effects noted here was

Figure 12: Sequence of alteration in Jones Camp syenodiorite dike:

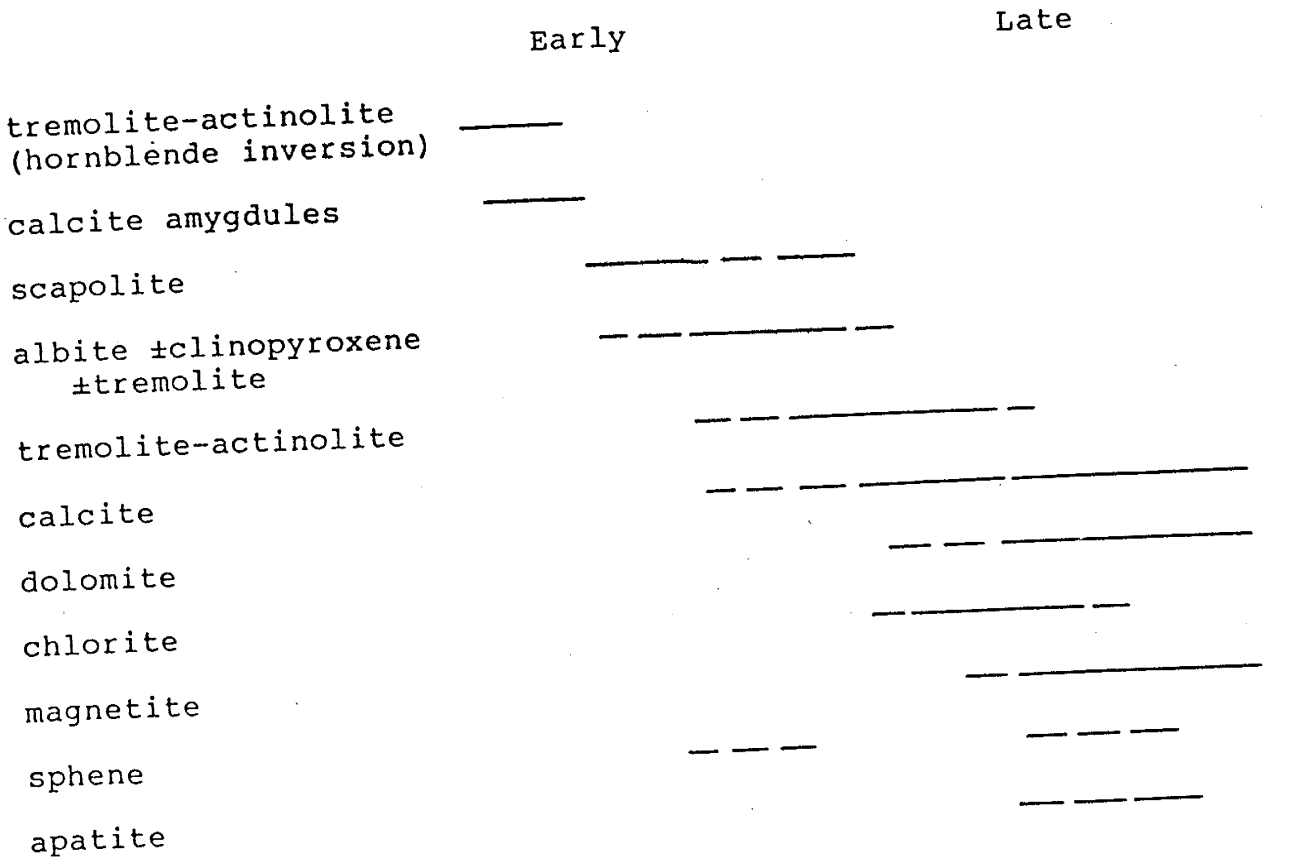

found to be consistently developed at other locations; however, some variations were noted at the Roof site where actinolitized Jones Camp syenodiorite is extensively mineralized.

As noted previously, the unaltered Jones Camp syenodiorite contains significant miarolitic cavities of variable size. Calcite filling miarolitic cavities and the inversion of primary hornblende to actinolite are recognized as the earliest hydrothermal alteration effects. This preceded pervasive recrystallization of primary mineralogy during subsequent scapolitization and albitization. Calcite occurs as fine-grained, equigranular mosaics in sharp contact with euhedral terminations of primary feldspar, hornblende, and clinopyroxene. Later, secondary scapolite may replace the calcite at the contact with primary minerals (Figure 13). The inversion of hornblende to actinolite is noted by a change to the pleochroism and extinction angle typical of the latter.

The occurrence of amygdaloidal calcite (which sometimes occurs as single crystals interstitial to primary feldspar) and scapolite after calcite and feldpsar were observed in J-12 and several of the thin sections of Jones Camp dike of Gibbons (1981). These rocks are otherwise unaltered and may be significantly removed from zones of intense hydrothermal alteration. This indicates a greater depth of penetration in the Jones Camp dike by the early secondary effects.

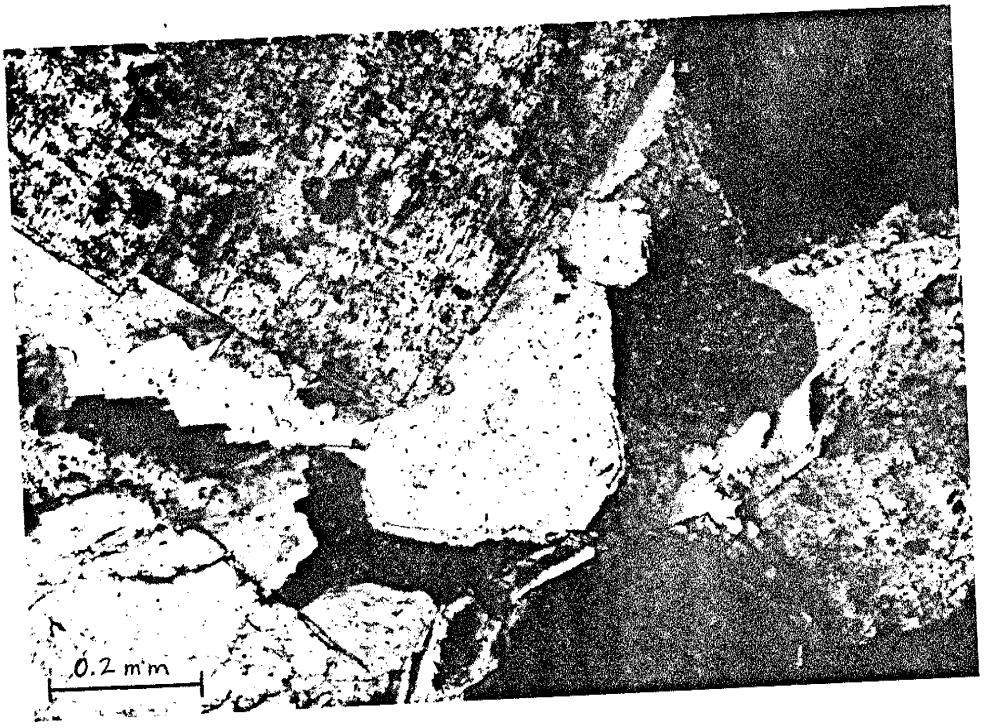

FIGURE 13: Photomicrograph of amygdaloidal calcite in Jones Camp dike. Scapolite replaces calcite at contact with euhedral primary alkali feldspar and clinopyroxene. X-nicols. Thin section J-10A.

Extensive scapolitization and albitization of the Jones Camp dike represents an intermediate stage in the alteration. Scapolite is anhedral or occasionally subhedral and indiscriminately replaces primary minerals. Zones of scapolite are commonly replaced by albite during albitization. The mottled texture seen in outcrop represents roughly concentric zones of scapolite occuring as remnants unreplaced during albitization. This texture is seen in Figure 14 of an outcrop of intensely altered dike.

Secondary plagioclase is fine-grained to microcrystalline and commonly shows a well-developed layered structure (defined by the alignment of plagioclase laths) in response to fluid migration during recrystallization. Plagioclase was determined to be of albitic composition using the Michel-Levy method. Nogueira (1971) confirmed the albitic composition of secondary plagioclase in the intensely altered Jones Camp dike from using refractive index oils and X-ray diffraction in addition to the Michel-Levy method.

Secondary clinopyroxene may accompany albite and occurs interstitial to albite laths. Interstitial tremolite blades also occur with secondary plagioclase at the Roof site. The tremolite in this occurrence also shows a parallel alignment.

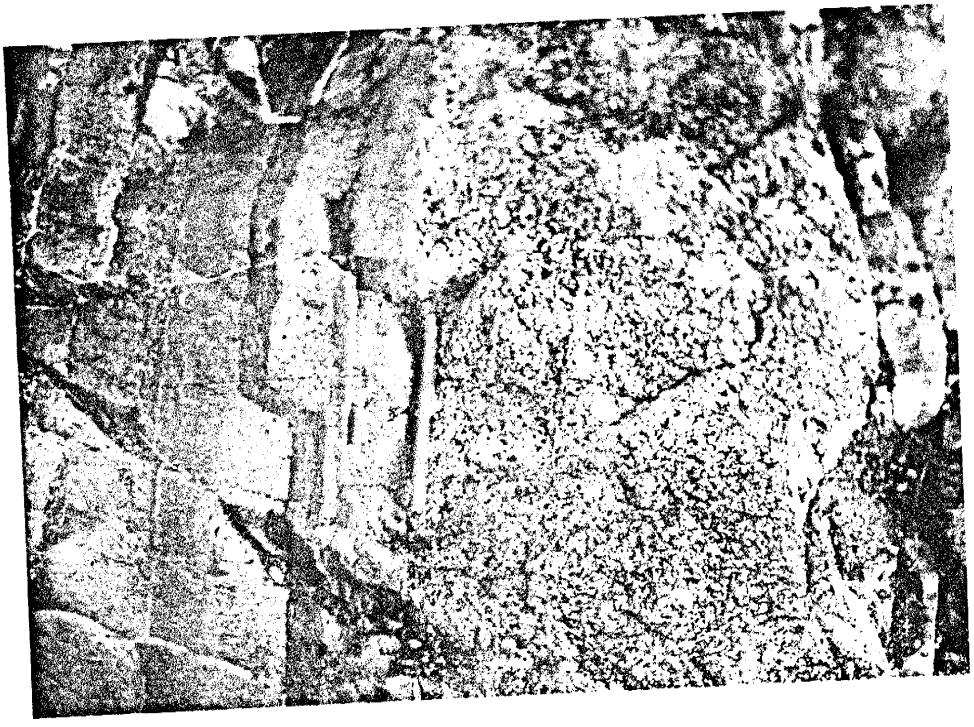

FIGURE 14: Outcrop of intensely altered Jones Camp dike showing mottled texture and layering in alteration which approximates attitude of prominent cooling joints. Pencil magnet is 5" in length.

The grain size of secondary plagioclase is variable and appears to be dependent on the extent of alteration. The contact between secondary albite of different grain size and/or zones of unalbitized rock is sharp. In addition, the concentration of concurrent clinopyroxene or tremolite ranges from zero to approximately 20% in different layers.

Some later scapolite, usually associated with calcite, is seen replacing previously albitized rock in the West Pit and "J" section (Figure 15). Scapolite forms a solid solution series between the end members mariolite $Na_4(Al_3Si_9O_{24})Cl$ and meionite $Ca_4(Al_6Si_6O_{24})CO_3$. Significant sulfate ions may also occur in the structure instead of chlorine or carbonate anions. The birefringence varies linearily with composition expressed as percent meoinite (Me) (Deer, et al., 1966). A relationship between the composition of scapolite with paragenesis is noted: the composition of scapolite after amygdaloidal calcite was determined to be approximately Me 50% or higher in Ca and CO_3 than later scapolite which ranged from approximately Me 20-45%.

Late secondary phases of the Jones Camp dike consist of pervasive fine-grained to microcrystalline tremolite-actinolite, chlorite, calcite or dolomite, magnetite, sphene, and apatite. Tremolite-actinolite and chlorite occur psuedomorphic after secondary albite and replacing interstitial clinopyroxene or as an alteration of

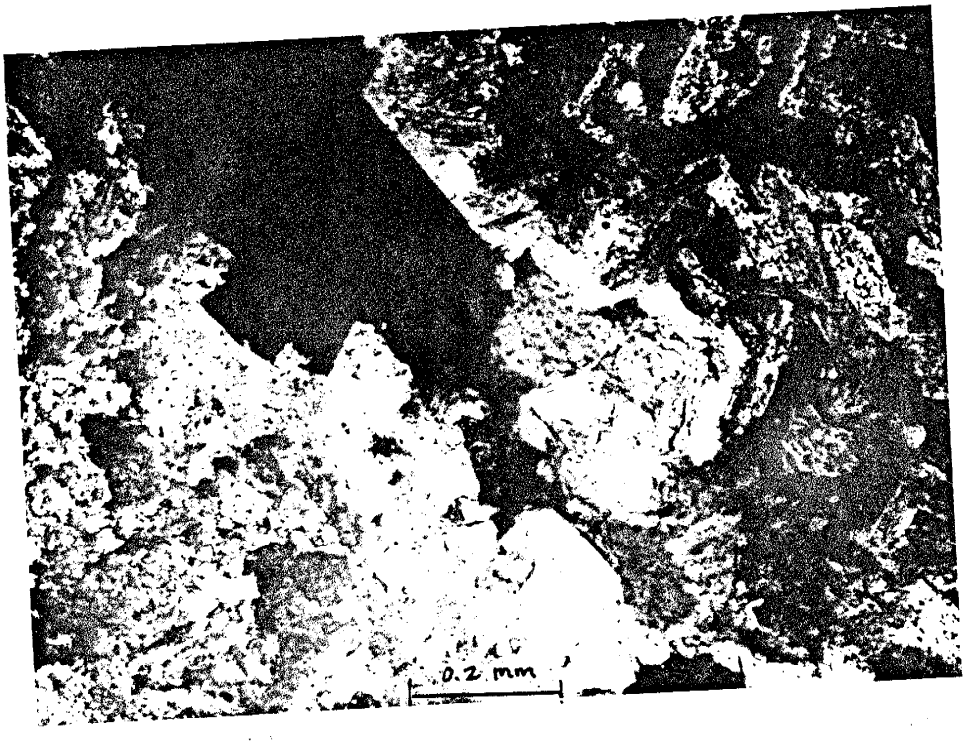

FIGURE 15: Photomicrograph showing sequence of alteration in intensely altered Jones Camp dike. Central zone of later calcite plus scapolite and magnetite crosscuts earlier scapolite (to the left) and albite (to the right). Secondary albite laths are 0.15 mm average length. X-nicols. Thin section J-10A.

scapolite, calcite mosaics, and remnants of primary mineralogy. Zones of scapolitization tend to be less affected by this late alteration. The relative concentrations of tremolite-actinolite and/or chlorite are variable as well as the extent of late alteration effects.

There is a tendency noted in some thin sections toward an increase in grain size of actinolite with continued alteration. Actinolite may occur as porphyroblasts or relatively coarse-grained aggregates exceeding the grain-size of secondary plagioclase. Some of the porphyroblasts occurring in intensely altered rock may be linked to tremolite resulting from inversion from hornblende.

With the exception of thin section RSA-3, samples from the Roof site showed the same sequence of alteration outlined in Figure 12. Late chlorite or carbonate are not abundant and significant secondary apatite associated with tremolite-actinolite and magnetite occurs in greater abundance here than at other localities. Extensive tremolite-actinolite is seen directly replacing primary feldspar not associated with albitization (Figure 16) in addition to rock subject to earlier albitization and scapolitization. Tremolite occurs as the principal gangue in the magnetite ore at this location. Thin section RSA-3 (from float) is a completely recrystallized sample in which plagioclase and actinolite are present in subequal amounts.

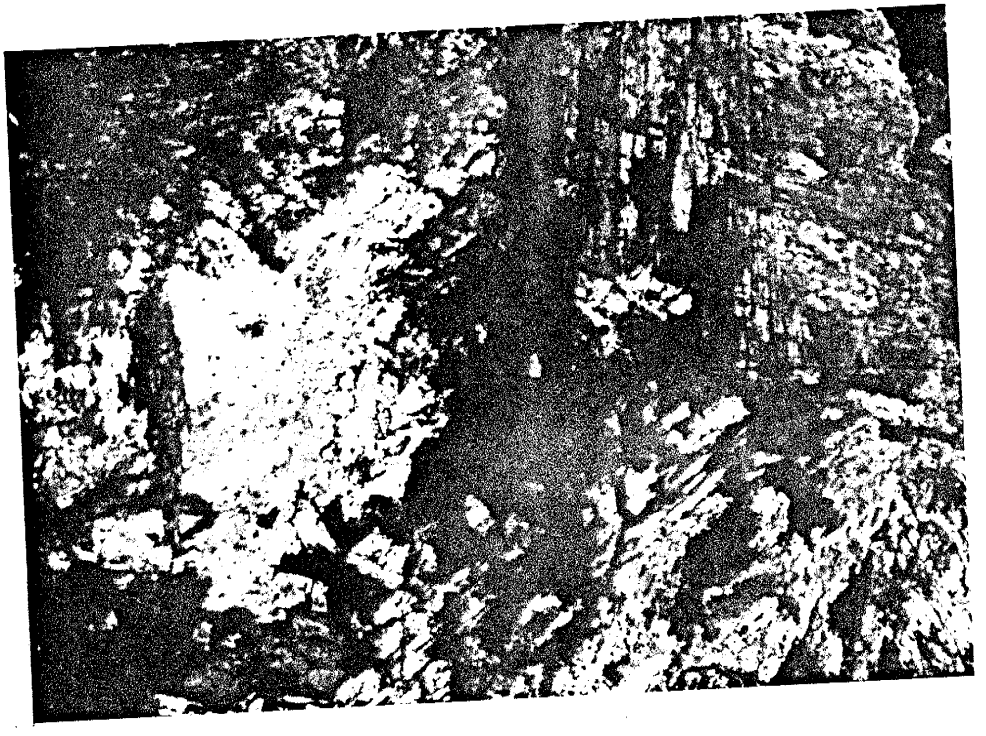

FIGURE 16: Scapolite (first order white to second order blue) and actinolite (top center) after scapolite and primary feldspar. Magnetite (center) replaces actinolite and scapolite. X-nicols. Thin section RSA-1.

(Figure 17). The occurrence of secondary plagioclase concurrent with actinolitization and subsequent mineralization was not noted at other locations. Medium to coarse-grained phenocrysts of euhedral plagioclase that appears to be vug filling is found in tremolitized ore at this location. These phenocrysts show inclusions of magnetite and tremolite.

Late calcite or dolomite occurs as equigranular mosaics in veins crosscutting earlier alteration or it may occur as an anhedral alteration of earlier secondary phases. These veins commonly host inclusions of magnetite, sphene, and tremolite-actinolite. In the field the margins of the Jones Camp dike have been flooded in places by secondary calcite where it occurs in a box-work configuration of veins up to 2 centimeters in width or as a matrix to brecciated (and altered) dike near the contact with the sediments (Figure 18).

Secondary magnetite in the Jones Camp dike is exclusively associated with the late stage alteration effects. Magnetite occurs in calcite veins or is disseminated and associated with tremolite-actinolite and chlorite alteration where it typically occurs in greater concentrations with chlorite. Magnetite is also seen replacing chlorite or tremolite-actinolite in addition to secondary albite, scapolite, or carbonate. Late magnetite in veins may be associated with sphene which is often seen

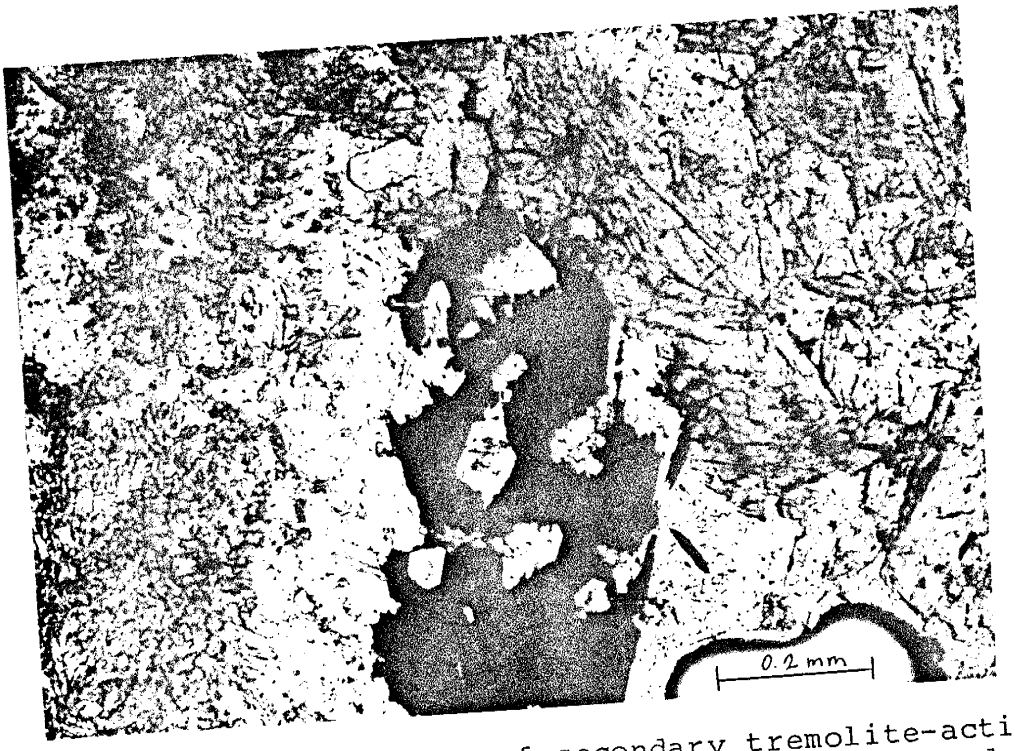

FIGURE 17: Photomicrograph of secondary tremolite-actinolite (green) and plagioclase plus later magnetite and apatite. Apatite crystal is left of center at top. Primary rock is Jones Camp dike. Plane light. Thin section RSA-3.

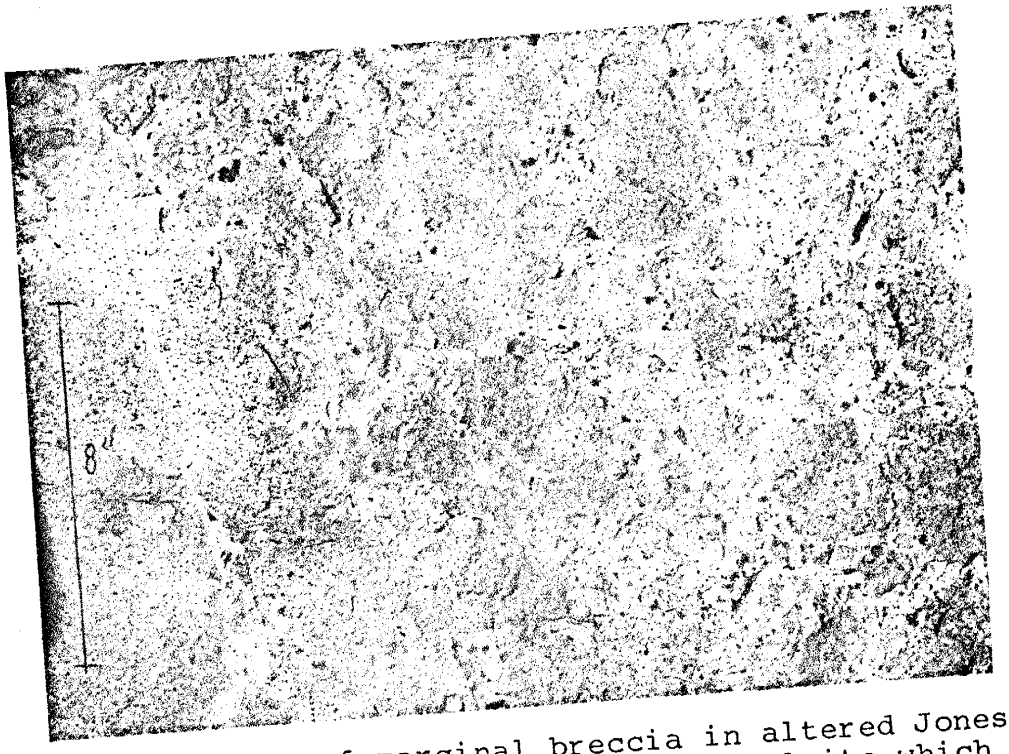

FIGURE 18: Outcrop of marginal breccia in altered Jones Camp dike. Matrix to clasts is predominantly calcite which hosts medium or coarse-grained magnetite grains.

replacing magnetite. Sphene also occurs replacing secondary albite. Late specular hematite is observed concentrated on some cooling joint surfaces in the field.

The depth of penetration of the late stage alteration in "J" location is less than earlier scapolitization and albitization. This trend is also observed in the section 18 samples of Gibbons (1981) with respect to scapolitization and amygdaloidal calcite which occur beyond the limit of extensive albitization, scapolitization, chlorite, tremolite-actinolite, and carbonate. The layered structure developed during hydrothermal alteration approximates the attitude of prominent cooling joints observed in unaltered dike which suggests the principal avenue for the ascending hydrothermal solutions was provided by these structures.

Major element chemical data for the Jones Camp dike of Gibbons (1981), plotted in Figure 4, includes both altered and unaltered samples. The accompanying thin sections for these chemical samples were rexamined by the author. Intensely altered samples are from the margins of the dike and include samples 1a, 1b, 2, 12, 13 all from the section 18 suite. Samples which include approximately 3-12% secondary scapolite, carbonate, tremolite (after hornblende), and minor albitization (where noted) include: 2, 3c, 3f (albite), 3h (albite) from section 24 and 3 (albite, no scapolite), 4, 5, 11 from section 18. The loss or gains in chemistry may be correlated with the secondary

mineralogy (see appendix III).

The decrease in total iron in the altered margins of the Jones Camp syenodiorite dike is significant in view of a model for the source of the iron in the magnetite deposits. The loss in iron is correlated to the destruction of primary ferromagnesian minerals and magnetite. High iron values in the unaltered Jones Camp syenodiorite are correlated with increased concentrations of ferromagnesian minerals and magnetite. These mafic rich rocks tend to occur marginally to the more felsic, mafic poor core zone. Intense alteration is concentrated along the margins of the Jones Camp dike; thus, the destruction of primary hornblende and magnetite during albitization and scapolitization must have enriched the hydrothermal solutions in iron from these minerals.

The loss of iron during the intermediate stages in the sequence of alteration of the Jones Camp syenodiorite is offset some by a gain of iron during the late stage of alteration. Iron rich phases actinolite, chlorite, and magnetite are included in the late secondary assemblages. Secondary actinolite and chlorite precede or overlap with magnetite mineralization in the sedimentary hosts and it is likely that the late stage of alteration in the Jones Camp dike is contemporaneous with mineralization in the district. The addition of significant CaO, MgO, and CO_2, as a result of replacement of carbonates, gypsum, and sandstones, may

account for a source of these elements in the extensive late carbonate in the altered dike.

Pyroxene syenodiorite dikes and sills

Hydrothermal alteration of the pyroxene syenodiorite dikes and sills includes: carbonate, chlorite, tremolite-actinolite, and magnetite. No scapolite, secondary albite, or amygdaloidal calcite was noted in thin section. Thin sections of altered pyroxene syenodiorite include RS4A, RS4B, and B16. Petrographic data from an additional 9 thin sections is found in Bickford (1980).

Anhedral calcite occurs as an alteration product of phenocrysts and groundmass feldspar and clinopyroxene. Microveinlets of calcite also occur cutting the groundmass and may show inclusions of tremolite, magnetite, or trace prismatic feldspar in thin section RS4B. Calcite filling relatively large fractures is noted in outcrop associated with areas of mineralization. These fractures also host fine or medium-grained crystals of magnetite.

Secondary magnetite also occurs as fine-grained disseminated rods or anhedral "blebs" which may show an interesting braided network in the former type (Figure 19). Secondary magnetite may be concentrated up to 15% (sample Db-2A Bickford, 1980). It occurs as an indiscriminate replacement of feldspar or clinopyroxene and may be

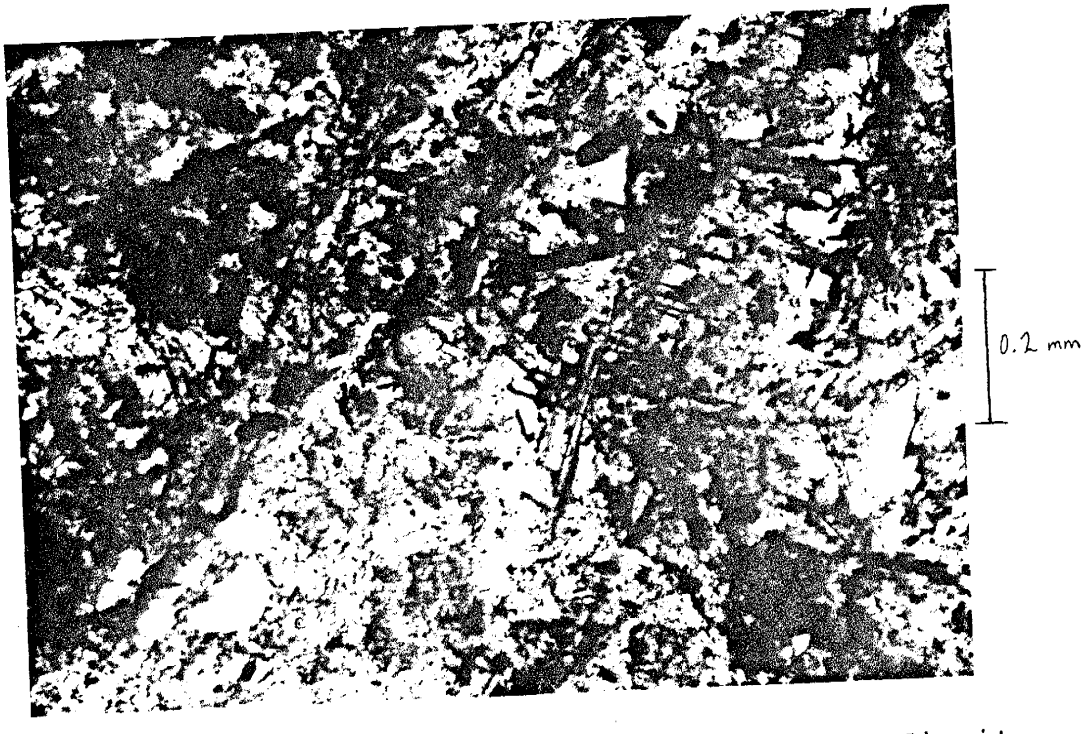

FIGURE 19: Photomicrograph of altered pyroxene syenodiorite. Plagioclase phenocryst in lower half. Secondary calcite is pink; chlorite and clinopyroxene are yellowish; magnetite is black. Note interesting braided pattern of secondary magnetite rods just right of center. X-nicols. Thin section B-16A.

associated with calcite.

Chlorite occurs as an alteration of feldspar phenocrysts or groundmass feldspar, clinopyroxene, and biotite. Tremolite occurs as fine-grained prismatic crystals replacing clinopyroxene or as fibrous masses of uralite after clinopyroxene (Bickford, 1980).

Carbonates

All the secondary mineral phases observed in carbonate hosted ore examined petrographically are believed to be metasomatic. Isochemical contact metamorphic phases were not identified in thin section (or outcrop) for the carbonate host. This observation is also true for the gypsum and sandstone in the district. The lack of a recognizable contact metamorphic aureole is probably principally due to: a) the occurrence of non-reactive sedimentary rocks i.e. non-siliceous, pure limestone and dolomitized limestone, gypsum, and clean sandstone; and b) extensive hydrothermal alteration obscuring contact metamorphic phases if present. Carbonate in contact with the Jones Camp dike or pyroxene syenodiorite dikes and sills has been recrystallized due to thermal metamorphism. It appears in outcrop as a white marble as seen in Figure 7 but no secondary phases are apparent in outcrop or thin section. A metamorphic texture in thin section is defined by well developed triple junctions in calcite and an increase in

grain size. Calcite grain boundaries may be straight or finely sutured (e.g. thin sections S-8, B7B).

Alteration-mineralization paragenesis in the carbonates falls into three general categories:

a) replacement of altered carbonate which includes higher temperature cordierite, garnet, idocrase (vesuvianite), spinel, and magnetite. This is exemplified by two suites of thin sections from the West Pit and section 24 pit;

b) mineralization preceded by extensive silicate metasomatism at locations in contact with the Jones Camp dike. Metasomatic phases include: clinopyroxene, tremolite-actinolite, feldspar, chlorite, and apatite. This is exemplified by samples from the Shaft site;

c) direct replacement of unaltered limestone, dolomite or dolomitized limestone by dissolution-precipitation. An example of this is thin section B16A of San Andres dolomite in contact with a pyroxene syenodiorite sill.

The upper two Torres member limestones of the Yeso Formation constitute the important carbonate units which host ore bodies in the Jones Camp district. The uppermost Torres member limestone, which marks the contact with the overlying Canas member, may be classified as micrite (Folk, 1969). This unit occurs in the West Pit and Section 24 pit.

Diagenetic effects determined petrographically include: a) aggrading neomorphism to microspar, and b) partial dolomitization. It is fossiliferous in part as noted in the field however no allochemical materials were observed in thin section.

Assemblages include: cordierite + garnet + magnetite + calcite; idocrase + calcite + magnetite; garnet + spinel + magnetite + calcite. Veins of late dolomite, lower temperature calcite, and magnetite concurrent with the main stage of mineralization also occur. Siderite was suspected as a secondary carbonate in thin sections WP14b, WP14C, WP1B, and others. These samples were checked for siderite by X-ray diffraction but none could be found. Garnet, idocrase, cordierite, spinel and higher temperature magnetite are locally abundant but do not exceed concentrations greater than approximately 25% of any thin section. Garnet and spinel are anhedral (amoeboid), fine-grained or occasionally medium-grained, and colorless or yellowish brown to orange. The garnet andradite was identified by X-ray diffaction (Nogueira, 1971). Spinel in thin section WP4 was identified as hercynite by C.T. Smith. Euhedral to suhedral cordierite and magnetite may occur as inclusions in garnet (Figure 20). Cordierite and idocrase are typically associated with secondary calcite after dolomite (Figure 21). These minerals are fine-grained, euhedral to subhedral, and are disseminated or occur in clusters. Idocrase may show anomalous blue birefringence.

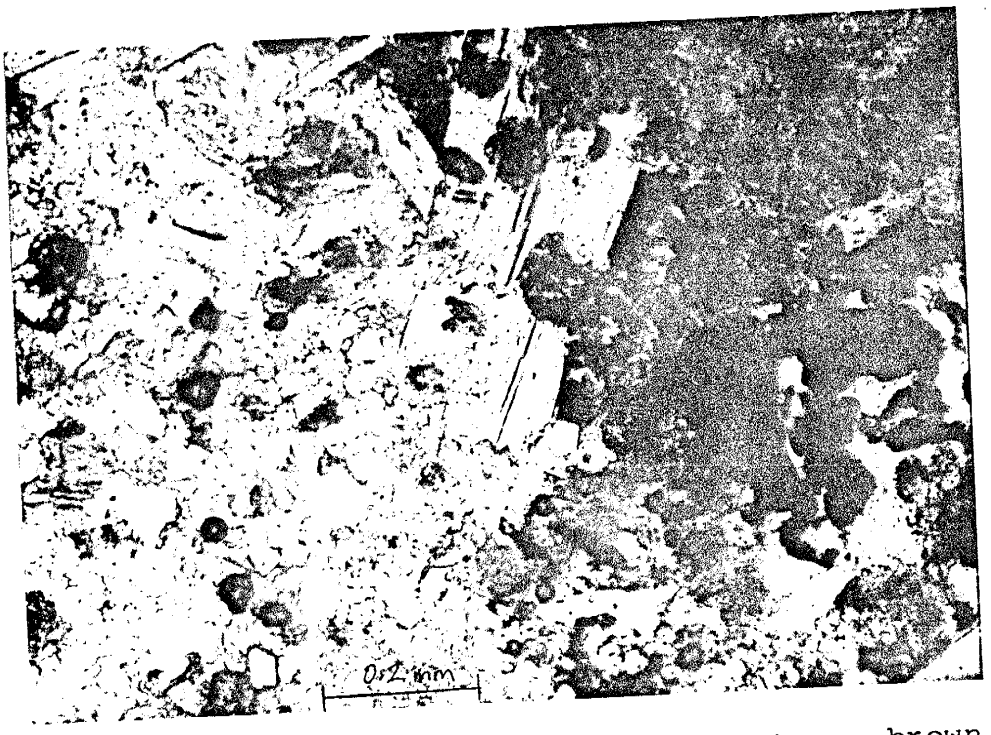

FIGURE 20: Photomicrograph of altered limestone: brown garnet showing inclusions of subhedral cordierite (colorless, top center) and higher temperature euhedral magnetite (black, right). Pink calcite replaces colorless, primary dolomite. Plane light. Thin section WP1B.

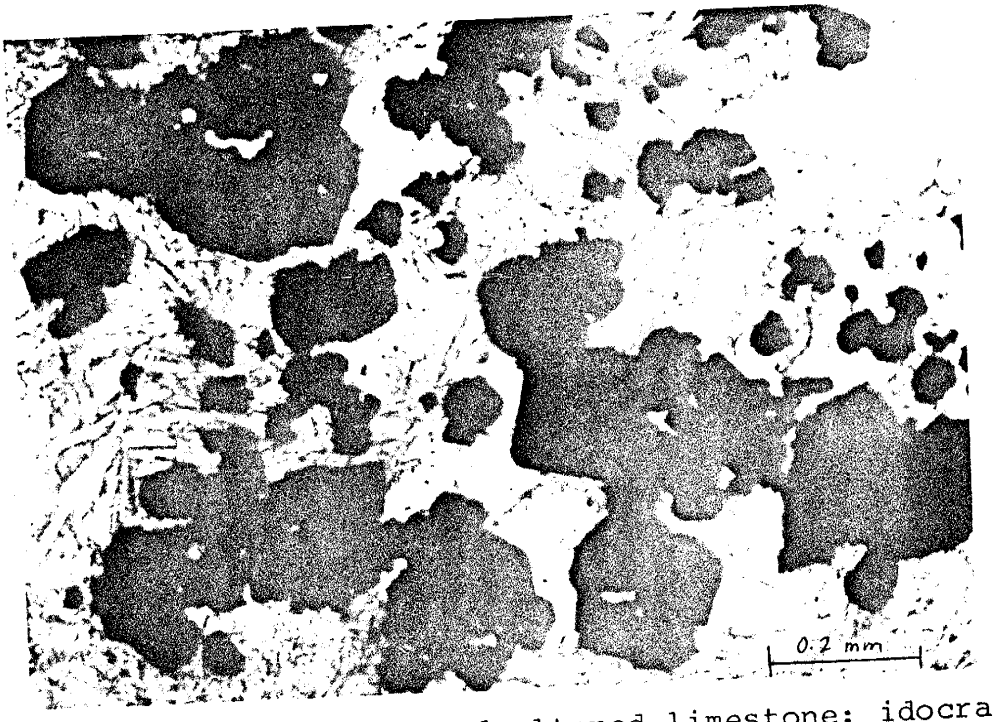

FIGURE 21: Photomicrograph of altered limestone: idocrase plus calcite after dolomite; subhedral magnetite replaces idocrase, calcite, and dolomite. Plane light. Thin section WP14C.

Cordierite also occurs replacing calcite as anhedral (ovoid) masses where it constitutes greater than 50% of the rock in thin section B7B. This form is common at lower temperature contact metamorphism (Deer, et al., 1966). Magnetite concurrent with the main stage of mineralization is late and replaces calcite or dolomite and earlier secondary phases. It is typically subhedral and grain size is variably microcrystalline to medium-grained. Recrystallized calcite concurrent with alteration-mineralization replaces dolomite. Late dolomite usually forms mosaics but is less common.

Development of a layered structure of secondary phases including magnetite is common. This layering coincides with bedding as measured in the field. Magnetite shows an increase in grain size with continued replacement and forms into aggregates parallel to layering. Some veins of dolomite are occasionally observed to crosscut this fabric.

The thinner limestone stratigraphically below the upper Torres member limestone is the host at the Shaft site. A 36 foot deep vertical shaft is sunk at the contact of the dike with the sediments. Two thin ore bodies occur near the surface at the shaft. Dips are away from the dike (to the north) at about 30 degrees. The interbedded limestone is intensely metasomatized and partly mineralized. Below this the degree of silicate metasomatism decreases and no ore is found.

The sequence of alteration at the Shaft site is outlined in Figure 22. Early clinopyroxene is seen in a radial arrangement centered at triple junctions in the calcite. Grain size increases to about 0.3 mm. Secondary tremolite occurs concomitant with replacement of the calcite by dolomite. A sieve texture of dolomite and inclusions of tremolite are common. Later feldspar is approximately euhedral and shows a sieve texture with clinopyroxene and tremolite inclusions.

Late chlorite, magnetite, and apatite replace earlier phases (Figure 23). Magnetite is also seen replacing chlorite. Intensely altered Jones Camp dike at the contact with the ore shows the typical sequence of alteration outlined previously. Late chlorite, carbonate, and magnetite are particularly well developed.

Mineralized San Andres dolomite was collected in association with a pyroxene syenodiorite sill. The dolomite is microspar. The contact between the mineralized and unmineralized rock is sharp. Calcite replaces the dolomite which is subsequently replaced by magnetite. Some dissolution vugs are developed which may be lined by calcite or magnetite. Abundant primary porosity developed in the dolomite was probably significant for the mineralization.

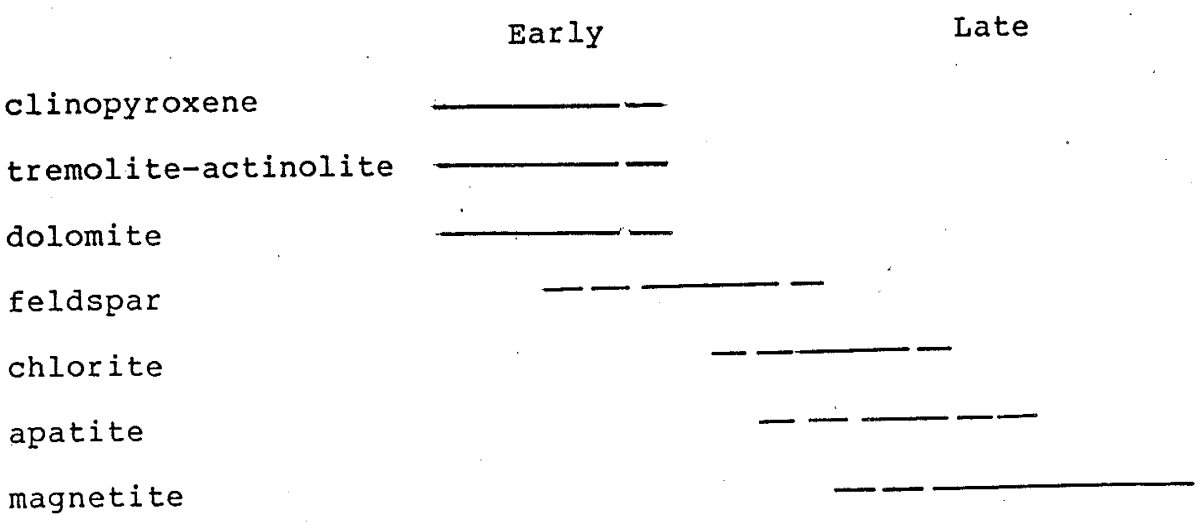

Figure 22: Sequence of alteration in silicated-mineralized limestone at Shaft site. Pure limestone was recrystallized during thermal metamorphism prior to metasomatism.

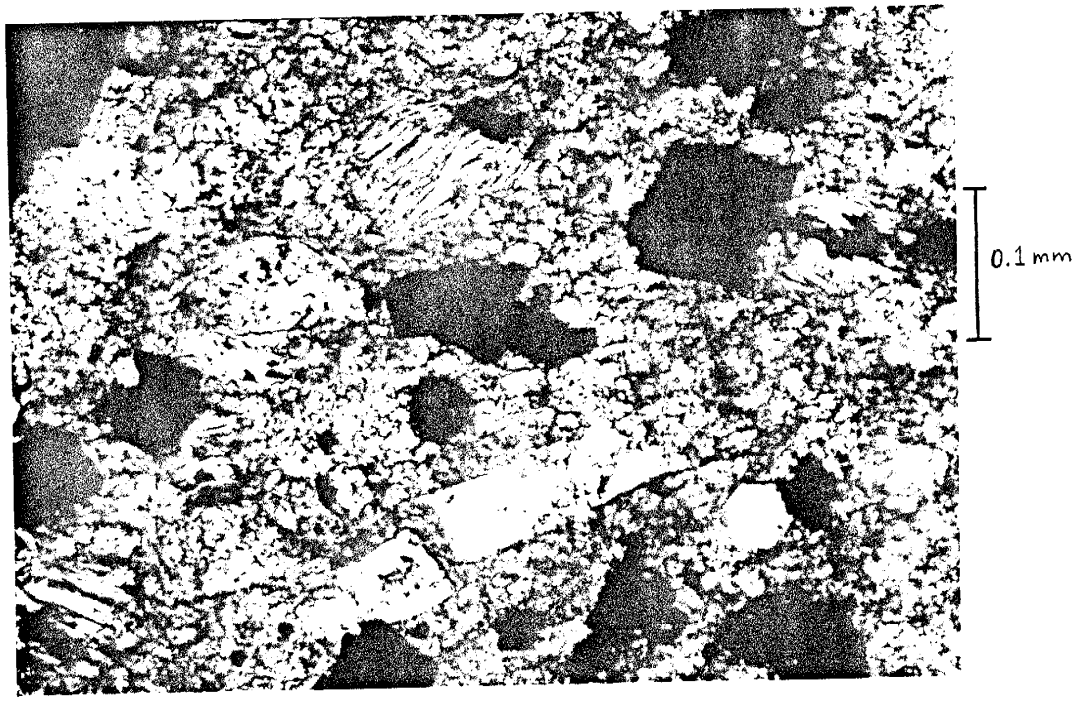

FIGURE 23: Photomicrograph of extensively metasomatized limestone. Early clinopyroxene after calcite. Later apatite (colorless, euhedral), chlorite, and magnetite. Some magnetite replaces chlorite. Plane light. Thin section S-3.

Gypsum

Gypsum beds in mineralized areas must have undergone dehydration to anhydrite as the upper stability limit of gypsum is 57 degrees. The paragenesis of gypsum ore is described by three parallel occurrences:

a) direct replacement of anhydrite by magnetite and minor pyrite.

b) replacement of anhydrite by magnetite and/or pyrite. However, anhydrite is reprecipitated as fibrous green colored variety during replacement.

c) mineralization is preceded by metasomatism and development of clinopyroxene.

Thin section EP (from the East Pit) is an example of the latter paragenesis. The rock consists of approximately 40% porphyroblasts of aegirine-augite and lesser augite in a matrix of microcrystalline gypsum; approximately 2% zones of anhedral quartz; and fine-grained, euhedral apatite. Pyrite occurs as psuedomorphs of clinopyroxene crystals or as a replacement of the matrix (Figure 24). Magnetite is seen is hand specimen as a matrix to some zones of pyrite. Gypsum is amorphous or has a fibrous habit and shows anamolous extinction and first order gray birefringence. The gypsum has probably been rehydrated at some later time. It is green colored in hand specimen.

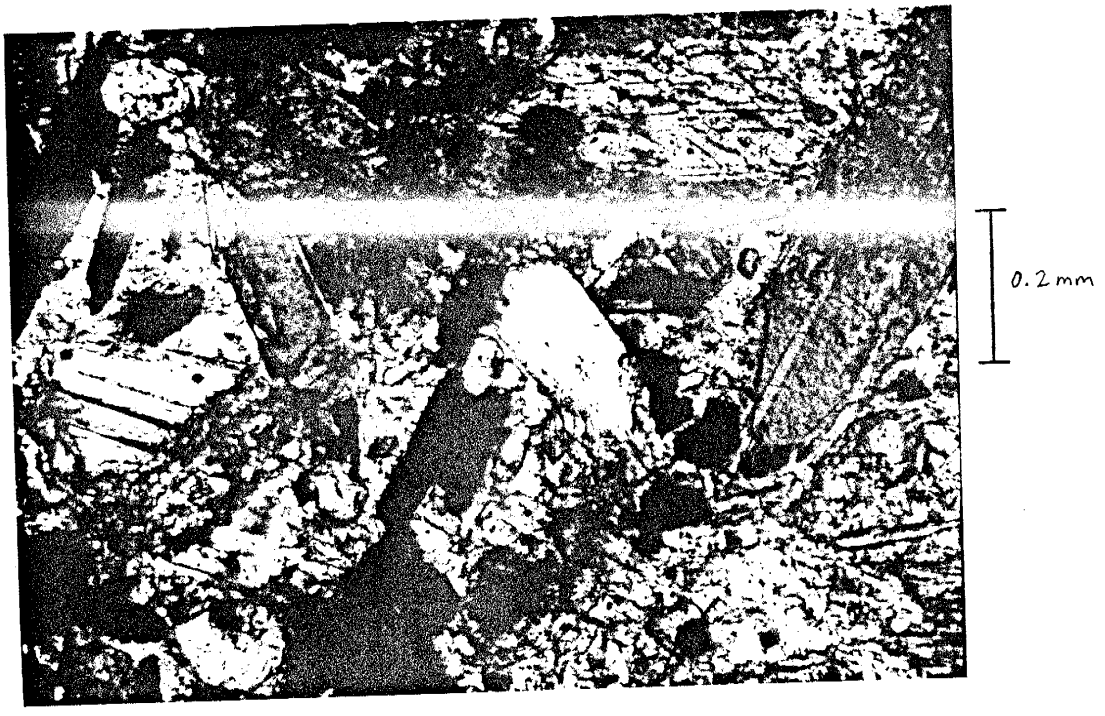

FIGURE 24: Photomicrograph of extensively metasomatized gypsum bed. Euhedral clinopyroxene is aegirine-augite, note some is twinned. Matrix is gypsum. Later apatite (colorless, in center) and magnetite psuedomorphic after clinopyroxene. X-nicols. Thin section EP.

Sandstone

As is the case with carbonate or gypsum hosted ore, sandstone may be mineralized by direct replacement of the primary mineralogy of the rock or preceeded by significant metasomatism and development of higher temperature secondary silicates or oxides which are later replaced by magnetite. Two thin sections of mineralized arkose at "J" location demonstrate this. In thin section J-1C calcite has replaced up to 20% of the rock with subsequent epidote after calcite. These zones are favored by magnetite replacement (Figure 25). Thin section J-2B shows magnetite as a direct replacement of detrital grains and cement. Secondary tremolite-actinolite, clinopyroxene, sphene, and apatite in addition to carbonate have also been identified in thin sections of altered sandstones in the Jones Camp district (Bickford, 1980). In the field some sandstone was observed to be completely actinolitized and subsequently mineralized.

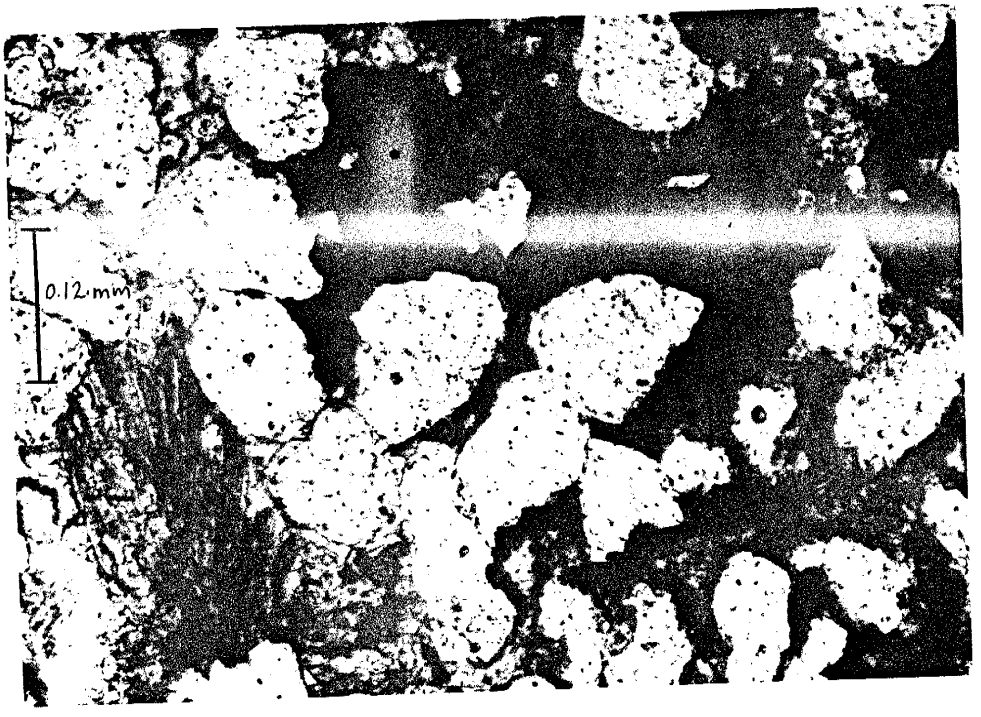

FIGURE 25: Photomicrograph of mineralized sandstone. Calcite is stained pink and replaces detrital quartz and feldpsar (colorless); epidote in lower left-hand corner, replaces calcite; magnetite is late and replaces calcite; detrital grains and epidote. Plane light. Thin section J-1C.

FLUID INCLUSION MICROTHERMOMETRY

Recognition of fluid inclusions as samples of ore forming fluids provides a means of direct estimation of the physical and chemical environment during ore deposition. Fluid inclusions also may be useful as geobarometers (Roedder, 1984). Calcite cogenetic with magnetite and pyrite associated with limestone ore was found to be the only suitable mineral which hosted measurable fluid inclusions in the Jones Camp district. Heating and freezing data were obtained from 11 polished sections from samples collected at two localities along the Jones Camp dike: the West Pit and a small pit in section 17.

Two sample types were found to contain numerous fluid inclusions. The first type is relatively common in areas of mineralization of limestone. The host rock is a slightly mineralized, tan-colored limestone which grades into high grade ore. The rock contains fine to medium-grained, equigranular calcite in zones up to 3 cm in width. The average grain size of calcite is one millimeter diameter. Fine-grained magnetite is concentrated at the interface between the coarse calcite and microcrystalline calcite of the groundmass. Lesser magnetite occurs disseminated. These samples are referred to as WPf and are from the West Pit.

The second sample type consists of coarse-grained calcite associated with fractures developed in limestone. Samples of this type were found in float at both locations sampled. This type is not considered common and could not be located in outcrop (or float) at other favorable locations in the district. The calcite is coarse-grained (up to 3.5 cm in diameter), white to translucent and rounded. At the West Pit coarse euhedral gypsum occurs as a matrix to the calcite crystals or as a cement to the angular limestone fragments. The limestone is typical of the upper Torres member and is dark grey and microcrystalline. Magnetite is concentrated at the contact between calcite crystals or calcite and gypsum. Pyrite is concentrated at the contact between gypsum and calcite. Minor magnetite also occurs widely disseminated in individual calcite or gypsum crystals. These samples are referred to as WPc. The calcite in the section 17 pit is similar to the above but did not contain gypsum or pyrite. These samples are referred to as S-17. The calcite and gypsum in these samples are probably related to open-space filling or replacement of clasts in fractures or faults in limestone.

Fluid Inclusion Types

Primary and secondary inclusions were recognized in the samples. Two types of primary inclusions occur: type A are two phase: liquid-vapor; and type B are three phase:

liquid-vapor-daughter crystals. Daughter crystals in type B inclusions were recognized as predominately anhydrite on the basis of crystal habit and anisotropic character. Lesser isotropic, cubic daughter crystals believed to be halite were observed in approximately 20% of the fluid inclusions. Figure 26 is a photomicrograph of two type B inclusions showing anyhdrite daughter crystals. Figure 27 is a photomicrograph showing the uncommon occurrence of both halite and anhydrite in a single primary inclusion. Occasionally inclusions containing two daughter crystals of anhydrite were observed.

Relatively minor, late secondary inclusions concentrated on cleavages or fracture planes are present in most of the samples measured. These inclusions are one or two phase and generally smaller than primary inclusions (average diameter less than 5 microns); they homogenized at considerably lower temperatures. Inclusions that have been modified by necking and partial decrepitation were also recognized. These modifications occurred at some time following phase changes upon cooling from the temperature of trapping which precluded their measurement for determining valid temperatures of homogenization and salinities. Criteria (after Roedder, 1984) to distinguish useful primary inclusions included: 1) separation of the inclusion from another inclusion by at least five times the distance of the diameter of the inclusion; 2) random occurrence in three dimensions in the host crystal; 3) large size relative to

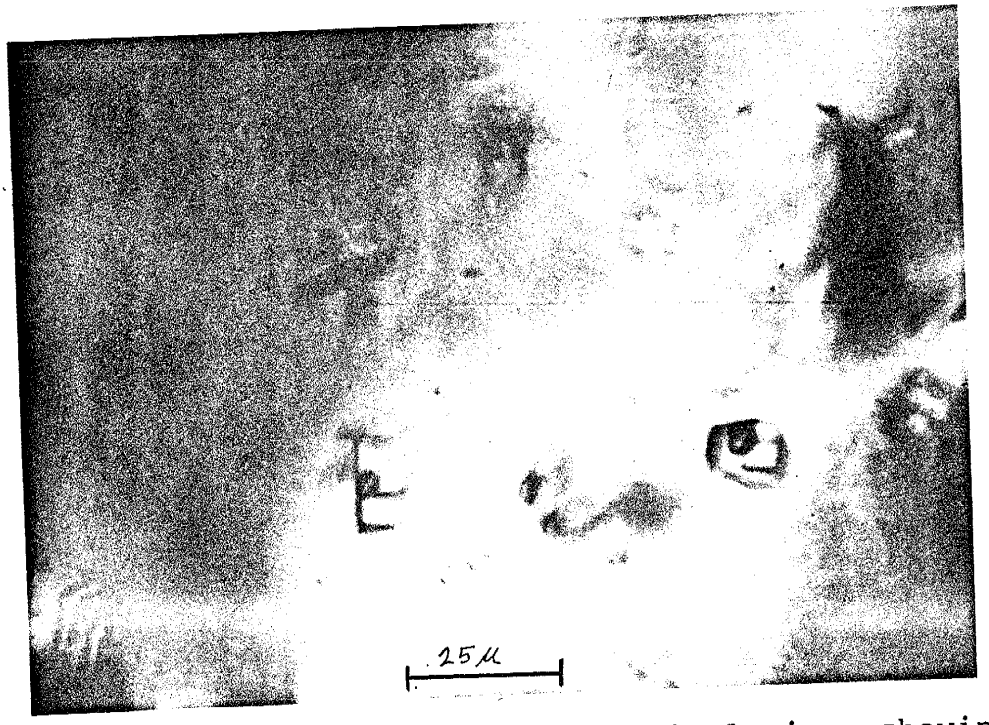

FIGURE 26: Photomicrograph of 2 type B inclusions showing daughter crystals of anhydrite.

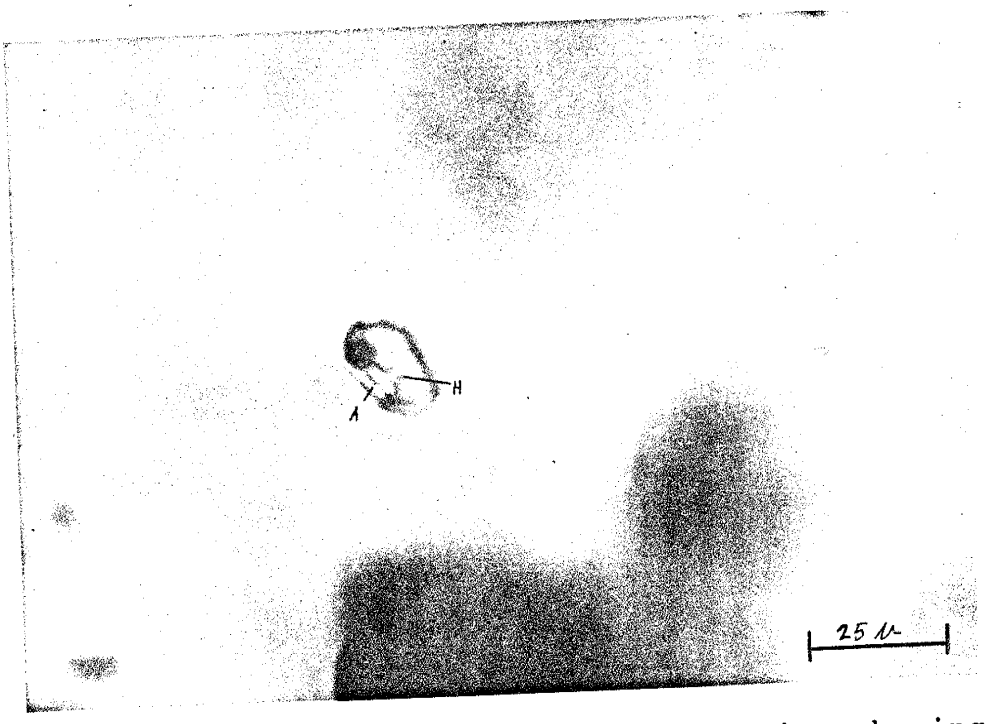

FIGURE 27: Photomicrograph of a type B inclusion showing daughter crystals of halite and anhydrite. Black solid is magnetite.

the host crystal (inclusions smaller than approximately 10-15 microns were not measured); 4) approximately constant volume ratio of phases; 5) inclusions with regular shape or negative crystal habit.

Partial decrepitation and stretching are related phenomena that result from adjustments in a fluid inclusion to internal pressures that may exceed the strength of the crystal (Roedder, 1984). In the process of stretching, the pressure is reduced by an increase in inclusion volume as opposed to partial decrepitation, where the pressure reduction is achieved by cracking of the walls of the inclusion allowing leakage of some of the fluid. These fractures are subsequently rehealed. Complete decrepitation occurs if this crack propagates to the edge of the crystal (or perhaps intersecting a pronounced cleavage). These effects can be caused by overheating in the laboratory or in nature. The susceptibility of fluid inclusions to stretching and decrepitation varies within a given sample and is greatest in large inclusions having steep isochores (i.e. low temperatures of homogenization) in soft, cleavable minerals such as calcite or fluorite. Decrepitation may also be the result from exposure to lower external pressures (Roedder, 1984).

Inclusions that resulted from partial decrepitation-rehealing were recognized on the basis of lower liquid to vapor ratios than unmodified, primary inclusions.

This was initially believed to be evidence for boiling in the system, however, this was determined not to be the case based on the following observations:
1) evidence for leakage by the occurrence of thin fractures emanating from the inclusion. These fractures are more obvious in nearly vapor filled inclusions. An example of this is seen in the lower inclusion in figure 28;
2) an association of these inclusions with completely decrepitated inclusions. The highest concentration of decrepitated and partially decrepitated inclusions occurred in the cores of the coarse-grained calcite (samples WPc and S-17); 3) frequent evidence for necking off (Figure 28); 4) highly variable liquid-vapor-daughter crystal size ratios. This indicates different degrees of partial decrepitation. In some cases differences may be principally due to necking down or a combination of necking down and partial decrepitation; 5) these inclusions typically decrepitated on heating or yielded spurious, non-reproducible temperatures of homogenization.

In addition to the above observations, a consideration of the confining pressure during formation of the inclusions indicates pressures that far exceeded the pressure required to inhibit boiling at the temperatures of trapping.

FIGURE 28: Photomicrograph of two partially decrepitated inclusions which may have necked-off prior to decrepitation.

Analytical Methods

Fluid inclusion sections were doubly polished to an average thickness of approximately 0.65 mm. A LinKam TH 600 stage and heating unit were used for heating and freezing measurements. A high quality Zeiss binocular microscope was used for optical determinations. Heating rates of 10-20 degrees per minute were used below 100 degrees centigrade but were slowed to approximately 0.5 degrees per minute in the range of homogenization. Typically one to four inclusions were measured simultaneously. The inclusion stage was calibrated; temperature corrections were found to be negligible.

Inclusions were often checked for decrepitation by allowing the inclusions to cool down from the temperature of homogenization to allow reversal of phase changes. Inclusions were found to be susceptible to stretching as a result of both freezing and heating. This effect is demonstrated by a higher temperature of homogenization on second heating (Roedder, 1984). The increase in temperature of homogenization ranged from a few degrees to 33 degrees centigrade. Stretching due to freezing was found to be more significant than due to heating therefore heating measurements were done before freezing. Because of the problems due to stretching in the laboratory no sample chip was measured for more than one grouping of inclusions.

Heating and Freezing Results

Figure 29 is a histogram of the homogenization temperatures for type A and type B primary inclusions. Temperatures of homogenization (Th) ranged from approximately 120 to 180 degrees centigrade. The average Th for the inclusions is 144 degrees centigrade. No difference in temperatures of homogenization between type A and type B inclusions was found. Both types homogenized to liquid: Th for type A inclusions was determined by the disapearance of the vapor bubble; Th for type B inclusions was determined by dissolution of daughter crystals (which followed homogenization of the vapor bubble). As previously noted, the system was determined to be non-boiling.

The presence of two immiscible liquids was noted in less than 10% of the inclusions included in figure 29. This observation was common on heating in type B inclusions, typically occurring between 50 to 100 degrees centigrade. Immiscible liquids at room temperature were occasionally observed in type A inclusions. The liquids did not become miscible at higher temperatures.

Observations of the temperature of final melting (Tm), temperatures of first melting (Te -eutectic temperature), and phase changes with regard to the formation and melting of salt-hydrate phases are used to estimate the salinity (or total dissolved salts) and in identifying the major species

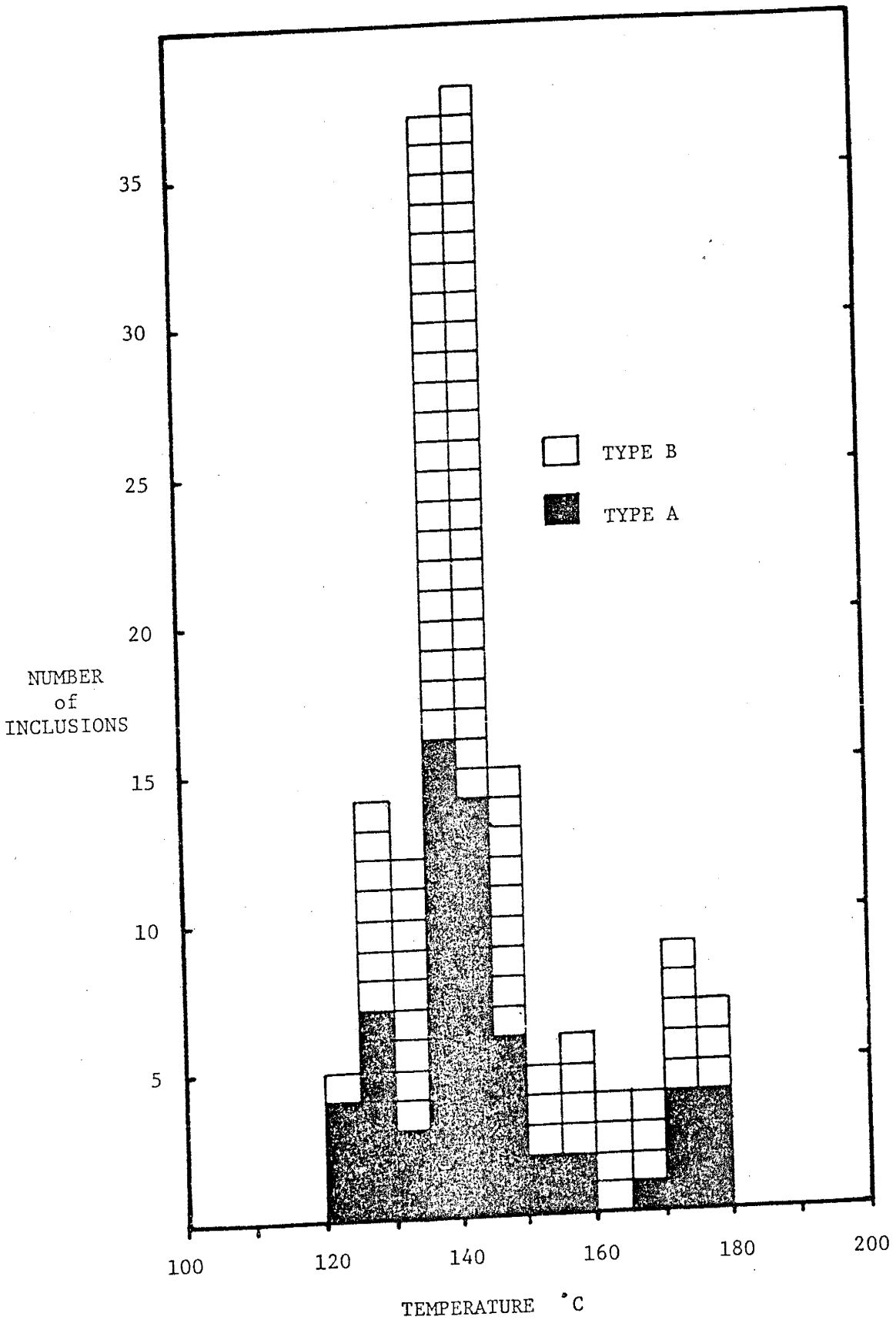

FIGURE 29: Histogram of fluid inclusion temperatures of homogenization.

in solution (Crawford, 1981). The freezing data for the samples is presented in table 2. Extreme difficulty was encountered in getting the inclusions to freeze despite holding the inclusions at temperatures as low as -120 C for up to 15 minutes. This was particularly true for type A inclusions and both types in samples WPf and S-17. This phenomenon is common in fluids with strong brines and at fast cooling rates (Roedder, 1984).

The Te for type B inclusions in WPc samples were typically -44.0 degrees centigrade and the Tm of a salt-hydrate phase at -33 to -31 degrees centigrade Type B inclusions for Wpf samples had a Te of -33 or -26 degrees centigrade. In these samples a salt-hydrate phase persisted to temperatures ranging from +11 to +20 degrees centigrade. If the last phase to melt is a salt-hydrate (and not ice) this indicates that the brine has a higher salt content than the eutectic composition (Crawford, 1981).

The specific behavior of multicomponent inclusion fluids on freezing-melting (such as temperature and amount of eutectic melting, and the nature of the various hydrate phases) cannot be fully understood without experimental data on closely matching compositions (Roedder, 1984). The presence of large anhydrite daughter crystals indicates solutions high in calcium and sulfate presumably due to the dissolution of the Permian gypsum beds. The lack of experimental data in the literature on systems high in these

Table 2: Fluid inclusion freezing data. Temperatures in degrees centigrade.

Type B inclusions:

Sample	Th	Tfm	Tm
WPc	140	--	-33
WPc	148	--	-33
WPc	141	-32	-12
WPc	158	-47	-34
WPc	137	-44	-34
WPc	136	-44	-32
WPc	127	-43	-33
WPc	141	-44	-32
WPc	132	-44	-33
WPc	133	-44	-32
WPf	149	--	-45
WPf	165	--	+20
WPf	176	-26	+11
WPf	165	-33	+18
WPf	130	-33	+19
WPf	132	-34	+20

Type A inclusions:

Sample	Th	Tfm	Tm
WPc	134	--	-45
WPc	144	-32	-5
WPc	138	-27	-20
S-17	142	-57	-28 ?
S-17	144	-63	-30
S-17	166	--	-11
S-17	138	--	-31

constituents and the unusual phase changes observed on freezing-melting limits the interpretation of the salinity of the fluid inclusions studied. Since most naturally occurring hydrothermal solutions are Na-K-Ca-Mg chloride brines, these systems have been studied in greater detail and has led to the convention of reporting salinities in terms of NaCl equivalents (i.e. the observed freezing point depression is used to calculate the amount of NaCl which would produce a similar lowering). In this system, hydrohalite ($NaCl \cdot 2H_2O$) is the last phase to melt if the concentration of NaCl is above the eutectic composition and has a greater concentration than other dissolved chloride species. The melting should occur in the pure $NaCl-H_2O$ system between -20.1 (temperature at the eutectic) and +0.1 degrees centrigrade at or above saturation (Crawford, 1981). In solutions saturated with NaCl, the salinity is determined from the solution of halite (not the melting of hydrohalite). These relationships suggest that hydrohalite was not the last phase to melt. No reference was found in the literature for the occurrence of a salt hydrate phase of calcium sulfate. It is possible that the concentration of Ca^{+2} exceeded Na^{+} in which case the salt-hydrate phase that melted would probably have been antarcticite ($CaCl_2 \cdot 6H_2O$). Alteration of the limestones and other rocks in the district provides a potentially rich source of additional calcium in the solutions. Further work is required for determining the composition and estimating the total dissolved salts of the

fluid inclusions in this study. Various methods (both destructive and nondestructive) are currently in use for determining the specific composition of liquids, gases, and solids in fluid inclusions. A discussion of the usefulness, practical problems and limitations of the various methods are discussed by Roedder (1984, chapters 4 and 5).

While an approximation of the salinity in terms of NaCl equivalents cannot be made, the presence of immiscible liquids on heating and the difficulty encountered in getting the inclusions to freeze suggest the inclusions may be saline or hyper-saline solutions (Roedder, 1984). The liquid-liquid immiscibility is probably an aqueous brine-aqueous brine immiscibility. This type of immiscibility in certain highly saline fluid inclusions has been reported in the literature (for example Kalyuzhnyi, 1956, 1958; Ermakov et al., 1957; Trufanov et al., 1970; Trufanov, 1970; and Ahmad and Rose, 1980; -cited in Roedder, 1984) however the significance of such immisciblity in terms of fluid composition is not well known (Roedder, 1984). According to Roedder, in view of the probable configurations of the pressure-temperature-composition (P-T-X) diagrams for water-salt systems, such immiscibility under conditions of rising temperature and constant volume is expectable.

As the system was determined to be non-boiling a pressure correction to the temperature of homogenization is required. The pressure correction is based on knowledge of the composition (salinity) and an estimate of the maximum confining pressure existing during mineralization. The Th and an estimate of the salinity limits the inclusion to an isochore on a pressure-temperature plot for the appropriate composition fluid.

A maximum confining pressure may be determined by an estimate of the thickness of the overburden during the time of mineralization. The mineralization in the West Pit and the bulk of the magnetite ore-bodies are post-emplacement of the igneous rocks. Since the major and trace element data suggests that the two principal intrusives are comagmatic (and thus penecontemporaneous) the amount of overburden consists of the sum of the thickness of all the units lying between the upper Torres member of the Yeso Formation and the youngest stratigraphic unit present at the time which was probably the early Tertiary Cub Mountain Formation (Arkell, 1983).

Griswold (1959) lists the approximate thicknesses of these units in Lincoln county just to the east of the Jones Camp dike. The greastest thickness given for a formation is used in order to assure that a maximum pressure has been derived (table 3).

TABLE 3: Maximum thickness of overburden for pressure estimate.

		maximum thickness*
Tertiary	Cub Mountain Fm.	2000 feet
Cretaceous	Mesa Verde Group	500
	Mancos Fm.	400
	Dakota Fm.	175
Triassic	Dockum Gp.	500
	Bernal Fm.	350
Permian	San Andres-Glorieta Fm.	1000
	Canas, Joyita mbrs.	
	Yeso Fm.	240**

Total estimated overburden----------5156' (1574.3 m)

Hydrostatic Pressure:

1 kilometer of water = 96.8 atm = 98 bars
5165' = 1.57 km = 154 bars

Lithostatic Pressure:

Assume average specific gravity of rocks = 2.6
1 km of rock = 260 bars
1.57 km = 408 bars

* Values from Griswold (1959); ** value from Bickford (1980).

The maximum thickness of the overburden was approximately 1.6 km. Thus the maximum lithostatic pressure would have been 408 bars, assuming an average density of 2.6 gram/cc and the maximum hydrostatic pressure of 154 bars, assuming the density of water equal to one. It is most likely that the hydrostatic head provided the principal pressure as the system was probably in the water saturated crust. This may be inferred based on the relatively shallow depth during mineralization and the predominance of clastic rocks in the stratigraphic section.

The presence of dissolved salts lowers the equilibrium vapor pressure on the liquid-vapor curve which means solutions would boil at a lower pressure or a higher temperature relative to the pure H_2O system. Since the inclusions show evidence of "exotic" or highly concentrated solutions the pressure correction can only be assumed to be equal to that for a 25 wt. percent NaCl solution (Roedder, 1984). Therefore the magnitude of the temperature correction at the estimated pressure for an average Th of 144 degrees centigrade would be approximately 25 degrees centigrade (Potter, 1977). This represents an average temperature of trapping of 169 degrees centigrade. At this temperature and salinity the minimum pressure to prevent boiling is 3.8 bars (25.2 m) (Haas, 1971). With a maximum hydrostatic pressure of 154 bars the maximum temperature without boiling is approximately 330 degrees centigrade (Roedder and Bodnar, 1982).

MODEL FOR THE ORIGIN OF THE JONES CAMP MAGNETITE DEPOSITS

The effects resulting from the emplacement and cooling of the Jones Camp dike and associated dikes and sills are of central importance to a model describing the origin of the magnetite ore-bodies. Forceful emplacement of the intrusive rocks created favorable structures for the localization of ore and provided secondary permeability which served as the principal channelways for the ascending hydrothermal solutions. The heat associated with the intrusive rocks provided the thermal energy necessary to establish a convective hydrothermal system required for the leaching, concentration, transport and deposition of the quantities of iron contained in the ore bodies.

Evidence from radiometric dating of hydrothermal ore deposits associated with volcanism or intrusive activity suggests the deposits are essentially coincident with igneous activity within the limits of measurement (Skinner, 1979). The presence of two intrusions in the Jones Camp district presents some uncertainties as to the exact timing and sequence of alteration and mineralization. Field relationships indicate that the ore is largely post-emplacement of the igneous rocks. This is demonstrated by the occurrence of the bulk of the ore directly associated with or relatively close to pyroxene syenodiorite dikes and sills; evidence indicates these later intrusions do not

crosscut magnetite bodies and do not show inclusions of ore suggesting that the ore is later than any of the intrusions. Major and trace-element chemical analysis of the igneous rocks suggest that the two intrusions are comagmatic and thus closely spaced in time. It is probable, considering the size of the deposits and extent of alteration (particularly in the Jones Camp syenodiorite dike), that the hydrothermal system responsible for the deposition of the magnetite ore was established by the emplacement of the Jones Camp syenodiorite dike and was maintained by the combined thermal energy of both intrusions subsequent to emplacement of the somewhat later pyroxene syenodiorite intrusions. The duration of the system (a quantity difficult to estimate) may have been extended by the cooling of a larger pluton at depth (which served as the source of the intrusive rocks) providing it was at a sufficiently shallow depth to develop thermal convection in the water-saturated crust.

Flow of solutions in a hydrothermal system occurs when density differences induced by local heat sources cause low-density (hot) water to rise (Skinner, 1979). Hydrothermal alteration associated with extensive metasomatism typically involves large amounts of fluid traversing rocks through fractures and connected pore space by the process of infiltration metasomatism. The effects of fluid transport by diffusion may be subordinate to this process (Rose and Burt, 1979).

Evidence for infiltration metasomatism at the Jones Camp deposits includes: 1) control of alteration-mineralization by secondary permeability (created by intrusion of igneous rocks), by primary permeability of the host sedimentary rocks, and by joints developed in the Jones Camp dike; 2) abrubt changes in alteration and sharp contacts between unaltered and altered or mineralized rock. These features contrast with alteration resulting from diffusion which often results in gradational contacts; 3) a tendency for the development of monomineralic assemblages e.g. magnetite ore-bodies (Rose and Burt, 1979); and 4) the non-specific host rock for the ore. The effects of permeability, temperature, and fluid composition are considered more important controls in hydrothermal alteration than composition or other features of original rock types (Henley and Ellis, 1983).

Hydrothermal solutions are recognized as brines in which the source and salinity of the solutions vary widely. Four types of hydrothermal solutions are recognized in the formation of hydrothermal ore-deposits (Skinner, 1979): 1) surface water (which includes rainwater, lake and stream water, seawater, and groundwater); 2) connate or deeply penetrating groundwater; 3) metamorphic water; and 4) magmatic water. The source and relative contribution of these types in most hydrothermal ore deposits is enigmatic.

The volume of fluids rich in H_2O and CO_2 resulting from dehydration and decarbonation reactions during prograde contact metamorphism is generally considered small (Skinner, 1979). This generalization is probably true with respect to the carbonates and sandstones in the district; however the presence of thick evaporite beds in the Yeso formation represents a potentially large source of water and dissolved constituents owing to the dehydration of gypsum plus assimilation of gypsum during emplacement of the Jones Camp syenodiorite and later pyroxene syenodiorite bodies.

An early magmatic component of the hydrothermal system may be inferred based on the occurrence of extensive miarolitic cavities in the Jones Camp dike and an estimate of a minimum water pressure of 500 bars (based on the composition of the magma and occurrence of the hydrous minerals hornblende and biotite). The volume and significance of volatile enriched magmatic waters evolved during crystallization of the igneous rocks (both seen and unseen) is unknown and difficult to determine. It is likely that pervasive sericite and sausserite is the result of deuteric alteration. Peripheral evidence for a relatively minor component of juvenile water is suggested by the minimum content of base metals and the absence of precious metals in the ore; e.g. copper is often associated with magnetite skarn deposits.

Emplacement of the Jones Camp dike and later dikes and sills in the relatively shallow, water-saturated crust would presume the involvement of local meteoric water and the interaction of these waters with the rocks through which they passed. Heated waters near the cooling igneous rocks would tend to migrate upwards along the contacts towards cooler and lower pressure areas. The fluids displaced upwards would initiate flow in the sediments towards the intrusive rocks. A convective hydrothermal system involving meteoric water (which would mix with waters derived from other sources) would most likely be established as the behaviour of groundwater in the permeable crust associated with local heat sources is dominated by thermal convection (Henley and Ellis, 1983).

The contribution of saline connate waters contained in the gypsum by assimilation during emplacement of the intrusive rocks, dehydration associated with contact metamorphism, or by reaction with the hydrothermal solutions is the likely source for the high salinity, sulfate enriched fluids recognized in the fluid inclusions. The source of high salinity in many formation waters is linked to the solution of evaporites at depth or by infiltration of hypersaline waters originally found in evaporite rocks (Hanor, 1979). This is believed to be the source of the saline groundwaters near Carrizozo, New Mexico which have reacted with the same sedimentary rocks that are exposed in the Jones Camp district (C.T. Smith, personal communication,

1984). This has also been the explanation for the salinities determined in the study of other ore deposits and in modern geothermal systems such as the Salton Sea (Ellis and Mahon, 1979).

Solubility is the controlling parameter in the precipitation or dissolution of a mineral (Rose and Burt, 1979). The equilibrium constant for the dissolution of magnetite according to the reaction:

$$Fe_3O_4 + 8H^+ = 2Fe^{+3} + Fe^{+2} + 4H_2O \qquad (1)$$

decreases with increasing temperature. It can be seen from equation (1) that the solubility of magnetite is pH dependent. In saline, chloride rich solutions the total amount of iron in solution coexisting with magnetite increases with increasing temperature owing to the formation of complexes with chloride ions which enhances the solubility of magnetite. At low temperatures the geologically dominant iron species are universally agreed to be the free ferrous ions (Crerar et al., 1978). With increasing temperature ferric chloride species become increasingly stable and may be effective in transporting reasonable quantities of iron in solution (Helgeson, 1969). At temperatures above approximately 250 degrees centigrade ferrous chloride species are believed to contribute to the transport of iron in hydrothermal brines and may be the dominant aqueous iron species above approximately 300 degrees centigrade (Crerar et al., 1978).

Assuming for simplicity that activity equals molality, the total molality of iron in the aqueous solution coexisting in equilibrium with magnetite can be calculated by adding the concentrations of each aqueous iron species at a specified pH. This is represented in figure 30 which was constructed from thermodynamic data contained in Helgeson (1969) and Crerar et al. (1978). The concentration of chlorine was taken to be equal to 3 molal; and the fugacity of oxygen used in the calculations represents a maximum for the system as it was determined from the equilibrium between magnetite and hematite. It should be noted that the pressure dependence on the equilibrium constants in hydrothermal solutions is negligible below 300 degrees centigrade and confining pressures up to several hundred bars (Helgeson, 1969). An outline of the method used to calculate these curves is contained in Appendix VI.

Although concentrations of metal carbonate, sulfide, bisulfide and polysulfide complexes are negligible in acid, low sulfide solutions, metal sulfate complexes may be important contributors to mineral solubilities in such solutions at temperatures below approximately 200 degrees centigrade (Helgeson, 1969). As no thermodynamic data was found for the stability of iron sulfate complexes the significance of these species could not be included in the calculations reflecting magnetite solubility.

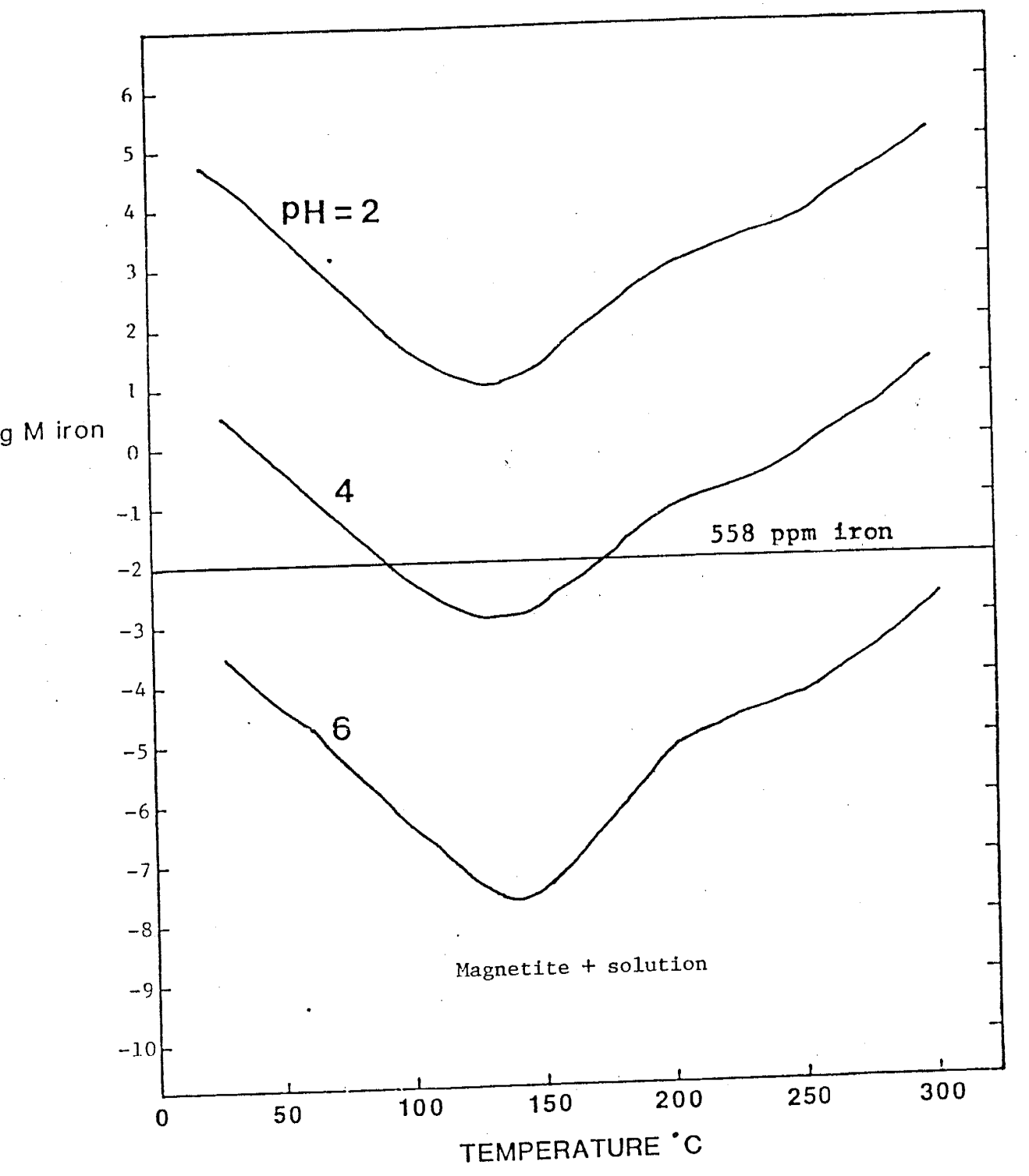

FIGURE 30: Solubility of iron in equilibrium with magnetite as a function of pH and temperature in a 3 molal Cl^- solution.

It can be seen in figure 30 that precipitation of magnetite can be promoted in several ways. A solubility minimum exists at around 145 degrees centigrade. At a constant pH with falling temperature the solution would be pushed toward saturation with respect to magnetite. This effect is due to the decreasing stability of chloride complexes with iron. The solubility minimum is approximately coincident with the temperatures of mineralization determined from fluid inclusion analysis. This suggests that the solutions were maintained below saturation until temperatures at or near the solubility minimum were reached.

The pH dependence of magnetite solubility provides the likely mechanism for the replacement of the host rocks by magnetite. A unit increase in pH would decrease the solubility of magnetite by approximately two orders of magnitude. The dissolution by hydrolysis of limestone, dolomite, anhydrite, sandstone, and altered sedimentary or igneous rocks represent hydrogen ion consuming reactions. In a saturated solution at constant temperature and pressure a slight increase in pH during dissolution of the host rocks would cause the precipitation of small amounts of magnetite. For example, dissolution of limestone would consume 2 moles of hydrogen for every mole of calcite destroyed:

$$CaCO_3 + 2H^+ = Ca^{+2} + H_2O + CO_2$$

If an iron saturated aqueous solution reacts with limestone

the resulting increase in pH decreases the solubility of iron, precipitating magnetite as a result.

The precipitation of magnetite (or the reverse of equation 1) creates hydrogen ions resulting from the hydrolysis of water. Thus a reciprocal reaction between hydrogen ion consuming reactions (i.e. the hydrolysis of the host rocks) and the precipitation of magnetite, which liberates hydrogen ions, can be envisioned as resulting in the gradual replacement of the various host rocks.

A consideration of figure 30 suggests that reasonable quantities of iron can be transported in solution. Ten ppm is considered a minimum for significant ore mineral transport (Barnes, 1979). If one assumes that saturation of magnetite is not reached until the mean temperature of mineralization determined by fluid inclusion analysis (169 degrees centigrade) the amount of iron in solution at a neutral pH at this temperature falls several orders of magnitude below the ten ppm minimum. Thus, an acid pH is required for the solutions. The fluid inclusion evidence indicates saline, sulfate enriched solutions which are correlated with a low pH (Henley and Ellis, 1983). In addition, thousands of ppm of iron have been found in solution in modern geothermal systems such as the Salton Sea (Browne et al., 1979) and in analysis of fluid inclusions from extinct hydrothermal systems (Roedder, 1979). By way of a reasonable example, if you assume the solutions did not

become saturated with iron until the mean temperature of mineralization determined by fluid inclusion analysis, at a pH of 4, 558 ppm Fe (log M Fe = -2) would be in solution. The amount of iron deposited from a liter of solution would be relatively small. A change in pH from 4 to 5 would result in the maximum amount of iron being precipitated as magnetite which amounts to 1×10^{-2} M Fe or 0.72 g of magnetite. Therefore in order to deposit the conservative estimate of 1,117,940 tons of probable reserves (Bickford, 1980) would require 2.4×10^{12} liters of solution to have passed through the system. The combined effects of decreasing temperature through the solubility minimum and gradual neutralization of the solutions by reaction with the host rocks would cause most of the iron in solution to be precipitated as magnetite.

As noted previously the intensely altered margins of the Jones Camp syenodiorite dike are depleted in iron due to the destruction of primary magnetite and ferromagnesian minerals during the intermediate stage in the alteration (i.e. albitization and scapolitization). This must have enriched the solutions with iron that was largely maintained in solution until favorable conditions for the precipitation of magnetite were achieved. Using a simple mass transfer calculation, the amount of iron depleted in the altered margins of the Jones Camp dike (approximately 3-4%) could provide more than enough iron contained in the estimated probable reserves.

The Jones Camp magnetite deposits are unusual compared to other New Mexico deposits as well as magnetite deposits that are described in the literature because of the association of high grade magnetite ore with gypsum and the relatively low temperatures determined for mineralization. The favorability of carbonate rocks to replacement by magnetite, and in hosting hydrothermal ore deposits in general, is well known and these rocks are often the principal ore bearing rocks in skarn deposits (Einaudi, et al., 1980). The solutions were apparently reactive with anhydrite which is not known to the author to be a common host for replacement type base or precious metal deposits. In view of the above considerations required for the leaching, transport, and deposition of magnetite from solution, it is probable that the presence of thick gypsum layers in the section improved the favorability for significant mineralization seen in the district. This association increased the salinity and lowered the pH of the solutions allowing more iron to be leached from the mafic margins of the Jones Camp syenodiorite dike and to be effectively transported in solution. The relatively high iron content of the marginal Jones Camp syenodiorite dike (10-12%) is probably also significant by providing potentially more leachable iron relative to other intermediate composition intrusive rocks. The temperature, pH, and salinity relations of iron in solution, suggest that potentially large concentrations of iron were maintained in

solution and that the solutions did not become saturated with iron until relatively low temperatures. The fluid inclusion evidence indicates the magnetite was deposited at temperatures below 200 degrees centigrade. This agrees with petrographic observations that the main stage of mineralization is late and magnetite occurs as a replacement of all earlier secondary assemblages. These temperatures are also compatible with calculated solubility minima for iron in saline solutions.

REFERENCES

Arkell, B.W., 1983: Geology and Coal Resources of the Cub Mountain Area, Sierra Blanca Coal Field, New Mexico, Unpublished Master of Science thesis, New Mexico Institute of Mining and Technology.

Barnes, H.L., 1979: Solubilities of ore minerals in Geochemistry of Hydrothermal Ore Deposits, ed. H.L. Barnes, Wiley Interscience, New York, p.404-460.

Bickford, D.A., 1980: Economic Geology of the Jones Camp Iron Deposits, Socorro County, New Mexico, Unpublished Master of Science thesis, New Mexico Institute of Mining and Technology.

Blount, C.W. and Dickson, F.W., 1969: The solubility of anhydrite ($CaSO_4$) in NaCl-H_2O from 100-450 °C and 1 to 1000 bars, Geochemica Et Cosmochimca Acta, v.33, p.227-245.

Chapin, C.E., Chamberlin, R.M., Osburn, G.R., White, D.W., and Sanford, A.R., 1978: Exploration framework of the Socorro geothermal area, New Mexico, N.M., Geol. Soc. Special Publication, v.7, p.115-117.

Clynne, M.A., 1977: Freezing point depression of synthetic brines, (abstr) Geol. Soc. Am. Abstr. Programs 10, 381 (296).

Crawford, M.L., 1983: Phase equilibria in aqueous fluid inclusions, in Fluid Inclusions: Applications to Petrology, eds. L.S. Hollister and M.L. Crawford, Mineralogical Association of Canada, Calgary.

Crerar, D.A., Susak, H.J., Borcsik, M., and Schwartz, S., 1978: Solubilities of the buffer assemblage: pyrite + pyrrhotite + magnetite in NaCl solutions from 200-350 °C, Geochim. Cosmochim. Acta. 43, p.1427-1439.

Deer, W.A., Howie, R.A. and Zussman, J., 1966: An Introduction to the Rock Forming Minerals, Longman Group Limited, London, 528 p.

Einaudi, M.T., Meinart, L.D. and Newberry, R.J., 1980: Skarn deposits, in Economic Geology Seventy-Fifth Aniversary Volume, ed. B.J. Skinner, Econ. Geol. Pub. Co., El Paso, Tx., p.317-391.

Ellis A.J. and Mahon, W.A., 1977: Chemistry and Geothermal Systems, Academic Press, New York, 392 p.

Emmons, N.W., 1906: The Jones iron fields of New Mexico. Mining Magazine v.13, p.109-113.

Gibbons, T.L., 1981: Geochemical and petrographic investigation of the Jones Camp magnetite ores and associated intrusives, Socorro Co., New Mexico, unpublished Master of Science thesis, New Mexico Insitute of Mining and Technology.

Grantham, R.M. and Soule, J.H., 1947: Jones iron deposit, Socorro County, New Mexico, U.S. Bureau of Mines, Report of Investigation 4010, 4 p.

Griswold, G.B., 1959: Mineral Deposits of Lincoln County, New Mexico, N.M. Institute of Mining and Technology, State Bureau of Mines and Mineral Resources Bull. 67, 112 pp.

Haas, J.L., Jr., 1971: The effect of salinity on the maximum thermal gradient of a hydrothermal system at hydrostatic pressure, Econ. Geol., v.66, p.940-946.

Hanor, J.S., 1979: The sedimentary genesis of hydrothermal fluids, in Geochemistry of Hydrothermal Ore Deposits, ed. H.L. Barnes, Wiley Interscience, New York, p.137-172.

Hanson, G.N., 1978: The application of trace elements to the petrogensis of rocks of granitic composition, Earth and Planet. Sci. Letters, 38, p.26-43.

Helgeson, H.C., 1978: Summary and critique of thermodynamic properties of rock forming minerals, Am. J. Sci., 278-A, p.1-229.

Henley, R.W., 1984: Fluid Mineral Equilibria in Hydrothermal Systems, Reviews in Economic Geology: vol. 1, Econ. Geol. Pub. Co., El Paso, Tx., 267 pp.

Henley, R.W. and Ellis, A.J., 1983: Geothermal systems ancient and modern: a geochemical review, Earth Sciences Reviews 19, p.1-50.

Holland, H.D. and Malinin, S.D., 1979: The solubility and occurrence of non ore minerals, in Geochemistry of Hydrothermal Ore Deposits, ed. H.L. Barnes, Wiley Interscience, New York, p.461-508.

Jones F.A., 1904: New Mexico Mines and Minerals, p.202-205.

Kelley, V.C., 1949: Geology and Economics of New Mexico iron-ore deposits, University of New Mexico Publications in Geology., no.2, 249 p.

Kelley, V.C. and Thompson, T.B., 1964: Tectonics and general geology of the Ruidoso-Carrizozo Region, central New Mexico, New Mexico Geological Society Guidebook, 15th Field Conference, p.110-120.

Keyes, C.R., 1904: Iron Deposits of the Chupadera Mesa, The Eng. and Mining Journal., vol.78, 632.

Keyes, C.R., 1915: Foundations of exact Geologic correlation, Iowa Academy Sci., PR., vol.22, p.249-267.

Lasky, S.G., 1932: Ore deposits of Socorro County, New Mexico Bur. Mines and Min. Res., Bull 8.

Lee N.B., 1909: The Manzano Group of the Rio Grande Valley, New Mexico, U.S.G.S. Bull. 389.

LeMaitre, R.W., 1976: The chemical variability of some common igneous rocks, J. Pet., v. 17, Part 4, p. 569-637.

Lindgren, W., Graton, L.C., and Gordon, C.H., 1910: The ore deposits of New Mexico, U.S. Geological Survey Prof. Paper 68.

Needham, C.E., and Bates, R.L., 1943: Permian type section in central New Mexico, Geol. Soc. of Amer. Bull., vol., 54 p.1653-1668.

Nockolds, S.R., 1954: The average composition of the major igneous rock types, Geol. Soc. Am., Bull., v. 65, p.1007-1032.

Nogueira, A.C., 1971: Mineralogy and geochemistry of contact metasomatic iron deposits at Jones Camp, Socorro County, New Mexico, Unpublished Master of Science thesis, New Mexico Institute of Mining and Technolgy.

Peacock, M.A., 1931: Classification of igneous rock series, J. Geol., v.11, p.15-32.

Potter, R.W., II, 1977: Pressure corrections for fluid inclusion homogenization temperatures based on the volumetric properties of the system $NaCl-H_2O$, U.S. Geol. Survey Jour. Res., v.5, p.603-608.

Ramdohr, P., 1980: The Ore Minerals and their Intergrowths, in two volumes, 2nd edition, Pergamon Press, Oxford, 1207 p.

Read, C.B., and Andrews, D.A., 1944: U.S. Geological Survey Oil and Gas Investigations, preliminary map 8.

Roedder, E., 1984: Fluid Inclusions, Reviews in Mineralogy volume 12, Mineralogical Society of America, Washington D.C., 644 p.

Roedder, E. and Bodnar, R.J., 1980: Geologic pressure corrections from fluid inclusion studies, Ann. Review Earth Planet. Sci., 8, p.263-301.

Roedder, E., 1979: Fluid inclusions as samples of ore fluids, in: Geochemistry of Hydrothermal Ore Deposits, H.L. Barnes, ed., Wiley Interscience, New York, p.684-737.

Rose, A.W. and Burt, D.M., 1979: Hydrothermal alteration, in Geochemistry of Hydrothermal Ore Deposits, ed. H.L. Barnes, Wiley Interscience, New York, p.173-235.

Schrader, F.C., 1910: Iron deposits of the northern Sierra Oscura, in U.S. Geol. Survey Prof. Paper 68: The ore deposits of New Mexico, p.203-205.

Schnake, D.W., 1977: Conditions of formation of the iron bearing skarns at Lone Mountain, Lincoln County, New Mexico, Unpublished Master of Science thesis, New Mexico Institute of Mining and Technology.

Skinner, B.J., 1979: The many origins of hydrothermal ore deposits, in Geochemistry of Hydrothermal Ore Deposits, ed. H.L. Barnes, Wiley Interscience, New York, p.1-21.

Streckeisen, A., 1976: To each plutonic rock its proper name, Earth Sci. Rev., v.12, p.1-33.

Uytenbogaardt, M. and Burke, E.A.J., 1971: Tables for microscopic identification or ore minerals, Elsevier Publishing Co,. Amsterdam, 423 p.

Weber, R.H., 1971: K/Ar Ages of Tertiary igneous rocks in central and western New Mexico, Isochron/West, no.71-1 Jan. 1971

Weissberg, B.G., Browne, P.R.L., and Seward, T.M., 1979: Ore metals in active geothermal systems, in: Geochemistry of Hydrothermal Systems, H.L. Barnes, ed., Wiley Interscience, New York, p. 738-780.

Appendix I: Single major element analysis of pyroxene syenodiorite from Nogueira (1971).

SiO_2	55.56
TiO_2	1.97
Al_2O_3	13.47
Fe_2O_3	8.11
MgO	6.66
CaO	7.19
Na_2O	5.26
K_2O	0.96
	99.18

APPENDIX II: Hand sample descriptions of pyroxene syenodiorite and Jones Camp syenodiorite chemical samples:

84-5A pyroxene syenodiorite dike

Very fine-grained, greenish gray, porphyritic: 2% feldspar phenocrysts 1-2 mm; approximately 35% total mafics, black color.

84-5B pyroxene syenodiorite dike

No discernable differences from 84-5A.

84-15A pyroxene syenodiorite dike

Very fine-grained, greenish gray, porphyritic: feldspar phenocrysts 1-3 mm length; groundmass feldspar, gray color; interstitial mafic minerals: black or green color; total mafics approximately 35%.

84-15B pyroxene syenodiorite dike

As above (84-15A).

84-15C pyroxene syenodiorite dike

Very fine-grained, gray, non-porphyritic: total mafics approximately 35%, black color.

84-11 pyroxene syenodiorite sill

Fine-grained, greenish gray, non-porphyritic: total mafics approximately 35%, black or green color; few percent biotite present.

84-33 Jones Camp syenodiorite dike

Medium-grained, inequigranular, hypidiomorphic: feldspars-1-3 mm, euhedral to subhedral, predominantly pink color; sparse (< 5%) quartz; mafics (17%): hornblende occurs as elongated blades to greater than 5 mm, black color; some greenish, shorter habit crystals probably clinopyroxene, some biotite present 1-3 mm; 3% miarolitic cavities to 7 mm in greatest dimension.

84-34 Jones Camp syenodiorite dike

Essentially same phase of dike as 84-33. Same texture and mineralogy and percent of phases except this rock shows minor and smaller miarolitic cavities.

84-35 Jones Camp syenodiorite dike

Fine-grained, inequigranular, hypidiomorphic, porphyritic. Feldspar white color; a few percent medium-grained phenocrysts also white; mafics (17%): hornblende blades are medium-grained, black color, groundmass mafics <1 mm, interstitial to feldspar, some suggestion of biotite, some of mafics show signs of oxidation; one large miarolitic cavity shows evidence of alteration as it is green in color however this was not included in chemical sample for analysis.

84-36 Jones Camp syenodiorite dike

Medium-grained (however finer grained than 84-33, 84-34), inequigranular, hypidiomorphic, porphyritic: feldspar-phenocrysts 2-4 mm, whitish color, groundmass feldspar shows pinkish color; mafics (17%): blades of hornblende to 3.5 mm, minor biotite noted; no quartz; no miarolitic cavitites.

84-37 Jones Camp syenodiorite dike

Medium-grained (comparable to 84-33, 84-34), inequigranular, hypidiomorphic. Feldspar: subhedral, predominantly pinkish color, minor show greenish tint; mafics (25%): black color, 2-5 mm, does not show elongated blades of hornblende, no biotite apparent, no quartz or miarolitic cavities.

APPENDIX III: Major element concentrations across the Jones Camp syenodiorite dike of Gibbons (1981).

Section 18 suite

sample number:	1a	1b	2	3	4	5	6
SiO_2	46.03	47.93	46.65	50.99	53.17	55.53	52.53
TiO_2	1.11	1.20	1.20	1.44	1.51	1.20	1.18
Al_2O_3	16.76	16.30	17.58	15.17	17.20	16.78	17.57
Fe_2O_3	5.47	5.99	4.47	9.70	8.69	3.76	4.52
MnO	0.04	0.05	0.05	0.08	0.07	0.05	0.08
MgO	7.57	7.55	5.81	5.75	6.05	4.15	4.06
CaO	12.18	10.92	13.27	7.58	8.66	4.06	4.50
Na_2O	3.79	4.51	4.30	4.74	3.94	6.18	6.94
K_2O	1.04	0.08	0.37	1.03	0.97	1.41	1.46
L.O.I.	4.37	3.62	4.52	0.96	1.60	1.28	1.93
TOTAL	98.36	98.15	98.22	97.44	98.80	94.38	98.58

	7	8	10	11	12	13
SiO_2	52.53	58.53	57.82	53.41	51.80	47.75
TiO_2	1.48	1.14	1.24	1.18	1.47	1.55
Al_2O_3	16.48	18.22	18.04	17.44	16.64	16.48
Fe_2O_3	8.21	5.27	5.90	3.88	5.94	4.69
MnO	0.09	0.06	0.06	0.05	0.06	0.06
MgO	4.50	2.60	2.75	3.48	4.59	4.10
CaO	6.71	3.12	2.91	6.90	7.12	13.17
Na_2O	5.44	8.42	8.60	6.87	6.07	5.78
K_2O	1.78	1.94	1.88	1.79	2.05	---
L.O.I.	1.29	0.88	0.73	2.49	2.10	3.31
TOTAL	98.87	100.18	99.93	97.49	97.84	96.59

Section 24 suite

sample number:	1	2	3a	3b	3c	3e	3f	3h
SiO_2	56.82	50.65	63.17	61.77	49.58	58.73	51.46	54.34
TiO_2	0.94	1.53	0.76	0.91	1.88	1.17	1.92	1.68
Al_2O_3	17.41	16.61	16.71	17.03	16.22	17.98	17.00	16.56
Fe_2O_3	3.73	10.21	3.37	3.76	12.47	5.51	9.36	5.69
MnO	0.05	0.08	0.04	0.06	0.09	0.06	0.08	0.09
MgO	3.07	5.70	1.65	2.79	5.82	2.39	4.89	4.57
CaO	5.07	8.61	2.42	2.46	8.25	3.01	6.33	6.16
Na_2O	7.91	4.08	9.78	8.65	4.84	7.87	5.53	6.42
K_2O	1.56	0.95	0.95	1.45	0.71	2.44	2.07	1.84
L.O.I.	1.54	2.18	0.65	1.13	1.70	0.85	0.85	1.65
TOTAL	98.10	100.60	99.50	100.01	101.56	100.01	99.49	99.35

APPENDIX IV

Table of ore polished section descriptions. A description of the locations and features of the local geology follows.

Shaft Site

S-1 Silicated limestone of Torres member.
60% magnetite 25% maghemite 3% gangue 12% vugs

Phenocrysts of euhedral magnetite (3 mm avg. size) occur growing in voids or set in a matrix of predominantly equant, subhedral fine-grained magnetite. Magnetite shows a light pink tint suggestive of unexsolved titanium (Ramdohr 1980). Matrix magnetite is replaced up to 80% by maghemite. Gangue consists of fine-grained tremolite blades or calcite- white or green in color.

S-2 Silicated limestone of Torres member.
70% magnetite 15% maghemite 15% gangue

Euhedral to subhedral magnetite; fine-grained, seriate. Larger grains may show inclusions of tremolite blades. Patchy alteration to maghemite up to 60% of individual grains. Magnetite is variable shades of brownish gray. Gangue occurs as matrix to magnetite and consists of white or green calcite and tremolite or clinopyroxene.

S-5A Silicated limestone of Torres member.
90% magnetite m maghemite 10% gangue

Magnetite occurs as euhedral phenocrysts (2 mm avg. size) in a matrix of anhedral to subhedral magnetite; fine-grained, seriate. Interstitial gangue consisting of calcite plus blades of tremolite. Minor maghemite. Magnetite phenocrysts show a slightly darker tint.

S-5B Silicated limestone of Torres member.
85% magnetite 10% maghemite 5% gangue

Anhedral-subhedral magnetite, fine-grained, seriate. Grain boundaries may not be distinct in zones of complete replacement describing a massive texture. Patchy alteration to maghemite irregularly distributed. Interstitial gangue consists of green silicates plus minor calcite.

Roof Site

RS4 Actinolitized Jones Camp syenodiorite dike host.
70% magnetite 20% martite 10% gangue m maghemite

Fine-grained, anhedral magnetite with a massive texture, poorly defined grain boundaries. Some near surface alteration to hematite (martite). Gangue consists of interstitial actinolite.

RS6 Actinolitized Jones Camp syenodiorite dike host.
83% magnetite 12% gangue 3% maghemite 2% vugs

Magnetite occurs as euhedral phenocrysts to 4 mm in diameter or is anhedral to subhedral, fine grained seriate. Euhedral magnetite is homogenous gray with minor maghemite alteration vs. matrix magnetite which shows a light pink tint. Magnetite occasionally occurs as psuedomorphs of actinolite blades. Gangue consists of interstitial actinolite.

RS7 Actinolitized Jones Camp syenodiorite dike host.
82% magnetite 12% gangue 6% vugs

Near complete replacement of silicated Jones Camp syenodiorite by magnetite. Magnetite phenocrysts are euhedral, 1-3 mm diameter, and contrast with matrix magnetite which is sub-anhedral, fine grained- seriate. Gangue: blades of tremolite; medium to coarse grained plagioclase phenocrysts occur in vugs and may host inclusions of magnetite.

East Pit

EP1 Canas gypsum member host.
60% magnetite 10% maghemite 10% pyrite 17% gangue
3% vugs

Anhedral, fine-grained magnetite and pyrite set in matrix of silicates and gypsum gangue. Pyrite appears to be psuedomorphic after magnetite in places and is unaltered. Some maghemite alteration of magnetite.

EP Canas gypsum member host.
60% magnetite 12% maghemite 15% pyrite 6% gangue
7% vugs

Magnetite is fine-grained, seriate (<0.5 mm) and subhedral. Individual grains grow into clusters as mineralization proceeds. Irregular patches of alteration to maghemite

common. Pyrite is fine to medium-grained (0.5-1.5 mm) and sub-anhedral. Largely associated with growth in vugs. Where pyrite contacts magnetite, it is partly altered to magnetite around the edges. Pyrite may show inclusions of clinopyroxene. Gangue: gypsum and clinopyroxene.

"J" location

J-3A Torres member, siltstone host.
68% magnetite 7% maghemite 25% vugs

High grade vuggy magnetite ore. Vugs result of near surface dissolution of gangue. Vugs irregular shape. Magnetite is euhedral or subhedral and polygonal grain boundaries developed. Patchy alteration of magnetite to maghemite in places.

J-3B Torres member, siltstone host.
64% magnetite 25% maghemite 6% gangue 5% vugs

Maghemite occurs in matrix of rounded magnetite grains which seem to directly replace detrital quartz and feldspar. Gangue is silicates and calcite irregularly distributed.

"B" location

B7D Upper Torres limestone host.
87% magnetite 13% gangue

Magnetite: anhedral-subhedral, fine-grained seriate. Massive texture developed. No alteration of magnetite. Gangue consists of white-opaque very fine grained calcite interstitial to magnetite.

Birthday Site

BS6A Upper Torres limestone host.
66% magnetite 7% maghemite 27% gangue

Bimodal grain size distribution on magnetite: coarser magnetite (0.75-1.5 mm) euhedral, distinct or grown together, light brown gray with pink tint, may show maghemite alteration; or fine grained (0.1-0.4 mm) subhedral-anhedral, where massive texture developed. Calcite gangue as matrix.

BS6B Upper Torres limestone host.
70% magnetite 15% maghemite 15% gangue

Same texture and mineralogy as BS6A.

West Pit

WP2 Upper Torres limestone host.
17% magnetite m martite 83% gangue

Anhedral-subhedral magnetite; fine-grained seriate. Magnetite occurs as individual grains in layers parallel to primary bedding. Gangue is calcite, fine to medium-grained. Calcite fine-grained granular and variously colored white, brownish yellow, green or clear. Late vein of calcite cuts layers of magnetite and earlier calcite.

WP3 Upper Torres limestone host.
63% magnetite 32% gangue 5% vugs

Subhedral magnetite 0.10-0.6 mm. Layered texture with calcite gangue as in WP2 but more complete replacement.

WP8C Upper Torres limestone host.
75% magnetite 18% gangue 7% vugs

Subhedral-euhedral magnetite, fine-grained, seriate. No alteration. No layered texture apparent. Polygonal grain boundaries well developed. Interstitial calcite gangue in variable amounts.

WP8D Upper Torres limestone host.
65% magnetite 32% gangue 3% vugs

Subhedral-euhedral magnetite, fine-grained. In areas of complete replacement, massive texture developed as no grain boundaries are distinct. A few percent of medium grained phenocrysts, 1-2 mm in size, may show calcite gangue inclusions.

WP8E Upper Torres limestone host.
87% magnetite 13% gangue

Ten percent of magnetite occurs as large euhedral phenocrysts in a matrix of calcite gangue. Other magnetite is anhedral and shows a massive texture. Minor interstitial calcite gangue.

WP8F Upper Torres limestone host.
78% magnetite 20% gangue 2% vugs

Same texture and mineralogy as WP8E.

WP9A Upper Torres limestone host.
78% magnetite 15% maghemite m gangue 7% vugs

Medium grained magnetite phenocrysts may show concentric zoning with some zones replaced by maghemite. Groundmass magnetite is anhedral and shows a massive texture. Minor calcite gangue. Irregularly shaped vugs probably due to near surface dissolution of calcite.

WP10B Upper Torres limestone host.
80% magnetite m hematite 17% gangue 3% vugs

Magnetite is subhedral, lesser anhedral. Bimodal fine grain size distribution: 0.05-0.1 mm or 0.5-0.75 mm. Matrix of opaque white calcite gangue.

WP14A Upper Torres limestone host.
50% magnetite 50% gangue

Fine-grained, euhedral-subhedral magnetite interlayered with calcite gangue. Variable grain size on calcite: fine to medium grained. Ratio of magnetite to gangue variable. Minor maghemite alteration.

WP14B Upper Torres limestone host.
12% magnetite 88% gangue

Magnetite is anhedral-subhedral and largely very fine-grained (0.03-0.06 mm). Occasional disseminated euhedral phenocrysts 1 mm ave. size. Layered structure of magnetite and fine-grained calcite gangue: white-yellow-orange in color.

WP15 Upper Torres limestone host.
83% magnetite 2% martite 12% gangue 3% vugs

Massive magnetite ore, no grain boundaries discernable. Calcite gangue fine-grained, granular. Martite alteration controlled by crystallographic planes in magnetite. Irregularly dispersed vugs, 0.1 mm avg. diameter.

WP23 Torres member gypsum host.
41% magnetite 20% maghemite 7% pyrite 32% gangue

Pyrite is anhedral and altered in part to magnetite. Magnetite is anhedral to subhedral and occurs as individual dispersed grains or in clusters. Patchy alteration to maghemite. Gangue predominantly gypsum.

Key to sample locations and local geology:

Shaft Site

The Shaft Site is located on the north side of the Jones Camp dike in section 13 (T5S R6E) just west of the 13/18 section line. Just below crest of the dike a 36' deep vertical shaft has been sunk at the contact of the dike and a limestone of the Torres member. Limestone hosted ore crops out for approximately 300 feet westward from the Shaft site and intermittently 250 feet to the east where outcrops of gypsum hosted ore also occur and are intruded by pyroxene syenodiorite. Samples for polished section and thin section were collected in the accessible upper 6 feet of the shaft where two thin ore bodies are interlayed with silicated carbonate. No ore exists in the rest of the shaft. It consists of intensely weathered altered dike, sandstone, and gypsum. Minor amounts of silicates occurred below the upper 6-8 feet. There is no direct road access to the Shaft site. It may be reached on foot from a ranch road on the south side of the dike.

Roof Site

The Roof site is located on top of the Jones Camp syenodiorite dike just below the crest of the dike in the NE quarter of sec. 30, T5S R8E. Some mining activity occurred at this location; however no ore crops out. Several small stockpiles occur (RS 4,6,7). A pyroxene syenodiorite dike intrudes the Jones Camp syenodiorite dike on the north side and occurs as dikes and sills to the south (cross section D-D', Plate 2). This location is interesting because it appears that intensely altered-actinolitized Jones Camp syenodiorite is the host for high grade ore. This is supported by numerous thin sections from outcrops of Jones Camp syenodiorite and pyroxene syenodiorite (thin sections RS1, RS2, RS3B, RS4A, RS4B) and float (RSA1, RSA2, RSA3). No sediment host is found in outcrop or float. A road branching from the old Socorro-Carrizozo highway on the north side of the Jones Camp dike provides ready access to the Roof site.

East Pit

The east pit is located in western half of section 19 (T5S R8E) and has been the site of surface mining activity as recently as 1981. Gypsum of the Canas member is the predominant host to large tonnages of variable grade iron ore. The ore shows 0-20% pyrite. Both unsilicated and green-silicated gypsum ore is present. Several large piles of unsorted, variable grade ore and gypsum waste are located here. The old Socorro-Carrizozo highway passes in front of the east pit. The east pit is floored by several ore outcrops. Polished section samples: EP1, EP. Thin section samples: EP.

"J" Location

This location is in the eastern half of section 18 (T5S R7E) on the north side of the Jones Camp dike just west of the ranch road which crosses the dike at this point. Sandstone of the Torres member hosts ore which was examined in polished section (J-3A, J-3B) and thin section (J-1B, J-1C, J-1D, J-2B). A well exposed, complete section of the Jones Camp dike is found here and was sampled in detail for petrographic examination of alteration (thin section samples J-4 to J-12). No pyroxene syenodiorite occurs in the immediate area but is present in relatively small bodies 1/3 mile to the east and 1/3 mile to the west. Direct access is provided by an access road to a drilling pad located here.

"B" Location

Ore section B7D was collected here at an open pit in sec. 24 on the south side of the Jones Camp dike. The crest of an anticline is exposed on the west side of the pit and hosts mineralized limestone, gypsum, and sandstone of the Torres member. The axis is faulted (cross section C-C', Plate 2). Pyroxene syenodiorite does not crop out at the pit but is seen intruding the Jones Camp dike on the north side, as sills to the south of the pit, and as sills and dikes to the east and west. Thin section samples: B3D, B7B, B7G1. Note that the deep drainage across the dike is the location of Gibbons sec. 24 Jones Camp dike samples and samples 84-33, 84-34 this study. Road access to the pit is available on mine roads from the old Socorro-Carizozo highway.

Birthday Site

The Birthday site is located in sec. 14 (T5S R7E). Ore was mined here to a limited extent but it appears that little was removed. Bold outcrops of glistening black, carbonate hosted magnetite ore contact the Jones Camp dike on the south side (polished sections BS6A, BS6B). The ore dips

into the dike and defines the north limb of an anticline the crest of which has been truncated by erosion. Farther to the west of this location both the north and south limbs of this structure host ore outcrops. Detailed mapping shows that anticlinal structures such as this occur for 5 miles on the south side of the Jones Camp dike. Most of the ore occurrences in this zone are associated with these structures. A ranch road branching off the old Socorro-Carrizozo highway at the prominent curve in section 13 crosses the Jones Camp dike and provides access to this location.

West Pit

The West pit is located in sec. 14 (slightly to the east of the Birthday site and on the opposite side of the Jones Camp dike). Vertical or near vertical limestone beds of the upper Torres member form the north wall of the pit and are cut by a near vertical dike of pyroxene syenodiorite. This is believed to have been emplaced along a fault in the axis of an anticline (cross section B-B', Plate 2). Altered gypsum and gypsum ore floor the pit and contact a thin, intensely altered (and weathered) pyroxene syenodiorite dike which intrudes intensely altered Jones dike on the south side of the pit. The West pit was sampled in detail for both polished sections (WP2, 3, 8C, 8D, 8E, 8F, 9A, 10B, 14A, 14B, 15, 23) and thin sections (WP1B, 4, 5, 14B, 14C, 22A, 22C, 24A, 26). East and west of the West pit are large pyroxene syenodiorite dikes intruding the north margin of the Jones Camp dike and spread out into the sediments as sills. Direct road access is on a old mine road branching off the old Socorro-Carrizozo highway at the prominent curve in section 13.

APPENDIX V

Thin section descriptions of altered and mineralized sedimentary and igneous rocks. Mineral percentages based on visual estimate. Grain size criteria: < 0.002 mm cryptocrystalline < 0.01 mm microcrystalline < 0.1 mm fine-grained < 1.0 mm medium-grained. Calcite was stained (using alizarin red) to distinguish from dolomite. Alkali feldspar was not stained but was distinguished from plagioclase based on differences in crystal form and twinning.

"J" Location

J-1C

Location: mineralized sandstone of Torres member of Yeso Formation.

Detrital grains: quartz and feldspar (67%); quartz:feldspar ratio=1:3; 0.1-0.3 mm; subround, moderately well sorted; feldspar is predominantly untwinned, occasionally albite twinning.

Cement: primary cement probably silica; largely replaced by secondary calcite, epidote, and magnetite.

Secondary minerals:

1) calcite (20%) shows straight or gently curved grain boundaries.
2) epidote (8%) microcrystalline to fine-grained; bladed; anomalous birefringence; occurs with calcite.
3) magnetite (5%) anhedral; fine-grained.

Alteration/mineralization:

Calcite occurs as an alteration of cement and detrital grains. Epidote and magnetite after calcite.

Name: mineralized fine-grained arkose.

J-2B

Location: mineralized siltstone of the Torres member.

Detrital grains: quartz and feldspar (35%); quartz:feldspar ratio 1:3; 0.02-0.4 mm; moderatelty well sorted; subangular.

Cement: replaced by hematite.

Secondary minerals:

1) mica (5%) microcrystalline to fine-grained; locally abundant; mostly chlorite and lesser biotite.
2) hematite (60%) yellow-orange-red, < 5% opaque.

Alteration/mineralization:

Secondary hematite after cement and detrital grains replaces up to 90% of the rock in places. Hematite is probably a near surface alteration of magnetite. No calcite.

Name: mineralized arkose.

Note: Samples J-4 through J-12 are altered Jones Camp syenodiorite. J-4 was collected close to the contact with the sediments. Distances from this sample across the dike normal to the contact with the sediments are given in paranthesis following the sample number. Sample J-4= 0'.

J-4 (0')

Primary minerals:		Secondary minerals:	
plagioclase	40%	calcite	20%
alkali feldspar	15%	scapolite	5%
microcrystalline feldspar	10%	magnetite	m
clinopyroxene	6%	chlorite	2%
sphene	2%		

Texture:

Thin section was poorly ground; approximately half useable for analysis. The rock is fine-grained to aphanitic, hypidiomorphic granular. Feldspar is 0.2-0.9 mm (ave. 0.3 mm) excluding approx. 15% microcystalline feldspar. Calcite mosaics up to 6 mm in length. Euhedral clinopyroxene is concentrated near calcite mosaics. Diverse crystal arrangement of feldspar and sutured grain contacts are common.

Alteration:

Early calcite mosaics filling variably sized miarolitic cavities. Scapolite is subhedral and occurs interstitial to feldspar where it has probably replaced amygdaloidal calcite. It also occurs as a direct alteration product of feldspar. Late calcite is anhedral and occurs as an alteration of feldspar. Chlorite is an alteration of feldspar. This thin section is interesting because it is near the contact with the sediments yet it is not

recrystallized by albitization and shows relatively minor early secondary scapolite.

J-5 (30')

Secondary minerals:

plagioclase (albite)	23%
scapolite	6%
actinolite	14%
chlorite	12%
clinopyroxene	3%
calcite-dolomite	13%
magnetite finely divided	9%
	20%

Texture:

Intensely altered, completely recrystallized, fine-grained to microcrystalline, allotriomorphic granular rock. Mottled texture seen in hand specimen result of approximately concentric zones of scapolite or carbonate mosaics. Large calcite vein is 5 mm wide. Magnetite is anhedral and disseminated or hosted in calcite veins.

Alteration:

Early scapolitization and albitization. Minor clinopyroxene occurs with secondary albite. Pervasive chlorite, actinolite, and magnetite alteration of earlier secondary minerals. Much of this alteration is finely divided and is commonly oxidized. Late calcite mosaics occur in crosscutting veins. These may show inclusions of actinolite and magnetite. Largest concentration of magnetite occurs in these veins. Actinolite also occurs aligned parallel to these fractures. Some scapolite is late associated with the carbonate and/or chlorite- actinolite. Some interstitial dolomite is contemporaneous with albitization or may be a remnant of amygdaloidal dolomite. No sphene or zircon.

J-6 (33')

Secondary minerals:

albite	29%
clinopyroxene	5%
scapolite	12%
chlorite	10%
tremolite	6%
dolomite	8%
magnetite	2%
finely divided	28%

Texture:

Completely recrystallized, fine-grained, allotriomorphic granular rock. Texture is similar to J-5. Secondary plagioclase laths 0.3 mm length.

Alteration:

Albitization (plus clinopyroxene) and scapolitization resulted in complete recrystallization of primary mineralogy. Scapolite is interstitial to plagioclase laths and exists as remnants of earlier scapolitization. Dolomite occurs interstitial to plagioclase laths or in relatively small mosaics hosting tremolite blades. Subsequent pervasive tremolite-actinolite, chlorite, and late magnetite replace earlier secondary phases. Much of this later alteration is finely divided. Some magnetite is altered to sphene around the perimeter of individual grains. Some of the sphene may be concurrent with albitization.

J-7 (60')

Primary minerals:		Secondary minerals:	
plagioclase	65%	calcite	3%
alkali feldspar	17%	tremolite	1%
clinopyroxene	5%		
cordierite	6%		
sphene	3%		
zircon	m		
apatite	tr		

Texture:

Fine-grained, allotriomorphic granular, monzodiorite. Most of the alkali feldspar is untwinned and is continously zoned. Plagioclase is commonly zoned. Sutured grain boundaries in feldspar common. Sphene is anhedral and typically shows interlocking grains interstitial to feldspar.

Alteration:

Rock shows relatively minor hydrothermal alteration. Occurs in the field as a narrow discontinuous zone within intensely altered dike rock. Relatively minor sericite and saussurite. Minor tremolite probably inverted from hornblende. Calcite occurs as individual grains interstitial to primary phases where it probably has filled tiny miarolitic cavitites. Anomalous cordierite is an anhedral late crystallizing phase which is often associated with calcite. This was believed to be quartz but all the grains were checked for optic sign and yielded biaxial-negative figures with a relatively large 2-V.

J-8 (70')

Primary minerals:		Secondary minerals:	
plagioclase	14%	scapolite	10%
alkali feldspar	2%	albite	25%
hornblende	5%	clinopyroxene	4%
clinopyroxene	3%	chlorite	5%
magnetite	1%	actinolite	13%
		calcite	6%
		magnetite	3%
		finely divided	9%

Texture:

Primary zones (unaffected by albitization) had a similar texture to J-7 but showed greater concentrations of hornblende and clinopyroxene. Secondary albite occurs with

interstitial clinopyroxene. Average grain size of albite is 0.1 mm.

Alteration:

Early scapolite occurs replacing primary feldspar and hornblende. Hornblende has inverted to tremolite. Calcite occurs interstitial to feldspar; or associated with scapolite; or as an alteration of feldspar, or scapolite. Some late magnetite. Approximately 70% of the section has been completely recrystallized during albitization which includes secondary clinopyroxene. Scapolite occurring in zones of albitization is sparsely distributed and exists as remnants of earlier scapolitization. Late actinolite, and chlorite alteration of primary and earlier secondary phases. Much of this is finely divided. Magnetite is the latest secondary phase and is seen replacing plagioclase, scapolite, actinolite, or calcite.

J-9 (105')

Secondary minerals:

plagioclase (albite)	30%
clinopyroxene	4%
scapolite	14%
calcite	3%
dolomite	5%
chlorite	18%
actinolite	6%
sphene	m
magnetite	3%
finely divided	17%

Texture:

Fine-grained to microcrystalline completely recrystallized rock. No prominent layering of secondary phases or flow structure. Secondary plagioclase laths are 0.15 mm ave. length.

Alteration:

Early scapolitization and albitization reducing grain size and indiscriminately replacing primary feldspar, ferromagnesian and accessory minerals, and in part after dolomite mosaics. Dolomite mosaics show inclusions of euhedral clinopyroxene (augite and aegirine-augite). Late tremolite-actinolite and chlorite alteration is pervasive but affects albitized areas greater than scapolitized areas or dolomite mosaics. Finely divided alteration is a combination of incipient tremolite-actinolite and chlorite. Late disseminated magnetite indiscriminately replaces plagioclase, scapolite, clinopyroxene, or calcite and is

also seen as pseudomorphic after clinopyroxene in dolomite mosaics. Chlorite is typically associated with magnetite. Approximately 20% of the rock shows an orange-red coloration due to the oxidation of iron in the late secondary phases particuarly chlorite.

J-9B (105')

Secondary minerals:

scapolite	25%
plagioclase (albite)	24%
clinopyroxene	5%
actinolite	5%
chlorite	5%
carbonate	17%
magnetite	3%
apatite	m
sphene	1%
finely divided	15%

Texture:

Fine-grained completely recrystallized, allotriomorphic granular rock. Prominent feature is layered structure developed as a result of intense alteration. This is also nicely displayed in outcrop. Layers are distinct according to the prominent secondary phases. Some veins of carbonate plus magnetite are normal to the prominent layering.

Alteration:

Early amygdaloidal dolomite mosaics and scapolitization. Minor primary clinopyroxene and feldspar associated with dolomite mosaics are preserved. Incomplete recrystallization of above during later albitization. Some later scapolitization of secondary albite. Late actinolite, chlorite, magnetite, and finely divided alteration. Late dolomite in vein cuts scapolitized and albitized areas and results in reprecipitation of plagioclase laths parallel to the vein. The vein also hosts inclusions of plagioclase, clinopyroxene, and magnetite. Secondary sphene is associated with magnetite.

J-10A (140')

Primary minerals:		Secondary minerals:	
plagioclase	23%	albite	13%
alkali feldspar	7%	clinopyroxene	4%
hornblende	2%	scapolite	15%
clinopyroxene	9%	calcite	10%
orthopyroxene	2%	chlorite	1%
sphene	1%	tremolite-actinolite	8%
magnetite	1%	magnetite	4%
apatite	tr	apatite	m

Texture:

Primary zone is medium-grained, hypidiomorphic granular, diverse crystal arrangement. Indiscriminate scapolite replacement. Sharp contact of primary zones with finer grained recrystallized zones resulting from albitization.

Alteration:

Relatively minor seritization of primary feldspar. Hornblende is largely inverted to tremolite. Calcite mosaics are amygdaloidal which preceded scapolitization and subsequent albitization. This is nicely displayed as the contact of the carbonate with euhedral primary minerals is sharp and the calcite may be replaced by scapolite at the interface. Approximately 20% of the section has been recrystallized during albitization which included clinopyroxene that is interstitial to the plagioclase laths. The grain size of secondary albite is variable-hiatal and a greater concentration of clinopyroxene occurs with the finer grained albite. Late calcite, chlorite and magnetite after scapolite, albite, and earlier calcite. Late calcite plus some magnetite also occurs in crosscutting veins. Some primary sphene is seen altering to magnetite. No late actinolite, chlorite, and finely divided alteration.

J-10B (140')

Primary minerals:		Secondary minerals:	
plagioclase	10%	albite	54%
alkali feldspar	3%	clinopyroxene	13%
hornblende	2%	scapolite	8%
clinopyroxene	m	calcite	3%
magnetite	1%	tremolite-actinolite	4%
apatite	tr	magnetite	2%
sphene	tr	chlorite	m

Texture:

Similar to J-10A.

Alteration:

Same alteration and paragenesis as in J-10A. Approximately 2/3 of this section has been albitized resulting in a reduction of grain size and complete replacement of primary mineralogy. The contact between albitized zones and altered diorite not subject to this alteration is sharp and nicely displayed in this thin section.

J-12 (194')

Primary minerals:		Secondary minerals:	
plagioclase	72%	calcite	2%
alkali feldspar	8%	scapolite	1.5%
hornblende	8%	chlorite	m
magnetite	2%	tremolite	4%
sphene	1%		
quartz	1%		
apatite	tr		

Texture:

Medium-grained, hypidiomorphic granular monzodiorite. Plagioclase may be rimmed by alkali feldspar. Plagioclase may be zoned and alkali feldspar commonly shows carlsbad twinning. Thin section shows some zones of very fine-grained (0.05-0.1 mm) subhedral primary feldspar of uncertain composition. Some is anhedral. Hornblende is commonly twinned. Magnetite is subhedral. Anhedral quartz is late. Calcite is interstitial.

Alteration:

Sericite is a common alteration product of feldspar. Hornblende is commonly inverted to tremolite. Scapolite after carbonate is interstitial to feldspar or hornblende and minor amounts occur as alteration products of these phases. Chlorite occurs as rosettes after plagioclase. Magnetite may be partly altered to sphene.

West Pit

Samples WP1B, WP4, WP5, WP14B, WP14C were collected from the upper limestone of the Torres member of Yeso Formation exposed in the West Pit. The primary rock is micrite (Folk, 1969). No allochemical materials were observed in thin section however the rock is fossiliferous in part as noted in outcrop. Diagenetic effects determined petrographically

include: a) incomplete aggrading neomorphism b) partial dolomitization. WP22A, WP22C, WP24A, and WP26 are altered Jones Camp dike collected from the south wall of the pit or adjacent outcrops farther south. Aspects of the local geology of the West Pit and other notes are found at the end of appendix IV.

WP1B

Primary mineralogy:

1) dolomite (38%) microspar to spar. Abundant intergranular porosity developed concomitant with dolomitization.
2) calcite (5%) microspar.

Secondary mineralogy:

1) calcite (20%) fine-grained, anhedral.
2) dolomite (7%) fine-grained mosaic in late vein.
3) garnet (5%) 1-3 mm, anhedral-amoeboid shape. yellowish brown color. Single grain in thin section which shows inclusions of cordierite, magnetite, calcite. Approximately 80% isotropic.
4) cordierite (10%) 0.1-0.3 mm, eu-subhedral. May show zoned extinction. Associated with secondary calcite.
5) magnetite (15%) eu-subhedral, 0.05-0.5 mm. Primarily associated with secondary calcite; lesser with cordierite and garnet.

Texture:

Layered structure developed in secondary mineralogy which is parallel to bedding. Some magnetite layers are at an angle to this. Late secondary dolomite vein is crosscutting. Dolomite occurs as a mosaic in form.

Alteration/mineralization:

Early garnet and calcite; later cordierite and higher temperature magnetite. Additional secondary calcite plus lower temperature magnetite concurrent with the main stage of mineralization. Late dolomite vein cuts all.

WP4

Primary mineralogy:

1) dolomite (40%) microspar

Secondary mineralogy:

1) garnet (15%) anhedral-amoeboid; 1.0 mm ave. grain size, lesser fine-grained (0.05-0.2 mm) and disseminated;

colorless; completely isotropic; may be associated with spinel; replaces primary dolomite.
2) spinel- hercynite (12%) anhedral-amoeboid; fine-grained; yellow to yellowish orange or colorless; isotropic to psuedo-isotropic; association with secondary dolomite.
3) dolomite (10%) anhedral, approximately equant; 0.1-0.5 mm.
4) magnetite (3%) eu-subhedral, fine-grained. May be concentrically zoned with non-isotropic, red colored phase which is probably hematite.
5) calcite (20%) anhedral; after dolomite.

Texture:

Primary dolomite is microspar and shows approximately 6% intergranular porosity. Secondary dolomite forms mosaics that may be linear in arrangement parallel to bedding. Secondary calcite occurs as a matrix to groundmass (primary) dolomite or as an alteration of coarser secondary dolomite.

Alteration/mineralization:

Early spinel, garnet, dolomite, and higher temperature magnetite; later calcite and lower temperature magnetite concurrent with the main stage of mineralization.

WP5

Primary mineralogy:

1) dolomite (42%) microspar

Secondary mineralogy:

1) calcite (30) anhedral; 0.1-0.3 mm.
2) dolomite (22%) subhedral; 0.1-0.2 mm.
3) quartz (1%) anhedral, 0.05-0.3 mm. occurs in vein with secondary calcite and magnetite.
4) magnetite (5%) an-subhedral, fine grained.

Texture:

Primary dolomite is microspar with high primary porosity as in WP4 and WP1B. Secondary dolomite tends to form mosaics. No primary calcite is apparent.

Alteration/mineralization:

Early secondary dolomite; later calcite and magnetite concurrent with the main stage of mineralization. Magnetite replaces calcite or dolomite. No late dolomite present.

WP14B

Primary mineralogy:

1) dolomite (10%) microspar

Secondary mineralogy:

1) cordierite (7%) eu-subhedral; 0.05-0.4 mm; usually occurs with secondary calcite; may be replaced by magnetite.
2) magnetite (18%) eu-subhedral; 0.01-0.7 mm; mean size 0.6 mm; after calcite or dolomite.
3) calcite (50%) anhedral; fine-grained.
4) dolomite (15%) anhedral, approximately equant; fine-grained.

Texture:

Well developed layered texture of secondary phases approximately parallel to bedding. Point growth of magnetite at carbonate grain boundaries. Secondary dolomite tends to form mosaics. Primary dolomite is microspar with high intergranular porosity. No primary calcite apparent.

Alteration/mineralization:

Nearly complete recrystallization. Early secondary calcite and cordierite. Later calcite plus magnetite concurrent with the main stage of mineralization. Some late dolomite in veins. Magnetite replaces all phases present.

WP 14C

Secondary mineralogy:

1) dolomite (10%) 0.05-0.4 mm; occurs as mosaics in zones or in veins.
2) idocrase (7%) euhedral; 0.3 mm ave. grain size; shows anomalous blue birefringence.
3) calcite (20%) anhedral; fine-grained; after dolomite.
4) magnetite (13%) euhedral; 0.5 mm mean grain size.

Texture:

Well developed layered texture as in WP14B.

Alteration/mineralization:

Early idocrase and secondary dolomite. Later magnetite and calcite concurrent with main stage of mineralization. Some late dolomite veins.

WP 22A

Primary minerals:	
feldspar	7%
clinopyroxene	2%

Secondary minerals:	
plagioclase (albite)	17%
clinopyroxene	4%
scapolite	18%
actinolite	13%
chlorite	20%
magnetite	6%
finely divided	13%

Texture:

Intensely altered, fine-grained, allotriomorphic granular rock. Secondary albite, chlorite, and actinolite show diverse crystal arrangement and an average length of 0.1 mm. Relatively minor medium-grained primary feldspar, clinopyroxene, and tremolite after hornblende unrecrystallized during scapolitization and albitization but show effects of later pervasive actinolite, chlorite and magnetite. Actinolite and chlorite typically occur as pseudomorhs after plagioclase or as fine-grained alteration of primary feldspar. Much of this alteration is finely divided.

Alteration:

Early scapolite indiscriminately replaces primary mineralogy. Scapolite after primary feldspar is preserved in one zone and not affected by later albitization which results in complete recrystallization and reduction in grain size. Pervasive actinolite and chlorite alteration of secondary and primary plagioclase and scapolite. Magnetite is predominately late and replaces plagioclase, scapolite, chlorite, and actinolite. Oxidation of iron in chlorite, actinolite, and magnetite is common.

WP 22C

Secondary minerals:	
plagioclase (albite)	15%
clinopyroxene	tr
actinolite	30%
chlorite	16%
magnetite	5%
sphene	3%
apatite	1%
calcite	tr
finely divided	30%

Texture:

Intensely altered diorite. Texture is similar to WP22A however secondary albite has an average length of 0.2 mm and actinolite also occurs as porphyroblasts. Secondary magnetite is anhedral and occurs in veins and fractures or is widely disseminated.

Alteration:

Early albitization resulting in near complete recrystallization of primary mineralogy. This thin section shows no primary feldspar preserved but does contain what appears to be primary clinopyroxene that was incompletely replaced during albitization and later actinolite and chlorite alteration. No evidence of scapolitization. Magnetite is predominantly late and replaces chlorite, actinolite, or albite. Secondary sphene is anhedral and associated with magnetite. Fine-grained euhedral apatite is concentrated in zones or occurs widely disseminated. Finely divided alteration is pervasive in some zones but is generally recognized as poorly crystallized, microcrystalline late chlorite and actinolite. Oxidation of iron in finely divided, chlorite, actinolite and magnetite is common.

WP 24A

Secondary minerals:

plagioclase (albite)	25%
scapolite	37%
chlorite	15%
actinolite	7%
finely divided	13%
magnetite	2%
sphene	1%
zircon	m

Texture:

Completely recrystallized, fine-grained; plagioclase laths are 0.1 mm ave. in length. Actinolite, chlorite, and finely divided material is microcrystalline to 0.3 mm in size. Actinolite is strongly pleochroic. Abundant widespread scapolite which commonly shows ghosts of secondary plagioclase laths. Disseminated anhedral magnetite.

Alteration:

Intensely altered syenodiorite. Early albitization and scapolitization of primary mineralogy. Scapolite is unusually widespread and has replaced some areas of albitization. Late chlorite, actinolite, finely divided,

magnetite, sphene, and zircon alteration affecting albite and scapolite.

WP 26

Secondary minerals:

plagioclase (albite)	23%
calcite	10%
scapolite	6%
clinopyroxene	1%
chlorite	11%
tremolite-actinolite	4%
magnetite	8%
sphene	2%
zircon	m
finely divided	35%

Texture:

Fine-grained to microcrystalline allotriomorphic granular. Secondary albite laths are 0.075 mm ave. length. Well developed flow texture in part. Prominent calcite mosaics hosting magnetite grains to 1.5 cm in length also host tremolite, sphene, and may show alteration to scapolite. Anhedral sphene also occurs crosscutting the plagioclase groundmass in veins to 2.2 mm length; zircon: 0.5 mm. Some calcite occurs as a matrix to secondary plagioclase. Late chlorite, actinolite, and finely divided alteration overprints secondary plagioclase. The latter is poorly crystallized green to greenish brown material showing anomalous extinction and first to second order birefringence. This is believed to be incipient chlorite and actinolite. Finely divided alteration, disseminated magnetite, chlorite and actinolite may show near surface oxidation of iron.

Alteration:

Intensely altered. Early albitization, minor remnants of scapolitization. Some of the calcite mosaics are probably partly preserved early amygdules and show trace associated primary clinopyroxene and early scapolite after calcite. Later pervasive chlorite, actinolite, and finely divided alteration. Sphene, magnetite, chlorite, and associated (late) calcite mosaics are the latest secondary effects.

East Pit

Sample EP was collected from float at the East Pit. Aspects of the geology of the East Pit are found at the end of Appendix IV.

EP

Secondary mineralogy:

1) gypsum (42%) anhedral-fibrous; microcrystalline; occurs as a matrix to clinopyroxene.
2) clinopyroxene (38%) euhedral; fine-grained- 0.2-1.0 mm; commonly twinned; largely aegirine-augite.
3) apatite (3%) euhedral; fine-grained; often clustered.
4) pyrite and magnetite (15%) fine-medium grained.
5) quartz (2%) anhedral; fine-grained; occurs in small zones; often triple junctions.

Alteration/mineralization:

Extensive metasomatism of gypsum bed resulting in clinopyroxene and quartz and dehydration of gypsum and concurrent reprecipitation as fibrous anhydrite. Apatite is later. Late pyrite determined in hand sample. Some magnetite in matrix of pyrite and partly replacing it. Pyrite is pseudomorphic after clinopyroxene or replaces matrix anhydrite. Gypsum is rehydrated.

"B" Location

Thin sections B3D, B7B, and B7G1 are from the section 24 pit. They are from the upper limestone of the Torres member. Primary rock is a micrite (Folk, 1969). No allochemical materials were observed in thin section however the rock is fossiliferous in part as observed in outcrop. Diagenetic effects determined petrographically include: a) incomplete aggrading neomorphism b) partial dolomitization. Aspects of the local geology and other notes are found at the end of appendix IV.

B3D

Primary mineralogy:

dolomite (63%) microspar

Secondary mineralogy:

1) dolomite (20%) anhedral, approximately equant; 0.2-0.5 mm; occurs in mosaics 0.4-3.0 mm wide.
2) calcite (12%) anhedral; 10-25 microns; after primary dolomite, also occurs lining dissolution vugs.
3) magnetite (5%) anhedral; fine-grained.

Texture:

Approximately 10% irregularly shaped vugs. Primary dolomite is microspar. Primary intergranular porosity of approximately 3-4%.

Alteration/mineralization:

Early dolomite mosaics. Magnetite concurrent with the main stage of mineralization, replaces predominantly secondary calcite and some dolomite.

B7B

Secondary mineralogy:

1) calcite (40%) anhedral, approximately equant; fine-grained seriate: 0.05-0.3 mm.
2) dolomite (15%) fine-grained; anhedral-subhedral.
3) cordierite (40%) an-subhedral; cryptocrystalline to fine-grained.
4) magnetite (5%) an-subhedral, fine-grained.

Texture:

Primary rock is probably an undolomitized limestone. Calcite occurs as equant grains typically showing triple junctions. Calcite-calcite grain boundaries are straight or sutured. Cordierite shows a diverse form. It may be amorphous cryptocrystalline to microcrystalline and equant or show a fibrous habit which may develop in radial arrangements. This finer-grained variety is pervasively stained yellow. Fine-grained varieties may occur as inclusions in the former type and are typically unstained and show zoned extinction. The coarser varieties also show triple junctions in places and trace amounts are euhedral. Zones of cordierite replacement are irregular in shape and size. Magnetite is anhedral and more commonly occurs replacing cordierite.

Alteration/mineralization:

Recrystallization of limestone during thermal metamorphism. No apparent recrystallization of calcite during hydrothermal alteration resulting in replacement of calcite by cordierite plus dolomite. Magnetite after cordierite and calcite at lower temperatures concurrent with the main stage of mineralization.

B7G1

Secondary mineralogy:

1) calcite (75%) anhedral; 0.05-2.0 mm.
3) magnetite (25%) eu-subhedral; fine-grained- seriate to 0.25 mm.

Texture:

Texture of calcite is similar to B7B however some of the coarser calcite was probably reprecipitated during hydrothermal alteration and mineralization. Magnetite is eu-subhedral; increase in grain size is gradual and individual grains may coalesce into aggregates during continued replacement of calcite.

Alteration/mineralization:

Occurrence of calcite suggests that the increase in grain size and development of triple junctions was the result of thermal metamorphism. Some of coarser calcite may be due to reprecipitation during mineralization. Magnetite replaces calcite.

B16A

Location: San Andres dolomite just above contact with pyroxene syenodiorite sill in section 15.

Allochemical material: none

Diagenetic changes:

1) complete dolomitization; individual dolomite rhombs are 10-50 microns in size; primary intergranular porosity of approximately 3-4%.

Primary mineralogy:

1) dolomite (50%) microspar

Secondary mineralogy:

1) calcite (15%) 0.05 mm average diameter
2) magnetite (35%) fine-grained; eu-subhedral much oxidized to hematite around perimeter of grains.

Mineralization:

The dolomite is replaced by calcite and magnetite. Sharp contact between unmineralized dolomite and magnetite plus calcite. Some calcite occurs in thin fractures emanating from the mineralized half of the thin section which in turn may be replaced by magnetite. Later calcite vein cuts some magnetite in earlier vein. Approximately 10% dissolution vugs occur in the mineralized half of the section and are lined by sparry calcite. Mineralized half shows alteration to hematite.

B16

Location: From pyroxene syenodiorite sill intruding San Andres dolomite collected just below sample B16A.

Primary minerals:		Secondary minerals:	
plagioclase	53%	calcite	10%
alkali feldspar	<5%	magnetite	7%
clinopyroxene	7%	chlorite	16%
magnetite	2%		
apatite	m		

Texture:

Fine-grained, porphyritic, hypidiomorphic granular pyroxene syenodiorite. Nine percent phenocrysts of plagioclase and minor alkali feldspar, 1.0-2.0 mm in size. Groundmass plagioclase diverse crystal arrangement, 0.3 mm ave. length. Secondary magnetite is anhedral or occurs as blades to 0.25 mm length which commonly show an interesting braided like network.

Alteration:

Secondary calcite occurs in the matrix and as an alteration product of phenocrysts. Chlorite is an alteration of primary clinopyroxene, feldspar, and biotite (?). Secondary magnetite is disseminated.

Roof site

Descriptions of the sample locations and aspects of the local geology of the Roof site can be found at the end of appendix IV.

RS-1

Secondary minerals:

scapolite	7%
tremolite	23%
plagioclase (albite)	60%
clinopyroxene	m
chlorite	5%
magnetite	3%
sphene	2%

Texture:

Fine-grained to microcrystalline. Subparallel or diverse arrangement of secondary plagioclase. Plagioclase laths 0.2 mm ave. length. No alkali feldspar apparent. Scapolite is

interstitial or as a matrix to secondary plagioclase. Tremolite is an-subhedral, fine-grained to microcrystalline and may show greenish brown pleochroism. It occurs: interstitial to secondary plagioclase laths; or as a psuedomorph of plagioclase; or occasionally as porphyroblasts. Anhedral sphene and magnetite occur disseminated.

Alteration:

Completely recrystallized Jones Camp syenodiorite rock. Scapolite exists as a remnant of early scapolitization of primary mineralogy. Near complete albitization plus concurrent tremolite and clinopyroxene at lower temperatures. Late tremolite, magnetite, chlorite, and apatite. Sphene is concurrent with albitization.

RS-2

Primary minerals:		Secondary minerals:	
plagioclase	4%	plagioclase	70%
alkali feldspar	tr	tremolite-actinolite	14%
clinopyroxene	1%	clinopyroxene	6%
		magnetite	2%
		sphene	3%

Texture:

Hypidiomorphic granular, fine-grained hydrothermally altered sample. A well developed parallel alignment of secondary plagioclase laths and tremolite due to fluid migration. 0.2 mm ave. grain size of secondary plagioclase laths; interstitial secondary clinopyroxene, tremolite-actinolite, magnetite, sphene.

Alteration:

Recrystallization of rock during hydrothermal alteration resulting in albite plus interstitial clinopyroxene, tremolite, magnetite and sphene. Tremolite also occurs as an inversion of primary hornblende as seen in zone unaffected by albitization. Chlorite alteration of primary clinopyroxene or plagioclase. No late tremolite, chlorite, or magnetite.

RS-3B

Primary minerals:		Secondary minerals:	
plagioclase	6%	plagioclase	70%
alkali feldspar	3%	alkali feldspar	12%
hornblende	1%	tremolite	5%
magnetite	tr	magnetite	3%
sphene	m	chlorite	1%
apatite	tr	apatite	tr
zircon	tr		

Texture:

Primary rock is medium-grained and hypidiomorphic. Diverse crystal arrangement. Feldspars are commonly zoned and alkali feldspar may show carlsbad twinning. Secondary plagioclase, alkali feldspar and interstitial actinolite are fine-grained and show a well developed subparallel or parallel alignment of crystals. Secondary plagioclase is relatively coarse-grained (0.4 mm ave. length).

Alteration:

Recrystallization of relatively felsic primary rock to plagioclase, alkali feldspar, and interstitial magnetite and tremolite. Sericitization of primary and secondary feldspar locally abundant. Actinolite occurs as an inversion of primary hornblende. Minor chlorite after feldspar. No early scapolite and calcite or late tremolite and magnetite.

RS-4A

Primary minerals:		Secondary minerals:	
plagioclase	69%	chlorite	5%
alkali feldspar	<5%	calcite	4%
clinopyroxene	5%	actinolite	3%
magnetite	7%	feldspar	1%
apatite	1%	magnetite	1%

Texture:

Fine-grained to microcrystalline, hypidiomorphic granular, porphyritic pyroxene syenodiorite. Diverse crystal arrangement. Phenocrysts are 1-3 mm length and predominantly plagioclase. Approximately 3% total phenocrysts. Groundmass plagioclase 0.1 mm ave. length. Interstitial clinopyroxene is anhedral, colorless or green. Disseminated subhedral magnetite.

Alteration:

Calcite, chlorite, magnetite occur as alteration products of phenocrysts, and groundmass clinopyroxene, feldspar, and biotite (?). Secondary magnetite is anhedral, finer-grained and is most abundant (as is chlorite) around a fracture cutting the section. The fracture hosts euhedral (prismatic) feldspar and calcite. Some iron oxide alteration around the fracture.

RS-4B

Thin section shows contact between pyroxene syenodiorite and Jones Camp syenodiorite.

pyroxene syenodiorite

Primary minerals:		Secondary minerals:	
plagioclase	48%	calcite	12%
alkali feldspar	2%	chlorite	15%
clinopyroxene	10%	magnetite	2%
magnetite	4%	actinolite	6%
		feldspar	1%

Jones Camp syenodiorite:

Primary minerals:		Secondary minerals:	
plagioclase	52%	calcite	10%
alkali feldspar	6%	chlorite	5%
clinopyroxene	10%	clinopyroxene	2%
hornblende	7%		
quartz	1%		
magnetite	4%		
biotite	3%		

Texture:

The pyroxene syenodiorite is fine-grained to microcrystalline, hypidiomorphic granular and porphyritic. The contact with the Jones Camp syenodiorite is sharp. The Jones Camp syenodiorite is medium-grained, hypidiomorphic granular and the feldspars are commonly zoned. Both rock types show a diverse crystal arrangement.

Alteration:

The pyroxene syenodiorite shows sericitization of feldspars. Chlorite replaces clinopyroxene and is an alteration of the phenocrysts. Calcite occurs as an alteration of groundmass minerals and phenocrysts. It also occurs as mosaics in

zones or in a fracture emanating from the chilled contact. Calcite mosaics host euhedral clinopyroxene, actinolite, or magnetite. The Jones Camp syenodiorite shows the same secondary effects as the pyroxene syenodiorite but includes some saussuritization of feldspars.

RSA-1

Primary minerals:		Secondary minerals:	
plagioclase	9%	plagioclase	25%
alkali feldspar	3%	scapolite	15%
		tremolite-actinolite	35%
		magnetite	8%
		chlorite	3%
		apatite	2%

Texture:

Fine-grained, hypidiomorphic granular hydrothermally altered sample. Secondary plagioclase is 0.3 mm ave. length. Secondary tremolite-actinolite and magnetite is relatively coarse grained.

Alteration:

Early scapolitization and albitization (plus interstitial tremolite-actinolite) of primary mineralogy. Extensive later actinolite plus magnetite. Some of actinolite is the result of inversion of primary hornblende at a higher temperature. Secondary apatite occurs in clusters of grains. Magnetite occurs in aggregates after actinolite or feldspar. Seritization and secondary chlorite in primary feldspar is common.

RSA-2

Secondary minerals:	
plagioclase	70%
tremolite-actinolite	17%
calcite	7%
chlorite	1%
magnetite	3%
apatite	2%

Texture:

Fine-grained hiatal, hypidiomorphic granular. Tremolite occurs: as porphyroblasts commonly greater than 1.0 mm; or pseudomorphic after secondary plagioclase (0.2 mm ave. length); or interstitial to secondary plagioclase (0.05-0.1

mm ave. length). Anhedral magnetite occurs in aggregates.

Alteration:

Early albitization precedes extensive tremolite-actinolite, calcite, and magnetite alteration. Some of the actinolite porphyroblasts may be relicts of earlier inversion of primary hornblende. Calcite occurs interstitial to plagioclase and actinolite or is an alteration of individual plagioclase crystals. Apatite is found in actinolitized zones. Magnetite may replace feldspar and tremolite-actinolite. Chlorite is an alteration product of feldspar. Magnetite may be associated with a minor high-relief, amorphous, unidentified secondary phase. No scapolite or early calcite.

RSA-3

Secondary minerals

tremolite-actinolite	50%
plagioclase	42%
magnetite	5%
apatite	3%

Texture:

Layered structure is defined by predominance of plagioclase or tremolite-actinolite and/or grain size variations. Grain size varies from 0.01 -0.2 mm however some tremolite occurs as porphyroblasts up to 1.0 mm. Plagioclase is predominantly anhedral and equant. A few percent of the plagioclase shows albite twinning and are subhedral.

Alteration/mineralization:

Complete replacement of primary rock by tremolite-actinolite, plagioclase, apatite, and magnetite. Tremolite-actinolite and plagioclase are believed to have coprecipitated in part; however, a tendency of the former to replace the latter is noted in some zones. Magnetite is late and replaces plagioclase and tremolite-actinolite but is predominately after the plagioclase in this section.

Shaft site

Sample locations and aspects of the local geology of the Shaft site can be found at the end of appendix IV. Allochemical materials and diagenetic changes were not identified due to complete recrystallization in response to contact metamorphism and hydrothermal alteration.

S-2

Secondary mineralogy:

1) tremolite-actinolite (37%) subhedral, 0.05-0.3 mm.
2) clinopyroxene (30%) subhedral, 0.1-0.3 mm.
3) calcite-dolomite (25%) 0.1-0.3 mm.
4) chlorite (2%) fine-grained.
5) magnetite (6%) sub-euhedral or pseudomorphs after actinolite; 0.1-1.0 mm.

Texture:

Well developed layered structure in response to fluid migration; individual layers are up to several mm's thickness and consist of: a) clinopyroxene + calcite b) dolomite + actinolite c) dolomite mosaics. Individual dolomite grains in the latter are 1.0-1.5 mm and show a sieve texture- hosting inclusions of actinolite or clinopyroxene. Clinopyroxene is 0.05-0.3mm in size. Grain size distribution is hiatal. Magnetite is pseudomorphic after actinolite and replaces calcite or dolomite. It may be rimmed by a high relief, amorphorous (unidentified) phase.

Alteration:

Extensive metasomatism of primary limestone resulting in clinopyroxene, actinolite, and dolomite. Later magnetite and chlorite.

S-3

Secondary mineralogy:

1) feldspar (12%) euhedral or anhedral, 0.75-1.25 mm.
2) clinopyroxene (48%) euhedral, 0.03 mm ave.
3) chlorite (17%) 0.05-0.2 mm.
4) apatite (3%) euhedral, 0.05-0.15 mm.
5) calcite (13%) anhedral, fine-grained.
6) magnetite (7%) sub-euhedral, 0.025-0.2 mm.

Texture:

Fine-grained to microcrystalline. Layered structure developed in response to fluid migration; layers are distinct based on the predominant secondary phase of either clinopyroxene, chlorite, feldspar, or magnetite. Calcite occurs as a matrix to clinopyroxene. Grain size of magnetite and apatite are an order of magnitude greater than clinopyroxene. As mineralization proceeded individual magnetite grains grew in size and formed into aggregates.

Alteration:

Complete recrystallization of primary limestone due to combined effects of contact metamorphism and metasomatism. Early clinopyroxene + calcite and feldspar. These phases may be replaced by later chlorite or magnetite. Apatite is also a late phase. No tremolite-actinolite or dolomite as seen in S-2.

S-4

Secondary minerals:

1) clinopyroxene (48%) euhedral, 0.01-0.1 mm, occasionally to 0.75 mm.
2) calcite (10%) anhedral, fine-grained.
3) chlorite (23%) cryptocrystalline to fine-grained.
4) actinolite (2%) euhedral, associated with calcite.
5) magnetite (17%) eu-subhedral, 0.1-0.3 mm.

Texture:

Similar to S-3.

Alteration:

Complete recrystallization of parent rock. Early secondary calcite + clinopyroxene and relatively minor actinolite; later chlorite and magnetite. Magnetite may replace all the phases present. Some oxidation of chlorite and magnetite.

S-6

Secondary minerals:

1) feldspar (11%) euhedral; 0.5-1.0 mm.
2) clinopyroxene (24%) eu-subhedral; 0.01-0.05 mm.
3) chlorite (30%) 0.1-0.5 mm.
4) magnetite (23%) subhedral; 0.2-0.5 mm some aggregates to 0.75 mm.
5) apatite (2%) euhedral; 0.1-0.2 mm.
6) calcite (10%) anhedral; fine-grained.

Texture:

Similar to S-3, S-4. Feldspar is untwinned and shows inclusions of clinopyroxene, magnetite, and chlorite. Calcite occurs as matrix to clinopyroxene.

Alteration:

Early clinopyroxene. The feldspar is later. Late chlorite, magnetite, and apatite. Magnetite may replace

clinopyroxene, chlorite, or calcite.

S-7

Secondary minerals:

1) calcite (71%) 0.1-0.3 mm.
2) feldspar (17%) subhedral-anhedral
3) clinopyroxene or tremolite (8%) subhedral; 20-60 microns; predominantly clinopyroxene.
4) chlorite (2%) 20-50 microns; radial aggregates.
5) dolomite (1%) anhedral; associated with tremolite.

Texture:

Triple junctions developed in calcite which controls occurrence of secondary feldspar and clinopyroxene. Clinopyroxene is typically elongated and shows radial arrangement at triple junctions in calcite. Feldspar may show sieve texture. Crude layering of secondary feldspar is developed.

Alteration:

Primary texture of recrystallized calcite is due to thermal metamorphism. No apparent recrystallization of calcite concomitant with silicate metasomatism. This relationship is also noted for the other samples however calcite may also be replaced by dolomite associated with tremolite-actinolite. Feldspar shows elongated fluid inclusions and may show relatively coarse chlorite alteration. No magnetite mineralization.

S-8

Secondary minerals:

1) calcite (61%) anhedral-approximately equant; 0.1-0.8 mm, ave. 0.2 mm.
2) clinopyroxene (12%) euhedral; 12 microns to 0.12 mm; green color, non-pleochroic.
3) feldspar (4%) eu-subhedral; 0.1-0.35 mm.
4) chlorite (15%) 0.05-0.5 mm, ave. 0.15 mm.
5) magnetite (8) eu-subhedral, 0.1-0.5 mm.

Texture:

Similar to S-7.

Alteration:

Recrystallization of primary calcite as a result of thermal metamorphism. Intergranular porosity controls occurrence of

secondary phases replacing calcite. Clinopyroxene is early; later feldspar; chlorite and magnetite are the latest secondary phases. Magnetite replaces clinopyroxene, chlorite, calcite.

S-9

Location: marginal Jones Camp syenodiorite at the Shaft site.

Secondary minerals:

plagioclase	48%
scapolite	8%
actinolite	30%
calcite	12%
magnetite	2%
apatite	m

Texture:

Fine-grained to microcystalline, hypidiomorphic granular. Diverse crystal arrangement of plagioclase laths. Remnants of primary feldspar occur as a matrix to secondary albite and actinolite. Mottled texture seen in hand specimen is due to roughly concentric zones of anhedral scapolite or mosaics of calcite. Anhedral magnetite occurs along fractures with calcite or is disseminated as individual grains (0.03 mm ave. diameter) or clustered in zones to 0.2 mm wide.

Alteration:

Albitization and scapolitization resulted in reduction of grain size and near complete recrystallization of primary mineralogy. Early calcite mosaics are amygdaloidal and are incompletely replaced by subsequent scapolitization and later albitization. Calcite also occurs as a later replacement of secondary albite, clinopyroxene (concurrent with albitization) and scapolite. It also occurs in late veins with magnetite cutting earlier alteration. Extensive late actinolitization after albitization is concurrent with chlorite, magnetite, and late calcite.

S-10

Location: Jones Camp syenodiorite collected above the shaft at the Shaft site.

Primary minerals:		Secondary minerals:	
plagioclase	55%	scapolite	15%
alkali feldspar	13%	tremolite-actinolite	10%
hornblende	4%	apatite	tr
magnetite	3%	uralite	1%

Texture:

Medium-grained hypidiomorphic granular, hydrothermally altered monzodiorite. Feldspar may be zoned. Euhedral hornblende is seen in transistion to inversion to tremolite-it has the extinction of tremolite but the pleocroism of hornblende. Hornblende is commonly twinned. No primary zircon, sphene, or apatite noted.

Alteration:

Extensive sericitization of primary feldspar replacing up to 85% of individual grains. Subhedral scapolite is interstitial to primary feldspar and probably replaces earlier amygdaloidal calcite. Anhedral scapolite showing lower birefringence also occurs as an alteration product of hornblende or feldspar. Relatively minor uralite after feldspar or hornblende. No carbonate.

APPENDIX VI:

The solubility of iron was calculated after a method outlined in Henley, et al. (1984, see Chapt.9 -Ore metals in hydrothermal fluids). Equilibrium constants for the various reactions are from Helgeson (1969) except for the stability of ferrous chloride complexes that were available in Crerar et al. (1978).

The solubility of iron determined by equilibrium with magnetite may be expressed as:

$$2Fe^{+3} + Fe^{+2} + 4H_2O = Fe_3O_4 + 8H^+ \qquad (1)$$

It is considered important to constrain both the pH and fugacity of oxygen in determining solubility. This is accomplished by adding an equation for the reduction of ferric to ferrous iron to equation (1):

$$2Fe^{+3} + Fe^{+} + 4H_2O = Fe_3O_4 + 8H^+ \qquad (1)$$

$$\underline{2Fe^{+2} + 1/2O_2 + 2H^+ = 2Fe^{+3} + H_2O \qquad (2)}$$

$$3Fe^{+2} + 1/2O_2 + 3H_2O = Fe_3O_4 + 6H^+ \qquad (3)$$

Metal ions such as iron, form complex ions by reaction with available ligands which is significant for ore metal transport. In acid, saline solutions, iron is transported as both ferrous and ferric chloride complexes:

$$Fe^{+3} + Cl^- = FeCl^{+2} \qquad (4)$$

$$FeCl^{+2} + Cl^- = FeCl_2^+ \qquad (5)$$

$$FeCl_2^+ + Cl^- = FeCl_3(aq) \qquad (6)$$

$$Fe^{+2} + Cl^- = FeCl^+ \qquad (7)$$

$$FeCl^+ + Cl^- = FeCl_2(aq) \qquad (8)$$

Equilibrium constants for these reactions are called stepwise formation constants. For example (parentheses denote molalities):

$$K_{<FeCl^{+2}>} = [Fe^{+3}][Cl^-]/[FeCl^{+2}] \qquad (9)$$

$$K_{<FeCl_2^+>} = [FeCl^{+2}][Cl^-]/[FeCl_2^+] \qquad (10)$$

These two expressions can be combined to give:

$$K_{<FeCl^{+2}>} \times K_{<FeCl_2^+>} = [Fe^{+3}][Cl^-]^2/[FeCl_2^+] = K'_{<FeCl_2^+>}$$

The new constant K' is the cumulative formation constant for the $FeCl^{+2}$ complex.

Constants such as this are assigned the symbol @n' where n is the ligand number for the complex. These constants for ferric and ferrous chloride complexes are tabulated in Table 1.

The total activity of a metal in solution is the sum of activities of each of its complexes in solution. For iron:

$$SUM\ Fe = [Fe^{+3}] + [Fe^{+2}] + [FeCl^{+2}] + [FeCl_2^+] + [FeCl_3] + [FeCl^+] + [FeCl_2]$$

or:

$$SUM\ Fe = [Fe^{+3}]\ (1 + [Cl^-]/@1a + [Cl^-]^2/@2a + [Cl^-]^3/@3a) + [Fe^{+2}]\ (1 + [Cl^-]/@1b + [Cl^-]^2/@2b) \qquad (12)$$

Since

$$K_3 = [H^+]^6/[Fe^{+2}]^3 + [O_2]^{1/2}$$

So that

$$\log[Fe^{+2}] = 1/3\log K_3 - 1/6\log[O_2] - 2pH$$

and

$$\log[Fe^{+3}] = \log[Fe^{+2}] + 1/4\log[O_2] - pH + \log K_2$$

These may be substituted nicely into equation (12) to give an expression for the solubility of iron in equilibrium with magnetite as a function of temperature, pH, fugacity of oxygen, and concentration of chlorine. No activity coefficients were added to equation (12); therefore activity equals molality in figure 30.

TABLE 1: Stepwise formation constants for ferric and ferrous chloride complexes.

Ferric chloride complexes:

$$@1a = [Fe^{+3}][Cl^-]/[FeCl^{+2}]$$

$$@2a = [Fe^{+3}]]Cl^-]2/[FeCl_{2}+]$$

$$@3a = [Fe^{+3}][Cl^-]^3/[FeCl_3]$$

Ferrous chloride complexes:

$$@1b = [Fe^{+2}][Cl^-]/[FeCl^+]$$

$$@2b = [Fe^{+2}][Cl^-]^2/[FeCl_2]$$

This thesis is accepted on behalf of the faculty of the Institute by the following committee:

Gary T. Smith
Advisor

James M. Roberts

Andrew Campbell

7/3/85
Date

Jenkins Thesis

Plate 2: Geologic cross sections

Scale: one inch=400 feet

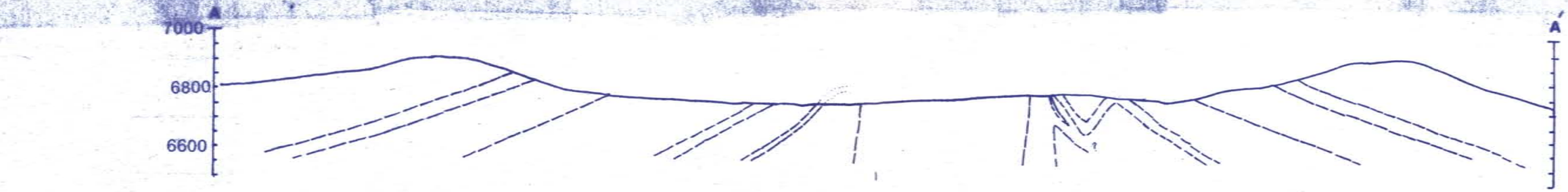

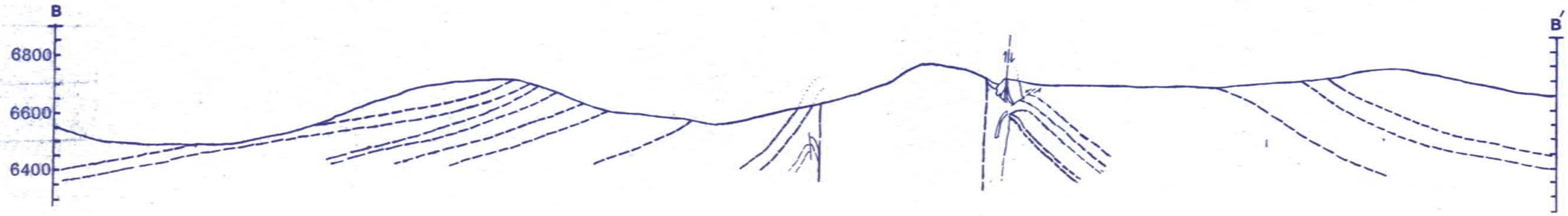

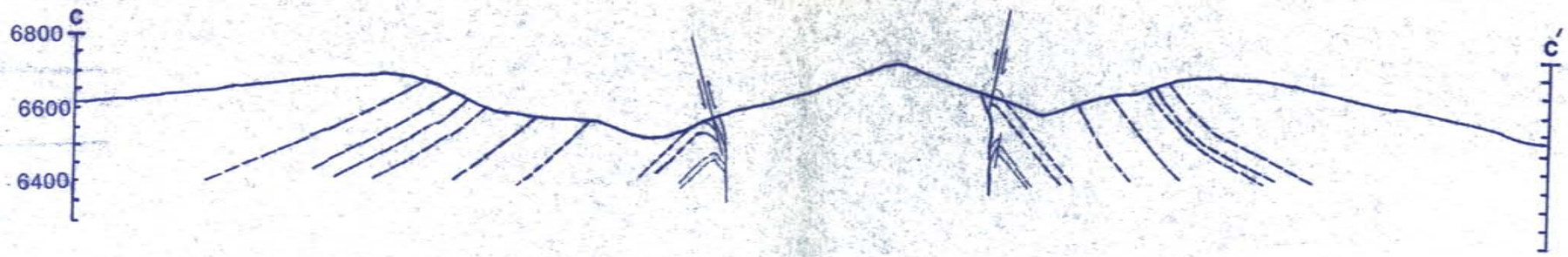


6400

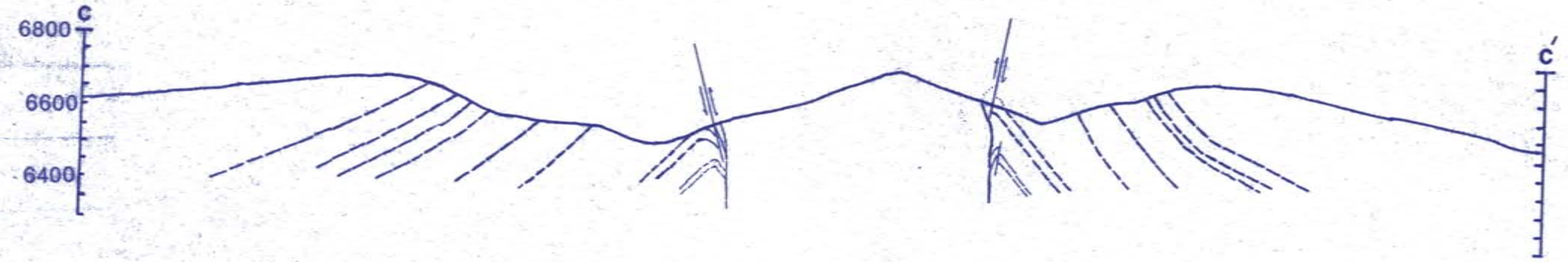
C
6800
6600
6400
C´

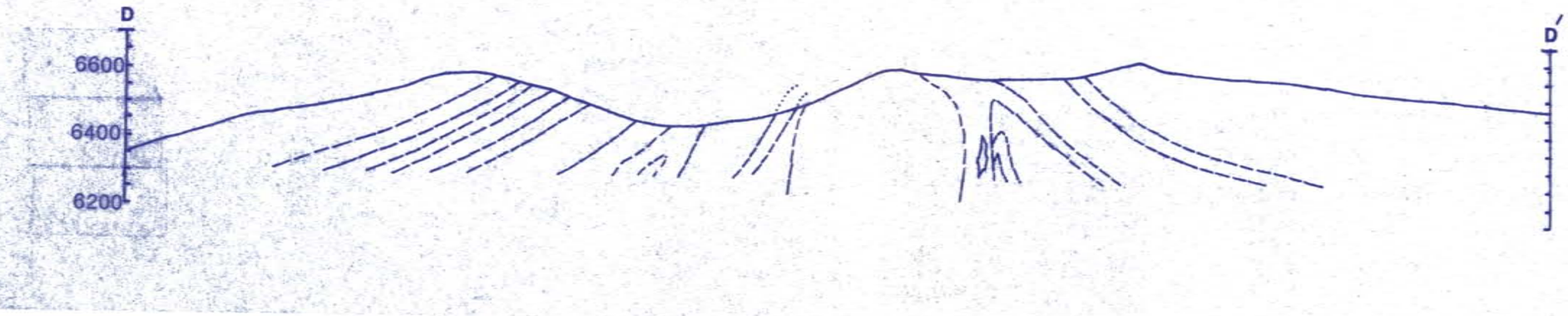
D
6600
6400
6200
D´